INTERNATIONAL ATOMIC ENERGY AGENCY
UNITED NATIONS EDUCATIONAL, SCIENTIFIC AND CULTURAL ORGANIZATION
INTERNATIONAL CENTRE FOR THEORETICAL PHYSICS
I.C.T.P., P.O. BOX 586, 34100 TRIESTE, ITALY, CABLE: CENTRATOM TRIESTE

UNITED NATIONS INDUSTRIAL DEVELOPMENT ORGANIZATION

INTERNATIONAL CENTRE FOR SCIENCE AND HIGH TECHNOLOGY
c/o INTERNATIONAL CENTRE FOR THEORETICAL PHYSICS 34100 TRIESTE (ITALY) VIA GRIGNANO, 9 (ADRIATICO PALACE) P.O. BOX 586 TELEPHONE (040) 224572 TELEFAX (040) 224575 TELEX 460449 APH I

SMR.550 - 6

SPRING COLLEGE IN MATERIALS SCIENCE ON

"NUCLEATION, GROWTH AND SEGREGATION IN MATERIALS SCIENCE AND ENGINEERING"

(6 May - 7 June 1991)

BACKGROUND MATERIAL

FOR LECTURE ON

TRANSPORT PROCESSES (INCLUDING RADIATION ENHANCED DIFFUSION)

W. FRANK
Max-Planck-Institut für Metallforschung
Institut für Physik
Heisenbergstrasse 1
7000 Stuttgart 80
Germany

Phenomenological and statistical description of diffusion

What is diffusion?

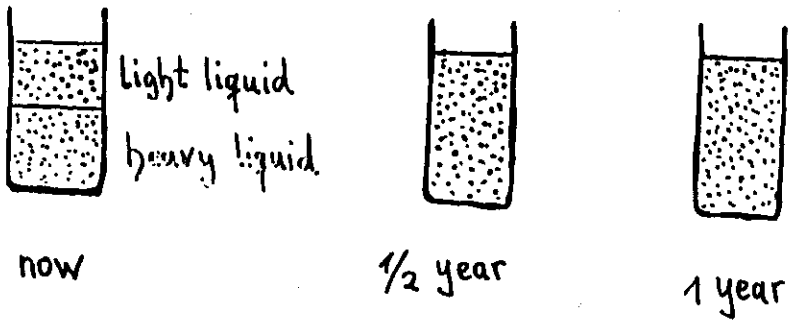

Phenomenological description

$$\vec{j} = -D \operatorname{grad} C \qquad (1)$$

Fick's 1st Law

D = diffusion coefficient $\left[\frac{m^2}{s}\right]$

- Onsager's linear irreversible thermodynamics: first-order kinetic coefficient
- tensor of rank 2 (anisotropic diffusion)

Conservation of diffusing particles (exclusion of particle reactions):

$$-\partial C/\partial t = \operatorname{div} \vec{j} \qquad (2)$$

Continuity Equation

(1) + (2):

$$\partial C/\partial t = \operatorname{div}(D \operatorname{grad} C) \qquad (3a)$$

Fick's 2nd Law (most general form)

Assumption: $D \neq D(I)$ $\left[D \neq D(C(I))\right]$

$$\partial C/\partial t = D \Delta C \qquad (3b)$$

Fick's 2nd Law (most popular form)

1-dimensional case: $\partial C/\partial t = D\, \partial^2 C/\partial x^2$

heat conduction eq.: $\partial T/\partial t = \chi\, \partial^2 T/\partial x^2$

Schrödinger eq.: $\partial \Psi/\partial t = (i\hbar/2m)\, \partial^2 \Psi/\partial x$

classical wave eq.: $\partial^2 W/\partial t^2 = c^2\, \partial^2 W/\partial x^2$

Statistical Description

1-dim. case :

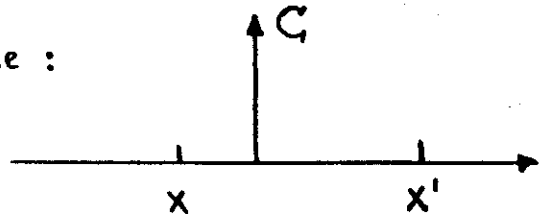

Random walK :

$P_t(x,x')$ = probability that a particle has migrated from $x \to x'$ during t

$$C(x',t) = \int_{x=-\infty}^{+\infty} C(x,0)\, P_t(x,x')\, dx \qquad (4)$$

Assumptions :

1) spatial homogeneity : $P_t = P_t(X)$, $X = x - x'$
2) isotropy : $P_t(X) = P_t(-X)$

$$C(x',t) = \int_{X=-\infty}^{+\infty} C(x'+X,0)\, P_t(X)\, dX \qquad (5)$$

Focker–Planck Equation

Expansion in power series of t and X :

Note : $\int_{-\infty}^{+\infty} P_t(X)\, dX = 1$ (normalization)

$$\int_{-\infty}^{+\infty} X\, P_t(X)\, dX = 0$$

$$\int_{-\infty}^{+\infty} X^2\, P_t(X)\, dX \equiv \overline{X^2} \neq 0$$

$\lim_{t\to 0} P_t(X) \neq 0$ only for small X

$$\partial C/\partial t + \ldots = \frac{\overline{X^2}}{2t}\, \partial^2 C/\partial x^2 + \ldots \qquad (6)$$

Comparison with FicK's 2nd Law :

$$D \equiv \frac{\overline{X^2}}{2t} \qquad (7a)$$

$$\overline{X} \simeq \sqrt{\overline{X^2}} = \sqrt{2Dt} \qquad (7b)$$

diffusion length

Basic diffusion mechanisms in solids

Specialization:
- crystalline solids
- thermally activated diffusion

p, T = const:

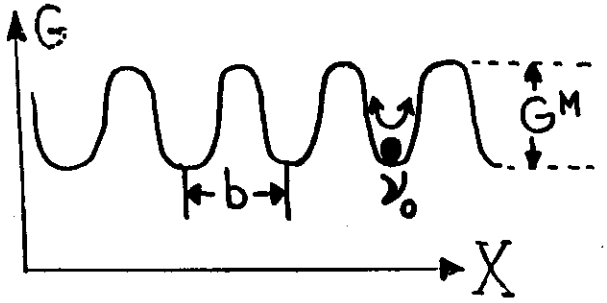

G^M = Gibbs free energy of migration

Jump frequency: $\nu = \nu_0 \exp(-G^M/kT)$

$G = H - TS$

$$\nu = \underbrace{\nu_0 \exp\left(\frac{S^M}{k}\right)}_{\nu_0^*} \exp(-H^M/kT) \quad (8)$$

Diffusion coefficient:

$$D = \overline{X^2}/2t$$

$$1/t \propto \nu$$

$$\overline{X^2} = b^2 \propto a^2$$

$$D^{(x)} = g a^2 \nu = g a^2 \nu_0^* \exp(-H^M/kT) \quad (9)$$

Direct vs. Indirect Diffusion

Direct diffusion (see above)

The diffusing particles perform **random walks.**

The diffusing particles are mobile per se; i.e., diffusion vehicles are not involved.

Indirect diffusion

Without the aid of diffusion vehicles the particles under consideration cannot move.

It is the **diffusion vehicles** which perform **random walks.**

The particles considered undergo a non-random, correlated diffusion as a result of the diffusion of the vehicles.

Direct Diffusion

Most prominent mechanism:

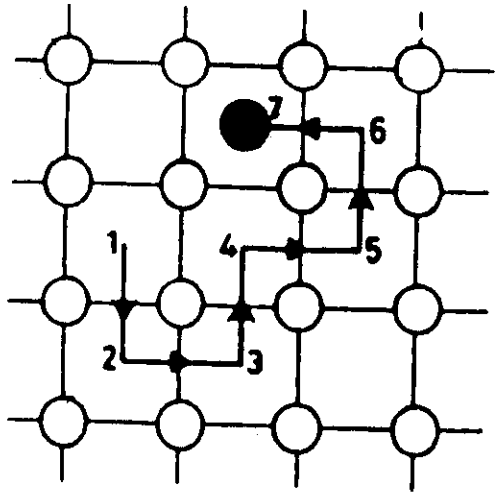

direct interstitial mechanism

Characteristic feature :

low migration enthalpy ($H^M \lesssim 1eV$)

Examples:

Fe, Cu, Li, Pd (see below) in Si

C, N in α-Fe

O in Ta

Indirect Diffusion

Most elementary mechanisms involve

vacancies or self-interstitials

1) Vacancy mechanism

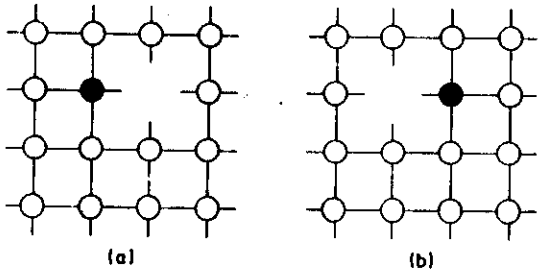

Examples:

self-diffusion in metals

diffusion of substitutional solutes in metals

self-diffusion in Ge

diffusion of substitutional Group-III and Group-V dopants in Ge

fat Group-V dopants (e.g. As, Sb) in Si

2) Indirect interstitial mechanism

(interstitialcy mechanism)

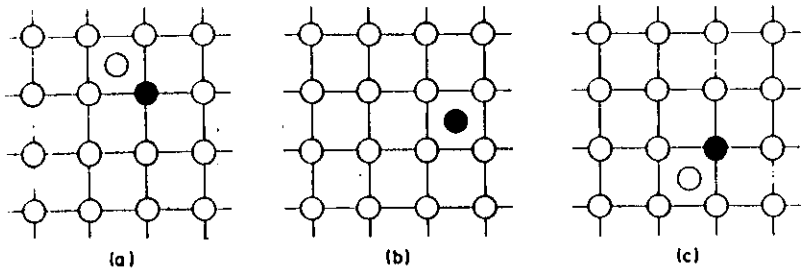

Examples:

self-diffusion in Si (above 1000 °C)

small Group-III dopants (e.g., B) in Si

self-diffusion in ice (above −50 °C)

Why is the vacancy mechanism widely known in contrast to the interstitialcy mechanism?

Diffusion Coefficients

Direct diffusion (see above [Eq. (9)]):

$$D = \underbrace{g a^2 \nu_0^*}_{D_0} \exp\left(-H^M/kT\right)$$

Indirect diffusion

Corresponding expression for the diffusion coefficient of the diffusion vehicles:

$$D_v = D_{v,0} \exp\left(-H_v^M/kT\right) \quad [v = V, I] \quad (10)$$

Diffusion coefficient of the particle diffusing via V or I:

$$D_v^s = f_v C_v D_v \quad (11)$$

$$0 \le f_v \le 1 \quad (12)$$

f_v: correlation factor (see below)

self-diffusion coefficient

or

diffusion coefficient of substitutional solutes

Thermal Equilibrium: $C_v = C_v^{eq} \equiv \exp\left(-G_v^F/kT\right)$

(10) + (13) in (11):

$$D_v^S = D_{v,0}^S \exp\left[-\left(H_v^F + H_v^M\right)/kT\right] \quad (14)$$

final expression for coefficient of indirect diffusion

Characteristic feature:

high self-diffusion enthalpy $\left(H_v^F + H_v^M \gtrsim 2\,eV\right)$

General case of indirect diffusion (superposition of vacancy mechanism and interstitialcy mechanism)

$$D^S = D_V^S + D_I^S \quad (15)$$

Note: Comparable significance of both contributions is restricted to a small temperature regime

Examples:
- self-diffusion in Si at about 1000 °C
- self-diffusion in ice at about −50 °C
- Group-III and Group-V elements in Si (> 1000 °C: fat Group-V dopants [e.g., Sb] prefer V mechanism, small Group-III dopants [e.g., B] prefer I mechanism)

Correlation factor

$$D_v^S = f_v C_v D_v \quad (11)$$

$$D_v^S = D_{v,0}^S \exp\left[-\left(H_v^F + H_v^M\right)/kT\right] \quad (14)$$

$$D_{v,0}^S \sim f_v$$

Demonstration for V mechanism

3d or 2d case:

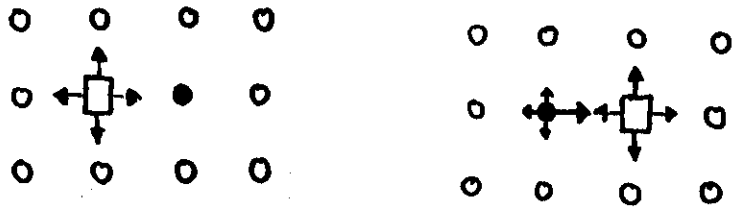

random walk of V
correlated walk of diffusing atom
→ high probability that preceding jump is cancelled
→ $f_V < 1$

linear chain:

→ $f_V = 0$

direct diffusion: $D_v^S \equiv D_{v(\equiv S)}$, $C_v = 1$, $f_v = 1$

(3)

ENHANCED DIFFUSION IN SEMICONDUCTORS

W.Frank, U.Gösele, and A.Seeger

Max-Planck-Institut für Metallforschung, Institut für Physik, and Universität Stuttgart, Institut für Theoretische und Angewandte Physik, Stuttgart, F.R.G.

After having reviewed the mechanism of enhanced diffusion in crystalline solids from the view-point of a new classification, the paper concentrates on current developments in the field of enhanced diffusion in semiconductors. As illustrated by various examples, the energy-release-type mechanisms appear to be most effective in raising the mobility of directly diffusing defects in silicon, germanium and gallium arsenide. Particular emphasis is given to the spatial redistribution of substitutional dopants in silicon under particle irradiation as well as to the enhanced dopant diffusion induced either by high phosphorus concentrations on the surfaces of the silicon specimens or by surface oxidation. In these cases the diffusion of dopants is enhanced, since the concentrations of self-interstitials, which serve as diffusion vehicles for the dopants (interstitialcy mechanism), are raised above their thermal-equilibrium values. Finally, a suggestion is made how information on the mechanism of the well-established substitutional-interstitial interchange diffusion of gold in silicon may be obtained from enhanced-diffusion studies.

1. Introduction and definitions

It is considered to be established that diffusion in crystalline solids takes place via the motion of crystal lattice defects /1-5/. The conceptionally simplest example is the 'direct' diffusion of foreign interstitial atoms (i.e. their jumping from interstice to interstice), since here the only defects involved are the foreign interstitials themselves. By contrast, 'indirect' diffusion (e.g., of radioactive isotopes of the matrix atoms [≡ self-atoms] or of foreign substitutional atoms) requires intrinsic defects as diffusion vehicles. Important examples for such vehicles are vacancies in metals or germanium (vacancy mechanism), or self-interstitials in silicon at high temperatures (interstitialcy mechanism) /6/.

'Normal' diffusion in solids is thermally activated and may take place under thermal-equilibrium or quasi-thermal-equilibrium conditions. In normal diffusion the diffusion coefficient D may be written as a weighted average

$$D = \sum_{\alpha} P_{\alpha} D_{\alpha} \qquad (1)$$

of diffusivities of the form*

$$D_{\alpha} = g_{\alpha} a^2 \nu_{\alpha}^{0} \exp(S_{\alpha}^{M}/k) \exp(-H_{\alpha}^{M}/kT) \qquad (2)$$

(a = lattice constant, k = Boltzmann's constant, T = temperature, g_{α} = geometrical factor, ν_{α}^{0} = attempt frequency, H_{α}^{M} [S_{α}^{M}] = enthalpy [entropy] of migration). The physical meaning of the diacritical parameter α and of the weight factors P_{α} depends on whether we consider direct or indirect diffusion.

In the case of normal direct diffusion, the diffusivities D_{α} refer to different states α of the defect species involved, e.g., to the different electric charge states in which a given foreign interstitial in a semiconductor may occur. Then the P_{α} denote the probabilities of population of these states in thermal equilibrium, normalized according to

$$\sum_{\alpha} P_{\alpha} = 1 \qquad (3)$$

Depending on whether the concentration of the foreign interstitials is equal to their solubility or not, one has normal direct diffusion under equilibrium or quasi-equilibrium conditions, respectively.

In the case of normal indirect diffusion, the D_{α} as given by (2) denote the diffusivities of the intrinsic defects of type α promoting diffusion. The quantities P_{α} are related to the thermal-equilibrium concentrations C_{α} of these defects according to

$$P_{\alpha} = f_{\alpha} C_{\alpha} , \qquad (4)$$

where

$$C_{\alpha} = \exp\left(\frac{S_{\alpha}^{F}}{k}\right) \exp\left(-\frac{H_{\alpha}^{F}}{kT}\right). \qquad (5)$$

Here H_{α}^{F} (S_{α}^{F}) denotes the formation enthalpy (entropy) of the intrinsic α-type defects. In the practically important case $C_{\alpha} \ll 1$, the factors f_{α} are independent of the defect concentrations. With (4), eq. (1) may be re-written as

$$D = \sum_{\alpha} f_{\alpha} C_{\alpha} D_{\alpha} . \qquad (6)$$

In the case of self-diffusion, D is the tracer self-diffusion

* For simplicity, we confine ourselves to cubic crystals. In crystals of lower symmetry, diffusion coefficients are second-rank tensors.

coefficient if, disregarding numerical factors of an entirely geometrical nature, the quantities f_α are identified with the correlation factors /2,5/. These account for the fact that, contrary to what is true for directly diffusing defects, the indirect diffusion of marked atoms (e.g., radioactive isotopes) is not random. Rather, successive jumps of the marked atoms are correlated in a manner that depends on the nature of the intrinsic defects involved. This holds also if D is identified with the diffusion coefficient of foreign substitutional atoms, with the additional feature that the correlation effects just described may be strongly influenced by interactions between substitutional atoms and intrinsic defects.

Whereas in the case of direct diffusion the subscript α discriminates between different states of the same defect species (see above), in indirect diffusion α distinguishes both between different states and between different kinds of intrinsic defects. This is illustrated by the following example: In the self-diffusion of silicon both self-interstitials (I) and vacancies (V) have to be taken into account, the first mechanism dominating above, the second below about 1220 K /1,6,7-9/. Both mechanisms may involve different electric charge states with different diffusivities D_α (for self-interstitials $\alpha = I^+, I^0$, and I^-; for vacancies $\alpha = V^+$, V^0, V^-, and V^{2-}). The populations of these states, i.e. the concentrations C_α, are determined by the position of the Fermi level, hence the self-diffusion coefficient is sensitive to chemical doping /1,7,9,10/.

Deviations from normal diffusion enforced by external influences, such as particle irradiation, illumination, carrier injection, or quenching, are referred to as 'enhanced diffusion'.* Direct diffusion (compare eq.(1)) may be enhanced either by establishing non-equilibrium populations P_α which favour equilibrium states α with high diffusivities D_α (whereby the form (2) of the D_α remains unchanged) or by the generation of new (non-equilibrium) states** in which the defect mobility is high (but, in general, no longer describable by(2)). At any rate, due to its very nature, direct

* 'Enhanced diffusion' comprises negatively enhanced diffusion, i.e. reduced diffusivities.

** Such new states may be electric charge states which do not occur in thermal equilibrium, excited electronic states, or excited states of vibration.

diffusion can be enhanced only by raising the average mobility of the diffusing defects. Indirect diffusion may be 'mobility-enhanced', too, if D (compare eq.(6)) is enhanced because of an increase of the average mobility of the intrinsic defects without a change in the total intrinsic-defect concentration $\sum_\alpha C_\alpha$. Alternatively, indirect diffusion may be 'concentration-enhanced', namely if the increase of the diffusion rate originates from an increase of $\sum_\alpha C_\alpha$. Mechanisms and examples of mobility-enhanced or concentration-enhanced diffusion will be presented in Sects. 2 or 3, respectively.

A further way in which indirect diffusion may be enhanced is the following: The factors f_α accounting for the correlation between the indirectly diffusing atoms and the intrinsic defects promoting diffusion may be changed by external influences. These changes give rise to 'correlation-enhanced' diffusion (compare (6)). This is particularly important if the correlation is mainly due to interactions between the indirectly diffusing atoms and the intrinsic defects. As suggested elsewhere /11/, correlation-enhanced diffusion appears to play a role in experiments on photon-irradiation-enhanced diffusion of dopants in silicon /12,13/ (Sect. 3.1.1).

2. Mobility-enhanced diffusion

2.1. Collision-enhanced mobility

The mechanisms of collision-enhanced mobility to be described in Sects. 2.1.1. to 2.1.4. are not specific for semiconductors but may operate in other crystalline solids as well. E.g., following Urban and Seeger /14/ we suggest that the diffusion of radiation-induced intrinsic defects in metals well below the temperatures at which these defects undergo thermally activated migration takes place via these mechanisms of collision-enhanced mobility, since other mechanisms of mobility-enhanced diffusion (Sects. 2.2 to 2.3) can exclusively operate in non-metals.

2.1.1. Direct collision displacement

If in an irradiation experiment an incident particle (electron, neutron, etc.) hits a lattice defect, e.g., an interstitial atom, the momentum transfer may suffice to directly displace the defect to another equilibrium position (direct Urban-Seeger mechanism /14/). The displacement barrier strongly depends on the crystallographic direction and, in general, is larger than the enthalpy H_α^M required for thermally activated migration. Temperature is expected to play a minor role in this mechanism.

2.1.2 Indirect collision displacement

A defect, say a self-interstitial, located at A may be displaced in the following indirect manner (Fig. 1): At B, which is inside the interstitial's recombination volume for vacancies, an atom is ejected by an incident energetic particle and deposited in the interstice at C. Then the interstitial at A will recombine with the vacancy generated at B, i.e., the net result is the transport of an interstitial from A to C (indirect Urban-Seeger mechanism /14/). It is emphasized that this mechanism may work even if the energy transferred to the atom at B is less than the threshold energy for the production of stable Frenkel pairs /15/: In this case a mechanically unstable Frenkel pair BC may be generated, and the interstitial at A may recombine with the vacancy at B before spontaneous recombination of BC takes place.

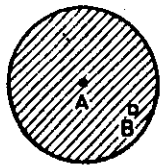

Fig.1. Indirect collision displacement of a self-interstitial.

The complementary mechanism of indirect collision displacement of vacancies is obvious. Similar mechanisms may give rise to indirect collision displacements of foreign atoms.

2.1.3. Thermally assisted collision displacement via excited states of vibration.

Excited states of vibration localized at defects may be populated by irradiation-particle-defect collisions. Provided

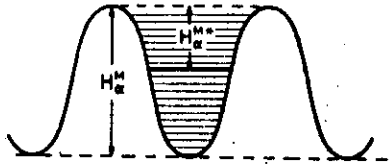

Fig.2. Thermally assisted collision displacement (Sect.2.1.3) or thermally assisted energy-release mechanism(Sect. 2.3.2) via the excited vibrational state marked by the fat horizontal line.

that the half-lives of these states are long enough, the defects can undergo thermally activated diffusional jumps from these excited states into neighbouring equilibrium positions (Fig.2). The efficiency of this mechanism is temperature-dependent. If only one excited state with sufficiently long half-life is populated or exists, a well-defined activation enthalpy H_α^{M*} ($<H_\alpha^M$) may be measured.

2.1.4. Mobility enhancement by irradiation heating

The overwhelming portion of the energy introduced into solids by irradiation ends up as heat, particularly if the energy per mass unit of the incident particles is high. Along the trails of such particles mainly electronic defects are generated. These recover to a large extent in a very short time. E.g., in metals electronic perturbations relax even completely within about 10^{-14} s. The energy released from these electronic excitations gives rise to an increase of temperature and thus to an enhancement of the mobility of defects migrating with the aid of thermal activation.

Mobility enhancement by irradiation heating is expected to play a particular role in radiation-induced recombinations of Frenkel pairs. At the ends of the projectile trails, where,in addition to electronic heating, nuclear stopping becomes important, the local temperature and hence the mobility of defects may temporarily become so high that a considerable fraction of the Frenkel pairs produced in these regions may recombine.

Presumably, collision-enhanced mobility always involves some contribution of mobility enhancement by irradiation heating, even in cases in which other mechanisms of mobility-enhanced diffusion are rate-controlling.

2.2. Electronic-state-controlled mobility changes

In non-metals defects may occur in different electronic states α, namely in different electric charge states and, in a given charge state, either in the electronic ground state or in an excited electronic state. In general, the Gibbs free energy of migration of a defect

$$G_\alpha^M = H_\alpha^M - TS_\alpha^M \quad , \qquad (7)$$

and thus its mobility depend on the electronic state of the defect. This may be realised from the following examples: The electron density may be more or less concentrated on the defect, i.e., a defect may exhibit different degrees of extension; the coupling between a defect and the matrix may be affected by the electronic state of the defect; even the geometrical configuration of a defect may depend on its electronic state, e.g., on its charge state.

An example for a defect whose migration enthalpy strongly depends on its electronic state is the self-interstitial in Si: /6,16,17/ H_I^M or $H_{I^+}^M$ is 0.35 eV or 0.85 eV, respectively. $H_{I_0}^M$ increases from 1.5 eV to 2 eV between 570 K and 1660 K. This is thought to be a direct consequence of the delocalization of the electrons of I^0 with increasing temperature.

As discussed already in Sect. 1, deviations of the electronic-state populations P_α of a given defect species from their equilibrium values can be achieved by particle irradiation, illumination, etc. As a consequence, the average mobility of the defects increases or decreases in comparison to normal diffusion /18/. This is a significant difference between electronic-state-controlled mobility changes and the other mobility-enhanced diffusion mechanisms: The latter can not give rise to a reduction of the diffusion rate*. A further specific feature of electronic-state-controlled mobility changes is that they are restricted to the mobility interval limited by the mobilities in the slowest and fastest diffusing electronic state of the defect species considered.

2.3 Mobility enhancement by electronic-energy release

2.3.1. Direct energy-release mechanism

If conduction electrons and (or) holes in a semiconductor recombine at (are trapped by) defects via non-radiative transitions, with the aid of the energy released in these processes the defects may be displaced /19,20/. The only difference between this direct energy-release mechanism and direct collision displacements (Sect. 2.1.1) is the source of the defect displacement energy: In direct collision displacements it originates from irradiation-particle - defect collisions, whereas in the direct energy-release mechanism the energy comes from the energy reservoir of the free charge carriers. These may be generated by irradiation, illumination, carrier injection, etc. Since the maximum energy which may be released from the electronic-energy reservoir of a semiconductor in a non-radiative transition is given by the width E_g of the energy gap, the direct energy-release mechanism works only if the defect migration enthalpy does not exceed E_g /11/.

* Note that in the case of concentration-enhanced diffusion the enhancement is always positive, whereas in the case of correlation-enhanced diffusion it may be negative, e.g., if a rapidly diffusing impurity-vacancy pair is decomposed by irradiation into less mobile constituents.

2.3.2. Thermally assisted energy-release mechanism via excited states of vibration.

In this mechanism the energy released from the electronic reservoir via non-radiative transitions is used to populate defect-localized excited states of vibration. Then by thermal activation the defects can jump from these excited states to neighbouring positions (Fig.2) like in thermally assisted collision displacements (Sect. 2.1.3). The mechanism is controlled by activation enthalpy barriers H_α^{M*} which are smaller than H_α^M /19,20/.

2.3.3. Bourgoin-Corbett-type mechanisms

A prerequisite for the operation of Bourgoin-Corbett-type mechanisms /18,21/ is that in different electronic states* the equilibrium positions of the defects are centred on crystallographically different sites. If the equilibrium positions in one electronic state lie symmetrically between those belonging to a different state, repeated transitions between these states may give rise to fully athermal diffusion (Fig. 3). In more complicated cases some thermal activation is usually required.

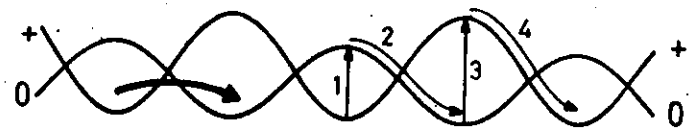

Fig. 3. Athermal Bourgoin-Corbett diffusion of a defect induced by repeated transitions between its positive and its neutral charge state (thin arrows 1 to 4). The fat arrow indicates a transition which is assisted by Jahn-Teller distortion.

* Originally, Bourgoin and Corbett regarded different electric charge states only.

The present authors /6,11/ have pointed out that, contrary to what might be implied by the original papers on the Bourgoin-Corbett mechanism, even the purely athermal mechanism may work if the enthalpies for thermal migration in the various electronic states are larger than Eg. This is so since a change in the electronic structure of a defect may induce a direct relaxation from the equilibrium position in the initial electronic state to that in the final one (Jahn-Teller effect), as indicated by the fat arrow in Fig.3.

2.4. Examples for mobility-enhanced diffusion.
As already mentioned in Sect. 2.1, in metals mobility-enhanced diffusion can occur exclusively by the mechanisms of collision-enhanced mobility (Sects. 2.1.1 to 2.1.4), i.e. under particle irradiation. The observation that radiation-induced mobility-enhanced diffusion (e.g., of vacancies) in metals increases with temperature can hardly be accounted for by direct collision displacements alone (Sect. 2.1.1). Hence, we presume that in metals other mechanisms of collision-enhanced mobility (Sects. 2.1.2 to 2.1.4) must be significant.

In semiconductors, mechanisms of mobility-enhanced diffusion which operate in non-metals only (Sects. 2.2 and 2.3) appear to play the main role. This is indicated by various examples in which mobility-enhanced diffusion has been demonstrated to occur under conditions not involving particle irradiation: (i) Illumination of low-temperature-irradiated n-type germanium with germanium-filtered light induces migration of self-interstitials at liquid-helium temperature/23/. This has been concluded from the fact that such an illumination extinguishes the recovery stage at 65 K which is found in unilluminated but otherwise equally treated n-type germanium, and which previously had been shown to be due to the thermally activated migration of self-interstitials /24/. (ii) Aluminium interstitials in silicon undergo mobility-enhanced diffusion under carrier injection and laser illumination /25/. (iii) The same is true for intrinsic defects in GaAs. In light-emitting diodes and lasers based on GaAs, light-induced defect migration is an important link in the chain of processes leading to degradation /26,27/.

The most detailed understanding of mobility-enhanced diffusion in a semiconductor has been achieved in the case of the carrier-injection-induced migration of aluminium interstitials (Al_i) in silicon /25/. There the thermally assisted energy-release mechanism via an excited state of vibration is realized (compare Sect. 2.3.2. and Fig.2): By carrier capture and recombination at the first donor level (corresponding to the charge-state transition Al_i^o/Al_i^+) the activation enthalpy is lowered to $H_\alpha^{M*} = 0.27$ eV, which has to be compared with the normal migration enthalpy of 1.2 eV in the usually populated charge state Al_i^{2+}. A decision whether H_α^{M*} corresponds to thermally activated defect jumps out of an excited vibrational state of Al_i^o or Al_i^+ has not yet been possible.

Concerning mobility-enhanced diffusion of intrinsic defects in GaAs, the operation of thermally assisted energy-release mechanisms (Sect.2.3.2.) has been established, too, though the defects undergoing mobility-enhanced diffusion have not yet been identified in a direct manner /26/. However, according to a degradation model for GaAs-base lasers suggested recently by two of us /27/, at least the Ga interstitials and the As vacancies must be capable of migrating by a thermally assisted energy-release mechanism via excited states of vibration.

The mobility-enhanced diffusion of self-interstitials in germanium or silicon below liquid-helium temperature presumably takes place via energy-release mechanisms, too (Sects. 2.3.1 and 2.3.2): In germanium collision-induced mobility (Sects. 2.1.) may be excluded, since mobility-enhanced diffusion occurs under illumination (see above)/23/.In silicon both electronic-state-controlled mobility changes (Sect.2.2) and Bourgoin-Corbett-type mechanisms (Sect.2.3.3) can be ruled out: The former would require an activation enthalpy which is at least equal to $H_I^M \approx 0.35$ eV and therefore would not work below liquid-helium temperature; the latter would require that the equilibrium positions of the self-interstitials in the various charge states are not centred on the same sites, contrary to what is the case for the split self-interstitials in silicon/6,16/. Hence, provided that in silicon and germanium mobility-enhanced diffusion of self-interstitials at extremely low temperatures is governed by the same mechanism, this must be of the energy-release type described in Sects. 2.3.1. and 2.3.2. In germanium the thermal assistance of this mechanism is extremely small (corresponding to $H_\alpha^{M*} = 0.0044$ eV) /28/, in silicon it may be even zero /29/, i.e., the direct energy-release mechanism may be realised.

3. Concentration-enhanced diffusion

3.1. Enhancement of the concentrations of intrinsic defects by irradiation

3.1.1. Spatially homogeneous defect concentrations

Indirect diffusion in solids may be concentration-enhanced if a super-saturation of intrinsic defects is introduced by irradiation /30,31/. If only monodefects are taken into account, the expression (6) for the coefficient of indirect diffusion reduces to

$$D = f_V D_V C_V + f_I D_I C_I \qquad (8)$$

and under steady-state conditions /31/,

$$D_V C_V = D_I C_I , \qquad (9)$$

further to

$$D = (f_V + f_I) D_V C_V = (f_V + f_I) D_I C_I \qquad (10)$$

The well-known Lomer-Dienes-Damask theory /32,33/, which has recently been reviewed by Sizmann /31/, is a straightforward rate-equation treatment of concentration-enhanced diffusion for a spatially homogeneous system, provided the above-mentioned simplifications are justified. The main results of this theory are the following: $D_I C_I = D_V C_V$ is temperature-independent if the disappearance of the radiation-induced defects is sink-controlled; by contrast, this quantity is proportional to $\exp\left(-\frac{H^M_{slow}}{2\,kT}\right)$, where H^M_{slow} is the migration enthalpy of the less mobile intrinsic defect species, if the intrinsic defects mainly disappear by mutual recombination. According to (10) these features should be directly reflected by the tracer self-diffusion coefficient, since in the case of self-diffusion f_V and f_I are temperature-independent correlation factors.

Unfortunately, to the authors' knowledge measurements of radiation-enhanced self-diffusion on semiconductors have not yet been performed. However, measurements of the radiation-enhanced diffusion coefficients of substitutional dopants in silicon show both a temperature-independent sink-controlled regime /12,34-37/ and a temperature-dependent recombination-controlled regime /12/, from which an activation enthalpy of $H^M_{slow} \gtrsim 1.5$ eV has been extracted /12/. This value is in agreement with the migration enthalpy of the less mobile intrinsic defect, the high-temperature configuration of the self-interstitial /6/. These are unexpected results, since at first sight the temperature dependences of the radiation-enhanced diffusion coefficients of substitutional dopants are expected to differ from those of $D_I C_I = D_V C_V$. The reason for this is that in the case of indirectly diffusing dopants the factors f_V and f_I in (10) ought to be temperature-dependent as a result of the interaction between the dopants and the intrinsic defects. The fact that this is not the case appears to indicate that effects of correlation enhancement, which 'switch off' the interaction between the dopants and the intrinsic defects during irradiation*, may play some role (Sect.1) /11/.

Although, in principle, investigations of concentration-enhanced diffusion under irradiation can yield valuable information on point defects in semiconductors, a number of difficulties may complicate the evaluations considerably: (i) In general, vacancies and self-interstitials enhance diffusion to different extents. (ii) Effects of mobility-enhanced diffusion and/or correlation-enhanced diffusion, e.g., via radiation-induced changes of the electronic states of the defects, may be intermixed. (iii) In practice, the defect concentrations use to be spatially inhomogeneous, so that the Lomer-Dienes-Damask theory is not applicable.

3.1.2. Spatially inhomogeneous defect concentrations

The production of intrinsic defects in semiconductors by irradiation with charged particles, say protons, is concentrated in the vicinity of the average penetration depth R_p of the irradiation particles (Fig.4a). The spatial inhomogeneities in the concentrations of vacancies and self-interstitials built up in this way lead to a redistribution of initially homogeneously distributed dopants, e.g., of boron in silicon /38,39/. This is a consequence of the coupling between the indirect diffusion of these dopants and the diffusion of the intrinsic defects.

Depending on the strength of the interaction between the dopants and the intrinsic defects two different approaches to the dopant redistribution phenomenon may be considered, both of which have originally been invoked in order to describe segregation in binary alloys under irradiation:

The formation of intrinsic-defect-dopant complexes/40, 41/ is expected to be important if a strong attraction between the dopants and the intrinsic defects exists.

*

* A 'switch-off' of interactions between point defects during irradiation may occur if the electronic states (e.g., the charge states) of the defects are changed

In this case mobile vacancy-dopant and/or self-interstitial-dopant complexes may be formed at a high rate in the vicinity of R_p where the concentrations of intrinsic defects are high. By preferentially migrating in the direction of their negative concentration gradients, these complexes leave the region around R_p, thus producing there a dip (between two smaller humps) in the dopant concentration (Fig. 4c).

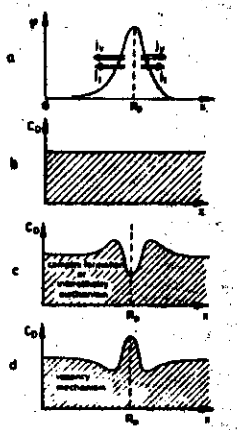

Fig. 4. Redistribution of dopants as a consequence of spatially inhomogeneous concentrations of intrinsic defects: Production rate φ of intrinsic defects as a function of depth x below the irradiated surface at x = o (a). Uniform dopant concentration C_D before irradiation (b). $C_D(x)$ after irradiation in the case of complex formation or of an interstitialcy mechanism (c). $C_D(x)$ after irradiation in the case of a vacancy mechanism (d).

The inverse Kirkendall effect /40,41/ can give rise to a redistribution of dopants without any attraction between the dopants and the intrinsic defects. This effect is a consequence of the conservation of matter during diffusion, which requires that, in the case of a vacancy mechanism, a vacancy flux (j_V) must be balanced by fluxes of matrix atoms (j_M) and dopants (j_D) in the opposite direction /42/, i.e.

$$j_V = -(j_M + j_D), \qquad (11)$$

whereas, in the case of an interstitialcy mechanism, a flux of self-interstitials (j_I) produces a combined flux of matrix atoms and dopants in the same directions and of the same magnitude /42/, i.e.

$$j_I = +(j_M + j_D) \qquad (12)$$

As a consequence, the out-flux of intrinsic defects from the region around R_p in which C_V and C_I are high, generates at R_p a peak (between two smaller dips) or a dip

(between two smaller humps) in the dopant concentration, depending on whether the dopants diffuse via a vacancy or an interstitialcy mechanism, respectively (Fig. 4d or c).

Proton irradiation of both boron- and phosphorus-doped silicon produces a dip in the dopant concentrations /38,39,43/. This means either that the complex-formation mechanism operates or, if the inverse Kirkendall effect is realized, that at high temperatures boron and phosphorus in silicon diffuse preferentially via an interstitialcy mechanism. Presumably, the latter is the case, since the attraction between dopants and intrinsic defects, which is a prerequisite for the operation of the complex-formation mechanism, appears to be switched off during proton irradiation (Sects. 1 and 3.1.1.). Moreover, the observations reported in Sects. 3.2 and 3.3 support the predominance of interstitialcy diffusion in silicon at high temperature.

3.2. Oxidation as a tool for studying concentration-enhanced diffusion.

There are various materials (e.g., Zn, Mg, or Si) into which intrinsic point defects are injected when oxide layers are grown on the surfaces /44-47/. In the case of silicon thin oxide surface layers grown below about 1400 K inject self-interstitials /48/. As a consequence, for dopants diffusing via an interstitialcy mechanism (e.g., boron or phosphorus at high temperatures) concentration-enhanced diffusion has been achieved by surface oxidation /41/. Unfortunately, attempts to demonstrate a different behaviour of arsenic /49/, which might diffuse via a vacancy mechanism / 11 / have failed for the following reason (41): With increasing thickness of the oxide surface layers the efficiency of these layers as self-interstitial sources decreases. Above a critical thickness (which depends on temperature) the oxide layers even become sinks for self-interstitials. This is the case before arsenic has diffused over a measurable distance, contrary to what is true for the faster diffusing phosphorus or boron.

Investigations of oxidation-enhanced diffusion have two big advantages over studies of radiation-enhanced diffusion: (i) By oxidation, one species of intrinsic defects can be introduced separately. Moreover, in the case of silicon these are self-interstitials, which predominantly control normal diffusion at high temperatures, too /6/. (ii) The enhancement of diffusion by oxidation is exclusively of the concentration-enhancement type, contrary to the diffusion enhancement under irradiation, which, at least in non-metals,

inevitably is a mixture of concentration-enhanced, mobility-enhanced, and correlation-enhanced diffusion. A disadvantage of surface oxidation is that it can enhance diffusion in silicon by a factor of about 2 only /47-49/, whereas under irradiation diffusion enhancements by a factor of 10^6 or more can be achieved /30/.

3.3. Generation of self-interstitial supersaturations in silicon by the in-diffusion of phosphorus

If phosphorus is deposited on a silicon surface in a high concentration at temperatures below about 1400 K, a supersaturation of silicon self-interstitials is pushed into the bulk in front of the in-diffusing phosphorus atoms /50-53/*. In turn, these extra self-interstitials enhance the diffusion of dopants which diffuse via an interstitialcy mechanism. Examples for these so-called anomalous diffusion phenomena are the 'emitter-push effect' and the 'movement of marked layers' /55-58/.

Compared to enhanced diffusion under irradiation, enhanced diffusion induced by high surface concentrations of dopants has the same advantages as oxidation-induced enhanced diffusion (compare (i) and (ii) in Sect. 3.2) whitout having the disadvantage of a small enhancement factor: By in-diffusing dopants the self-interstitial concentration is enhanced by typically a factor of 10^2, in some cases by 10^4, which produces an easily measurable 'pushing' of dopants /55-58/. The present authors therefore suggest to study the pushing of arsenic in silicon by in-diffusing phosphorus and to compare this to the phosphorus-induced pushing of phosphorus and of boron under identical experimental conditions. Should the relative diffusion enhancement of arsenic turn out to be equal to the diffusion enhancements of phosphorus or boron (which are virtually the same), although normal diffusion of arsenic is considerably slower than that of phosphorus or boron, this would indicate that under high-temperature thermal-equilibrium conditions arsenic diffuses via an interstitialcy mechanism like boron or phosphorus.

* The in-diffusion of other dopants into silicon, e.g., of boron, produces extra self-interstitials, too, although to a smaller extent /54/. Mechanisms which may give rise to these effects are discussed elsewhere /41/.

3.4. How
silicon by
Gold in
interchan
the major
(Au_S), on
The diffu
exceeds
silicon by
The
establishe
mechanis

or via sil
mechanis

This inter
mena, son
If go
the fast d
lished wit
concentrat
librium bel
or I (kick-
the formati
generation
of V or a
whether th
minates. In

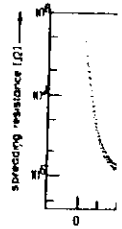

gold in sili
patible eith
an I supers
concentrati
erably hig

3.4. How to elucidate the diffusion mechanism of gold in silicon by diffusion-enhancement studies

Gold in silicon diffuses via a substitutional-interstitial interchange mechanism /59/. Under equilibrium conditions the majority of the gold atoms sit on substitutional sites (Au_S), only a small fraction occupy interstitial sites (Au_i). The diffusivity of Au_i is much higher than that of Au_S and exceeds the diffusivity of Group-III or Group-V elements in silicon by several orders of magnitude /1,59/.

Thermal equilibrium between Au_S and Au_i may be established via vacancies according to the Frank-Turnbull mechanism /59,60)

$$Au_i + V \rightleftharpoons Au_S \qquad (13)$$

or via silicon self-interstitials according to the 'kick-out' mechanism /61/

$$Au_S + I \rightleftharpoons Au_i \qquad (14)$$

This interchange diffusion gives rise to interesting phenomena, some of which are briefly described below.

If gold is diffused into a thin silicon wafer, due to the fast diffusion of Au_i the following equilibria are established within a short time: a global uniform Au_i equilibrium concentration throughout the whole wafer and a local equilibrium between Au_i, Au_S, and V (Frank-Turnbull mechanism) or I (kick-out mechanism /62/. According to (13) or (14) the formation of Au_S requires the consumption of V or the generation of I, respectively. In this way an undersaturation of V or a supersaturation of I is built up, depending on whether the Frank-Turnbull or the kick-out mechanism dominates. Indeed, it has been shown that the diffusion of

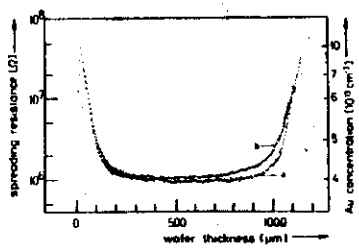

Fig. 5. Distribution of Au_S in a Si wafer measured by the spreading-resistance technique after Au_S deposition both surfaces (a) or on the left-hand surface only (b) and subsequent diffusion annealing for 5 h at 1100 K. For details see Ref. 62.

gold in silicon induces dislocation climbing which is compatible either with the existence of a V undersaturation or an I supersaturation /63/. In agreement with this picture the concentration of Au_S near the wafer surfaces is considerably higher than in the centre of the wafer (Fig. 5),

since the surfaces may act as V sources or I sinks, respectively.

A distinction between the Frank-Turnbull mechanism and the kick-out mechanism should be feasible in the following manner: Let gold diffuse into a boron-doped silicon wafer. Since the diffusivity of boron is known to be enhanced by supersaturation of self-interstitials (compare the emitter-push effect /53,55/) but can never be increased by an undersaturation of vacancies, the observation of a gold-induced enhancement of the boron diffusion in the centre of the wafer would be an unambiguous decision in favour of the kick-out mechanism. This prediction demonstrates the potential power of enhanced diffusion as a tool for investigating point defects and diffusion processes in semiconductors.

References

1. A.Seeger and K.P.Chik. Phys.Stat. Sol. 29, 455 (1968)
2. A.Seeger and H.Mehrer, in Vacancies and Interstitials in Metals edited by A.Seeger, D.Schumacher, W.Schilling, and J.Diehl. North-Holland, Amsterdam 1970, p.1
3. A.Seeger. J. Phys. F: Metal Physics 3, 248 (1973)
4. N.L.Peterson. J. Nuclear Materials 69/70, 3 (1978)
5. H.Mehrer. J. Nuclear Materials 69/70, 38 (1978)
6. A.Seeger, W.Frank, and U.Gösele. Inst. Phys. Conf. Ser. 46, 148 (1979)
7. A.Seeger. Radiat. Effects 9, 15 (1971)
8. A.Seeger, H.Föll, and W.Frank, Inst. Phys. Conf. Ser. 31, 12 (1977)
9. G.Hettich, H.Mehrer, and K.Maier. Inst. Phys. Conf. Ser. 46, 500 (1979)
10. J.M.Fairfield and B.J.Masters. J. Appl. Phys. 38, 3148 (1967)
11. U.Gösele, W.Frank, and A.Seeger. Inst. Phys. Conf. Ser. 46, 538 (1979)
12. B.J.Masters and E.F.Gorey. J. Appl. Phys. 49, 2717 (1978)
13. B.J.Masters. Inst.Phys.Conf.Series 46, 545 (1979)
14. K.Urban and A.Seeger. Phil.Mag. 30, 1395 (1974)
15. K.Dettmann, G.Leibfried, and K.Schroeder. Phys.Stat. Sol. 22, 423 (1967)
16. W.Frank. Radiat. Effects, 21, 119 (1974)
17. W.Frank. Inst. Phys. Conf. Ser. 23, 23 (1975)
18. J.C.Bourgoin and J.W.Corbett. Radiat. Effects 36, 157 (1978)
19. J.D.Weeks, J.C.Tully, and L.C.Kimerling. Phys. Rev. B 12, 3286 (1975)

20. L.C.Kimerling. Inst.Phys. Conf. Ser. 46, 56 (1979)
21. J.C.Bourgoin and J.W.Corbett. Phys.Lett.38A, 135, (1972)
22. M.Kiritani and H.Takata. J. Nuclear Materials 69/70 277 (1978)
23. J.Arimura and J.W.MacKay, in Radiation Effects in Semiconductors, edited by F.L.Vook, Plenum Press, New York 1968, p.204
24. J.Bourgoin and F.Mollot. Phys.Stat. Sol. (b) 43, 343 (1971)
25. J.R.Troxell, A.P.Chatterjee, G.D.Watkins, and L.C. Kimerling. Phys. Rev. B 19, 5336 (1979)
26. L.C.Kimerling and D.V.Lang. Inst. Phys. Conf. Ser. 23, 589 (1975)
27. U.Gösele and W.Frank, in these conference proceedings
28. W.D.Hyatt and J.S.Koehler. Phys.Rev. B4, 1903, (1971)
29. R.E.McKeighen and J.S.Koehler. Phys. Rev. B 4, 462 (1971)
30. Y.Adda, M.Beyeler, and G.Brebec, Thin Solid Films 25, 107 (1975)
31. R.Sizmann. J. Nuclear Materials 69/70 386 (1978)
32. W.M.Lomer. AERE, Harwell Report 1540 (1954)
33. G.J.Dienes and A.C.Damask. J. Appl. Phys. 29, 1713 (1958)
34. D.G.Nelson, J.F.Gibbons, and W.S.Johnson. Appl. Phys. Lett. 15, 246 (1969)
35. K.Gamo, K.Masuda, S.Namba, S.Ishihara, and I.Kimura. Appl.Phys. Lett. 17, 391 (1970)
36. S.Namba, K.Masuda, K.Gamo, A.Doi, S.Ishihara, and I.Kimura. Radiat. Effects 6, 115 (1970)
37. M.I.Guseva and A.N.Mansurova. Radiat. Effects 20, 207 (1973)
38. P.Baruch, J.Monnier, B.Blanchard, and C.Castaing. Appl. Phys. Lett. 26, 77 (1975)
39. P.Baruch. Inst. Phys. Conf. Ser. 31, 126 (1977)
40. P.R.Okamoto and L.E.Rehn. J. Nuclear Materials 83, 2 (1979)
41. U.Gösele and H.Strunk. Appl. Phys. 20, (1979), in press
42. F. Seitz. Acta Cryst. 3, 355 (1950)
43. W.Akutagawa, H.L.Dunlop, R.Hart, and O.J.Marsh. J.Appl.Phys.50,777,(1979)
44. R.E.Smallman. Modern Physical Metallurgy, Butterworths, London 1976, 3rd Edition, p.339
45. J.E.Harris. Acta Met. 26, 1033 (1978)
46. S.M.Hu. J. Appl. Phys. 45, 1567 (1977)
47. S.M.Hu. J. Vac. Science Technology 14, 17 (1977)
48. R.Francis and P.S.Dobson. J. Appl. Phys. 50, 280 (1979)

since the surfaces may act as V sources or I sinks, respectively.

A distinction between the Frank-Turnbull mechanism and the kick-out mechanism should be feasible in the following manner: Let gold diffuse into a boron-doped silicon wafer. Since the diffusivity of boron is known to be enhanced by supersaturation of self-interstitials (compare the emitter-push effect /53,55/) but can never be increased by an undersaturation of vacancies, the observation of a gold-induced enhancement of the boron diffusion in the centre of the wafer would be an unambiguous decision in favour of the kick-out mechanism. This prediction demonstrates the potential power of enhanced diffusion as a tool for investigating point defects and diffusion processes in semiconductors.

References

1. A.Seeger and K.P.Chik. Phys.Stat. Sol. 29, 455 (1968)
2. A.Seeger and H.Mehrer, in Vacancies and Interstitials in Metals edited by A.Seeger, D.Schumacher, W.Schilling, and J.Diehl. North-Holland, Amsterdam 1970, p.1
3. A.Seeger. J. Phys. F: Metal Physics 3, 248 (1973)
4. N.L.Peterson. J. Nuclear Materials 69/70, 3 (1978)
5. H.Mehrer. J. Nuclear Materials 69/70, 38 (1978)
6. A.Seeger, W.Frank, and U.Gösele. Inst. Phys. Conf. Ser. 46, 148 (1979)
7. A.Seeger. Radiat. Effects 9, 15 (1971)
8. A.Seeger, H.Föll, and W.Frank. Inst. Phys. Conf. Ser. 31, 12 (1977)
9. G.Hettich, H.Mehrer, and K.Maier. Inst. Phys. Conf. Ser. 46, 500 (1979)
10. J.M.Fairfield and B.J.Masters. J. Appl. Phys. 38, 3148 (1967)
11. U.Gösele, W.Frank, and A.Seeger. Inst. Phys. Conf. Ser. 46, 538 (1979)
12. B.J.Masters and E.F.Gorey. J. Appl. Phys. 49, 2717 (1978)
13. B.J.Masters. Inst.Phys.Conf.Series 46, 545 (1979)
14. K.Urban and A.Seeger. Phil.Mag. 30, 1395 (1974)
15. K.Dettmann, G.Leibfried, and K.Schroeder. Phys.Stat. Sol. 22, 423 (1967)
16. W.Frank. Radiat. Effects, 21, 119 (1974)
17. W.Frank. Inst. Phys. Conf. Ser. 23, 23 (1975)
18. J.C.Bourgoin and J.W.Corbett. Radiat. Effects 36, 157 (1978)
19. J.D.Weeks, J.C.Tully, and L.C.Kimerling. Phys. Rev. B 12, 3286 (1975)

20. L.C.Kimerling. Inst.Phys. Conf. Ser. 46, 56 (1979)
21. J.C.Bourgoin and J.W.Corbett. Phys.Lett.38A, 135, (1972)
22. M.Kiritani and H.Takata. J. Nuclear Materials 69/70 277 (1978)
23. J.Arimura and J.W.MacKay, in Radiation Effects in Semiconductors, edited by F.L.Vook, Plenum Press, New York 1968, p.204
24. J.Bourgoin and F.Mollot. Phys.Stat. Sol. (b) 43, 343 (1971)
25. J.R.Troxell, A.P.Chatterjee, G.D.Watkins, and L.C. Kimerling. Phys. Rev. B 19, 5336 (1979)
26. L.C.Kimerling and D.V.Lang. Inst. Phys. Conf. Ser. 23, 589 (1975)
27. U.Gösele and W.Frank. in these conference proceedings
28. W.D.Hyatt and J.S.Koehler. Phys.Rev. B4, 1903, (1971)
29. R.E.McKeighen and J.S.Koehler. Phys. Rev. B 4, 462 (1971)
30. Y.Adda, M.Beyeler, and G.Brebec. Thin Solid Films 25, 107 (1975)
31. R.Sizmann. J. Nuclear Materials 69/70 386 (1978)
32. W.M.Lomer. AERE, Harwell Report 1540 (1954)
33. G.J.Dienes and A.C.Damask. J. Appl. Phys. 29, 1713 (1958)
34. D.G.Nelson, J.F.Gibbons, and W.S.Johnson. Appl. Phys. Lett. 15, 246 (1969)
35. K.Gamo, K.Masuda, S.Namba, S.Ishihara, and I.Kimura. Appl.Phys. Lett. 17, 391 (1970)
36. S.Namba, K.Masuda, K.Gamo, A.Doi, S.Ishihara, and I.Kimura. Radiat. Effects 6, 115 (1970)
37. M.I.Gusava and A.N.Mansurova. Radiat. Effects 20, 207 (1973)
38. P.Baruch, J.Monnier, B.Blanchard, and C.Castaing. Appl. Phys. Lett. 26, 77 (1975)
39. P.Baruch. Inst. Phys. Conf. Ser. 31, 126 (1977)
40. P.R.Okamoto and L.E.Rehn. J. Nuclear Materials 83, 2 (1979)
41. U.Gösele and H.Strunk, Appl. Phys. 20, (1979), in press
42. F. Seitz. Acta Cryst. 3, 355 (1950)
43. W.Akutagawa, H.L.Dunlop, R.Hart, and O.J.Marsh. J.Appl.Phys.50,777,(1979)
44. R.E.Smallman. Modern Physical Metallurgy, Butterworths, London 1976, 3rd Edition, p.339
45. J.E.Harris. Acta Met. 26, 1033 (1978)
46. S.M.Hu. J. Appl. Phys. 45, 1567 (1977)
47. S.M.Hu. J. Vac. Science Technology 14, 17 (1977)
48. R.Francis and P.S.Dobson. J. Appl. Phys. 50, 280 (1979)

since the surfaces may act as V sources or I sinks, respectively.

A distinction between the Frank-Turnbull mechanism and the kick-out mechanism should be feasible in the following manner: Let gold diffuse into a boron-doped silicon wafer. Since the diffusivity of boron is known to be enhanced by supersaturation of self-interstitials (compare the emitter-push effect /53,55/) but can never be increased by an undersaturation of vacancies, the observation of a gold-induced enhancement of the boron diffusion in the centre of the wafer would be an unambiguous decision in favour of the kick-out mechanism. This prediction demonstrates the potential power of enhanced diffusion as a tool for investigating point defects and diffusion processes in semiconductors.

References

1. A.Seeger and K.P.Chik, Phys.Stat. Sol. 29, 455 (1968)
2. A.Seeger and H.Mehrer, in Vacancies and Interstitials in Metals edited by A.Seeger, D.Schumacher, W.Schilling, and J.Diehl, North-Holland, Amsterdam 1970, p.1
3. A.Seeger, J. Phys. F: Metal Physics 3, 248 (1973)
4. N.L.Peterson, J. Nuclear Materials 69/70, 3 (1978)
5. H.Mehrer, J. Nuclear Materials 69/70, 38 (1978)
6. A.Seeger, W.Frank, and U.Gösele, Inst. Phys. Conf. Ser. 46, 148 (1979)
7. A.Seeger, Radiat. Effects 9, 15 (1971)
8. A.Seeger, H.Föll, and W.Frank, Inst. Phys. Conf. Ser. 31, 12 (1977)
9. G.Hettich, H.Mehrer, and K.Maier, Inst. Phys. Conf. Ser. 46, 500 (1979)
10. J.M.Fairfield and B.J.Masters, J. Appl. Phys. 38, 3148 (1967)
11. U.Gösele, W.Frank, and A.Seeger, Inst. Phys. Conf. Ser. 46, 538 (1979)
12. B.J.Masters and E.F.Gorey, J. Appl. Phys. 49, 2717 (1978)
13. B.J.Masters, Inst.Phys.Conf.Series 46, 545 (1979)
14. K.Urban and A.Seeger, Phil.Mag. 30, 1395 (1974)
15. K.Dettmann, G.Leibfried, and K.Schroeder, Phys.Stat. Sol. 22, 423 (1967)
16. W.Frank, Radiat. Effects, 21, 119 (1974)
17. W.Frank, Inst. Phys. Conf. Ser. 23, 23 (1975)
18. J.C.Bourgoin and J.W.Corbett, Radiat. Effects 36, 157 (1978)
19. J.D.Weeks, J.C.Tully, and L.C.Kimerling, Phys. Rev. B 12, 3286 (1975)

20. L.C.Kimerling, Inst.Phys. Conf. Ser. 46, 56 (1979)
21. J.C.Bourgoin and J.W.Corbett, Phys.Lett.38A, 135, (1972)
22. M.Kiritani and H.Takata, J. Nuclear Materials 69/70 277 (1978)
23. J.Arimura and J.W.MacKay, in Radiation Effects in Semiconductors, edited by F.L.Vook, Plenum Press, New York 1968, p.204
24. J.Bourgoin and F.Mollot, Phys.Stat. Sol. (b) 43, 343 (1971)
25. J.R.Troxell, A.P.Chatterjee, G.D.Watkins, and L.C. Kimerling, Phys. Rev. B 19, 5336 (1979)
26. L.C.Kimerling and D.V.Lang, Inst. Phys. Conf. Ser. 23, 589 (1975)
27. U.Gösele and W.Frank, in these conference proceedings
28. W.D.Hyatt and J.S.Koehler, Phys.Rev. B4, 1903, (1971)
29. R.E.McKeighen and J.S.Koehler, Phys. Rev. B 4, 462 (1971)
30. Y.Adda, M.Beyeler, and G.Brebec, Thin Solid Films 25, 107 (1975)
31. R.Sizmann, J. Nuclear Materials 69/70 386 (1978)
32. W.M.Lomer, AERE, Harwell Report 1540 (1954)
33. G.J.Dienes and A.C.Damask, J. Appl. Phys. 29, 1713 (1958)
34. D.G.Nelson, J.F.Gibbons, and W.S.Johnson, Appl. Phys. Lett. 15, 246 (1969)
35. K.Gamo, K.Masuda, S.Namba, S.Ishihara, and I.Kimura, Appl.Phys. Lett. 17, 391 (1970)
36. S.Namba, K.Masuda, K.Gamo, A.Doi, S.Ishihara, and I.Kimura, Radiat. Effects 6, 115 (1970)
37. M.I.Guseva and A.N.Mansurova, Radiat. Effects 20, 207 (1973)
38. P.Baruch, J.Monnier, B.Blanchard, and C.Castaing, Appl. Phys. Lett. 26, 77 (1975)
39. P.Baruch, Inst. Phys. Conf. Ser. 31, 126 (1977)
40. P.R.Okamoto and L.E.Rehn, J. Nuclear Materials 83, 2 (1979)
41. U.Gösele and H.Strunk, Appl. Phys. 20, (1979), in press
42. F. Seitz, Acta Cryst. 3, 355 (1950)
43. W.Akutagawa, H.L.Dunlop, R.Hart, and O.J.Marsh, J.Appl.Phys.50,777,(1979)
44. R.E.Smallman, Modern Physical Metallurgy, Butterworths, London 1976, 3rd Edition, p.339
45. J.E.Harris, Acta Met. 26, 1033 (1978)
46. S.M.Hu, J. Appl. Phys. 45, 1567 (1977)
47. S.M.Hu, J. Vac. Science Technology 14, 17 (1977)
48. R.Francis and P.S.Dobson, J. Appl. Phys. 50, 280 (1979)

49. D.A.Antoniadis, A.M.Lin, and R.W.Dutton, J. Appl. Phys. 33, 1030 (1978)
50. A.Armigliato, M.Servidori, S.Solmi, and I.Vecchi, J.Appl. Phys. 48, 1806 (1977)
51. C.L.Claeys, G.J.Declerk, and R.J.van Overstraeten, in Semiconductor Characterization Techniques, P.A.Barnes and G.A.Rozgonyi, Electrochem. Soc., Princeton 1978, p.366
52. W.F.Tseng, S.S.Lau, and J.W.Mayer, Phys. Lett. 68A, 93 (1978)
53. H.Strunk, U.Gösele, and B.O.Kolbesen, Appl. Phys. Lett. 34, 530 (1979)
54. C.L.Claeys, G.J.Declerck, and R.J.van Overstraeten, Revue Physique Appliquée 13, 797 (1978)
55. A.F.W.Willoughby, J. Phys. D: Applied Physics 10, 455 (1977)
56. R.B.Fair and J.C.C.Tsai, J. Electrochem. Soc. 124, 1107 (1977)
57. S.Matsumoto, E.Arai, H.Nakamura, and T.Niimi, Jap. J. Appl. Phys, 16, 1177 (1977)
58. D.Lescronier, M.Gauneau, J.Paugam, G.Pelous, F.Richou, and P.Henoc, Appl. Phys. Lett. 34, 224 (1979)
59. W.R.Wilcox and T.J.LaChapelle, J. Appl. Phys. 35, 240 (1964)
60. F.C.Frank and D.Turnbull Phys. Rev. 104, 617 (1956)
61. W.Frank, U.Gösele, and A.Seeger, Inst. Phys. Conf. Ser. 46, 514 (1979)
62. M.J.Hill, M.Lietz, R.Sittig W.Frank, U.Gösele, and A.Seeger, In these conference proceedings.
63. W.C.Dash, J.Appl. Phys. 31, 2275 (1960)

(4)

Materials Science Forum 15-18, 369 (1987)

DIFFUSION MECHANISMS AND THERMAL-EQUILIBRIUM DEFECTS IN SILICON AND GERMANIUM

W. Frank[1] and N.A. Stolwijk[2]

[1]Max-Planck-Institut für Metallforschung, Institut für Physik,
and
Universität Stuttgart, Institut für Theoretische und Angewandte Physik,
P.O. Box 800 665, D-7000 Stuttgart 80, Fed. Rep. of Germany

[2]Universität Münster, Institut für Metallforschung,
Domagkstr. 75, D-4400 Münster, Fed. Rep. of Germany

ABSTRACT

After a review of the early developments in the understanding of self- and substitutional-solute diffusion in Si and Ge, the phenomena of enhanced and retarded substitutional-solute diffusion in Si as well as the interstitial–substitutional diffusion of Au or Pt in Si and of Cu in Ge are highlighted. The enhanced/retarded-diffusion studies lead to the *qualitative* conclusions that in Si self-interstitials and vacancies coexist under thermal-equilibrium conditions and that small Group-III atoms (e.g., B) mainly diffuse via self-interstitials whereas big Group-V atoms (e.g., Sb) prefer vacancies as diffusion vehicles. The interstitial–substitutional-diffusion studies show that Au or Pt in Si preferentially diffuses via the kick-out mechanism and that Cu in Ge undergoes dissociative diffusion. Furthermore, these investigations provide *quantitative* evidence that above about 1270 K Si self-diffusion predominantly takes place via an interstitialcy mechanism whereas self-diffusion in Ge occurs via vacancies in the entire temperature interval investigated.

1. INTRODUCTION AND EARLY DEVELOPMENTS

In Fig. 1 the self-diffusion in the elemental semiconductors Si, Ge, Se, and Te is compared with that in Cu, Ag, and Au [1]. It is seen that, compared with these metals, in both the cubic (Si, Ge) and the trigonal (Se, Te) semiconductors self-diffusion is a very slow process. This was already emphasized almost two decades ago by Seeger and Chik [2]. These authors also noticed that the ratio of the self-diffusivities in metals and semiconductors, which at the melting temperatures T_m amounts to several powers of ten, becomes even larger at lower normalized temperatures T/T_m. Hence, in the Arrhenius laws

$$D^T = D_0^T \exp(-H^{SD}/kT) \qquad (1)$$

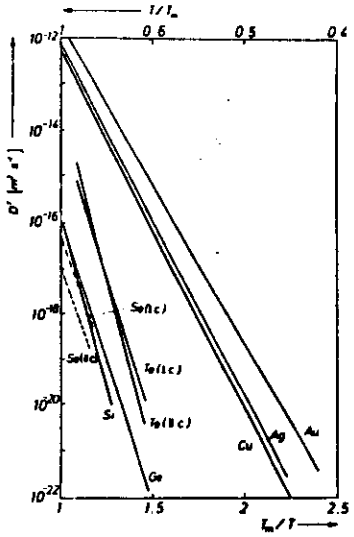

Fig. 1. Comparison between the self-diffusivities in the elemental semiconductors Si, Ge, Se, and Te and the metals Cu, Ag, and Au [1]. In the trigonal semiconductors Se and Te the diffusivities parallel and perpendicular to the c axis are different.

(k = Boltzmann's constant) obeyed by the tracer self-diffusion coefficients D^T of the elemental semiconductors in the temperature regimes investigated, both the pre-exponential factors D_o^T and the self-diffusion activation enthalpies H^{SD} are distinctly larger than in the case of Cu, Ag, or Au. In Ge and Si, to which in the present paper the discussion will be restricted, D_o^T exceeds 10^{-4} m^2s^{-1} — which may be taken as a D_o^T value characteristic of metals — by more than one and two to three orders of magnitude, respectively (Sect. 4).

Generally speaking, the origin of the differences between the diffusion in metals on the one hand and in Si and Ge on the other hand must be searched for in the difference between metallic and homopolar bonding. Here it will not be attempted to answer this fundamental question. Rather, as in the case of metals, we are interested "only" in whether self-diffusion in Si and Ge occurs *directly* (through an exchange of nearest-neighbour atoms or a ring mechanism) or *indirectly* (via a vacancy or an interstitialcy mechanism) [1]. The further discussion (in particular on the relation between interstitial–substitutional foreign-atom diffusion and self-diffusion in Sect. 4) will show unambiguously that for Si and Ge direct mechanisms may safely be excluded, in spite of the fact that very recently Pandey [3] has proposed a "novel concerted exchange mechanism for the diffusion in semiconductors".

In the case of metals monovacancies are the dominant intrinsic point defects under thermal-equilibrium conditions and provide the main contribution to self-diffusion [4-6]. (In some metals, in the vicinity of T_m divacancies [4-6] contribute to self-diffusion, and — according to recent investigations [7,8] — contributions by self-interstitials and/or direct mechanisms must not be excluded beforehand.) This has been demonstrated by separately determining the diffusivities D_V and the equilibrium concentrations C_V^{eq} of vacancies in metals as functions of temperature and showing that they account for the measured self-diffusivities, i.e., that they obey the relationship

$$D^T = D_V^T \equiv f_V D_V C_V^{eq} , \qquad (2)$$

where D_V^T and f_V are the contribution by monovacancies to D^T and the correlation factor for diffusion via monovacancies, respectively. The corresponding way is not practicable in the case of Si or Ge, since up to now none of the techniques successfully applied in the study of high-temperature defects in metals (thermal expansion, specific heat, positron annihilation, quenching from high temperatures) has yielded reliable results on point-defect equilibrium concentrations in semiconductors. It appears likely that the failure of these conventional techniques in the case of Si and Ge is due to extremely small equilibrium concentrations of vacancies and self-interstitials in these materials. The smallness of the self-diffusivities in Si and Ge may be a reflexion of this. Indeed there is indirect evidence, which will be discussed below, that in Si self-interstitials are the dominant thermal-equilibrium defect species, though their concentration C_I^{eq} at T_m is about 10^{-6} or smaller. A positive aspect of such small equilibrium concentrations of intrinsic defects is that contributions to the self-diffusion by multiple defects (e.g., divacancies) may be neglected.

Seeger and Chik [2] have realized early that an understanding of self-diffusion in Ge and Si has to be achieved in another way than in the case of metals. They included in their considerations the diffusion of substitutional Group-III and Group-V dopants as well as the dependence of both self-diffusion and dopant diffusion on the nature and concentration of the dopants, i.e. on the position of the Fermi level. They demonstrated that the enhancement of both self-diffusion and dopant diffusion in Ge by n doping and the opposite effects of p doping may be understood in terms of diffusion via an intrinsic defect species that possesses a shallow acceptor level in the lower half of the band gap. Since such a level had been predicted for the monovacancy [9], Seeger and Chik [2] concluded that self- and dopant diffusion in Ge occur via vacancies. No doubts have been raised on this interpretation until its recent confirmation, on which will be reported in Sect. 4.2.

In the case of Si the doping dependences of self- and dopant diffusion are by far more complicated than for Ge. For details the reader is referred to a recent review by Frank, Gösele, Mehrer, and Seeger [1]. Here it suffices to mention that Seeger and Chik [2] arrived at the conclusions (i) that in Si self-interstitials and vacancies coexist in thermal equilibrium, (ii) that Si self-diffusion is dominated by an interstitialcy mechanism or a vacancy mechanism above or below about 1270 K, respectively, and (iii) that in Si Group-III or Group-V elements preferentially diffuse via self-interstitials or vacancies, respectively. The main hypotheses on which this interpretation has been based are the acceptor nature of the vacancy [9] (see above) and Blount's model [10], according to which a self-interstitial introduces a donor level in the lower half of the band gap and an acceptor level in the upper half.

Various authors [11-13] formally accounted for the doping dependence of Si self-diffusion above 1270 K in terms of a monovacancy mechanism by arbitrarily endowing the vacancy with essentially the same electronic levels that Seeger and Chik [2] had attributed to the self-interstitial. Hence, experiments giving more specific information on the nature of the intrinsic defects involved in Si self-diffusion are of great importance. In this context the discussion on the nature of so-called A-type swirl defects found in dislocation-free Si single crystals grown by float-zone techniques at suitable rates played a significant role [14-17]. Using transmission electron microscopy it has been shown that the A swirls are interstitial-type dislocation loops [16,17]. Föll and co-workers [16,18] have suggested that A swirls are formed by clustering of the high-temperature equilibrium point defects that can neither reach the crystal surface nor disappear at grown-in dislocations during the cooling of the crystals and that therefore it is very likely that the thermal-equilibrium defects dominating in Si at high temperatures are self-interstitials. From the concentration of self-interstitials "precipitated" in swirl defects, the self-interstitial concentration in Si at T_m was estimated as $2 \times 10^{-8} \leq C_I^{eq} \leq 2 \times 10^{-6}$ [19,20]. In spite of the rapid progress made in the understanding of diffusion in Si and Ge during the last

years (Sects. 2 to 4) this scarce information on equilibrium defect concentrations has not been improved. In retrospect two desperate attempts to explain the generation or nature of A swirls in a way that avoids the conclusion that the dominant high-temperature equilibrium defect species in Si is the self-interstitial appear worth mentioning. Petroff and de Kock [21] argued that A swirls may be created by freezing in a non-equilibrium concentration of self-interstitials, whereas van Vechten [22] postulated that the thermal-equilibrium defects in Si are exclusively vacancies and that the A swirls are agglomerates of vacancies of a fancy structure which makes them look like interstitial-type dislocation loops in the electron microscope. In the meantime the controversial views of swirl-type defects have ceased to be significant in the discussion of the self-diffusion mechanisms in Si, since recent experiments (Sects. 3 and 4) have clarified this question in favour of the proposal by Seeger and Chik [2] (see above).

The observation previously made in self-diffusion studies that in Ge and Si the pre-exponential factors D_0^T of the self-diffusion coefficients are considerably larger than in metals [1] has been confirmed recently by another type of experiments (Sects. 3 and 4) and therefore deserves to be briefly considered here. Seeger and Chik [2] have proposed that this phenomenon reflects high self-diffusion entropies in Ge and Si, which they explained in terms of a spreading out of vacancies and self-interstitials, respectively, at high temperatures. A spread-out vacancy in Ge may be visualized as a region of, say, 5 atomic volumes having a lower density than perfect crystalline Ge and thus resembling the amorphous state. Such an extended defect corresponds to a larger number of microstates and may perform diffusional jumps via more paths than a "point" defect, i.e., it possesses larger entropies of formation and migration. The spreading out of a self-interstitial in Si leads not only to an increase of its formation and migration entropies but to a decrease of its formation enthalpy, too. The cause of this is the anomalous, pronounced density increase of Si when it melts. The compressive strains around a "point"-like Si self-interstitial and thus its formation enthalpy may be diminished by local "melting". So a spread-out self-interstitial in Si corresponds to a quasi-liquid droplet whose density is larger than that of crystalline Si. An atomistic model of the gradual transition of Si self-interstitials from "point" defects at low temperatures to spread-out configurations at high temperatures has been presented elsewhere [23].

The break-through in the understanding of self-diffusion in Si and Ge has been achieved by proceeding further in the direction in which the first steps had been done by Seeger and Chik [2], namely by intensifying the interest in studies of foreign-atom diffusion. It is clear that in this respect investigations of atoms diffusing via a direct interstitial mechanism (e.g., O, Cu, or Li in Si) are useless, whereas the diffusion of substitutional Group-III or Group-V elements that use intrinsic point defects as diffusion vehicles can yield valuable information. In effect, the coexistence of self-interstitials and vacancies in Si in thermal equilibrium has been convincingly demonstrated by means of substitutional-dopant diffusion experiments (Sect. 2). However, a final decision which self-diffusion mechanisms operate in Si and Ge as well as an indirect, quantitative determination of self-diffusion coefficients have become possible through diffusion studies of amphoteric foreign atoms (Au or Pt in Si and Cu in Ge) which, during their diffusion, interchange between substitutional and interstitial sites with the aid of intrinsic point defects (Sect. 3).

2. ENHANCED AND RETARDED DIFFUSION OF SUBSTITUTIONAL SOLUTES IN SILICON

2.1. The emitter-push effect

Diffusion of Group-III and Group-V elements in Si shows several striking features which have been termed "anomalous". The essence of these phenomena, which were recently reviewed by Frank et al. [1], will be demonstrated for the so-called emitter-push effect.

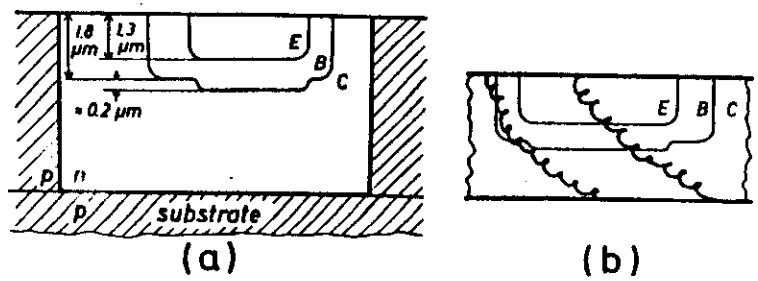

Fig. 2. Schematic illustration of the emitter-push effect in a bipolar transistor. (a) Specimen consisting of the emitter E, the base B, and part of the collector C. (b) Helical dislocations formed by climb of the edge components of dislocations originally being almost purely screw-type.

In the industrial production of bipolar transistors (Fig. 2a) the transistor base is generated by the in-diffusion of a Group-III element, say, B, in a first diffusion anneal. In a second step the emitter is produced by diffusing a Group-V element, usually P, into a part of the region pre-diffused by B. In this second diffusion anneal, below the part of the specimen surface through which the in-diffusion of P takes place, the diffusion of B is enhanced, i.e., the emitter diffusion seems to push the base-diffusion front ahead.

The interpretation of the emitter-push effect is straightforward. Due to the high P concentration on the specimen surface in the second diffusion anneal, a supersaturation of intrinsic point defects is produced. Potential mechanisms via which such a P-induced self-defect injection may occur have been discussed elsewhere [1]. In addition to the thermal-equilibrium defects, these injected defects act as diffusion vehicles for the B and thus enhance the B diffusivity.

The remaining question is whether the P-injected self-defects are vacancies or self-interstitials. The answer has been given by Strunk et al. [24], who found by means of transmission electron microscopy that isolated screw dislocations piercing the emitter–base region wind up to helices during the emitter-diffusion treatment in a manner that indicates dislocation climb by absorption of self-interstitials and/or emission of vacancies (Fig. 2b). This implies that the intrinsic defects injected by P diffusion are self-interstitials. It follows further that a supersaturation of self-interstitials enhances the diffusivity of B. However, these observations alone do not allow us to decide whether in *thermal equilibrium* B diffuses via self-interstitials and/or vacancies.

2.2. Injection of self-interstitials by surface oxidation or oxynitridation, injection of vacancies by surface nitridation

In 1966 Booker and Tunstall [25] and Jaccodine and Drum [26] discovered that surface oxidation of Si may lead to the nucleation and growth of interstitial-type dislocation loops on {111} planes. Hu [27] was the first who realized that under the same oxidation conditions the diffusivity of B is enhanced. He concluded that diffusion enhancement requires a supersaturation of intrinsic defects and that therefore the oxidation-induced growth of interstitial loops is due to self-interstitial injection into the Si bulk from the oxidized surface. Obviously, this result is in accordance with the conclusion drawn from the emitter-push effect that a supersaturation of self-interstitials enhances the B diffusion (Sect. 2.1). Whereas the detailed mechanism of the oxidation-induced injection of self-interstitials is controversial, there is agreement upon the fact that it is driven by the large volume increase of about 125% taking place at the SiO_2–Si interface when new SiO_2 material is formed by the diffusion of oxygen from the gas phase through the SiO_2 surface layer [1].

The further development in the field of enhanced and retarded substitutional-solute diffusion has been summarized up to 1983 by Frank et al. [1] and henceforth by Fahey and Dutton [28]. The latter, who have contributed much in order to elucidate these phenomena, report that the nitridation of an already oxidized Si surface — so-called oxynitridation — also injects Si self-interstitials into the Si bulk, as indicated by the growth of interstitial loops and the simultaneous enhancement of the diffusion of B or P. More important, however, is another discovery: During direct surface nitridation the diffusion of B or P is retarded, and concomitantly interstitial-type dislocation loops shrink. Since from the emitter-push effect and from surface-oxynitridation studies it is known that a supersaturation of self-interstitials enhances the diffusivities of B and P (see above), it follows that *under thermal-equilibrium conditions* these dopants diffuse preferentially via self-interstitials and that surface nitridation reduces the self-interstitial equilibrium concentration via either the injection of vacancies or the extraction of self-interstitials. A decision between the two possibilities is brought about by the observation that surface nitridation enhances the diffusivity of Sb. This is understandable only if surface nitridation injects vacancies. The picture is rounded off by the fact that surface oxidation enhances the diffusivity of Sb in its early stage but later retards it. Remembering that under surface oxidation a supersaturation of self-interstitials exists, these findings lead to the following conclusions: Whereas the transitory Sb-diffusion enhancement shows that Sb can diffuse via self-interstitials, too, if these are offered in a sufficiently high supersaturation, the final Sb-diffusion retardation indicates that continuous injection of self-interstitials generates a steady state in which a vacancy undersaturation coexists with a self-interstitial supersaturation and that, in contrast to B or P, Sb prefers the diffusion via vacancies. It should be noted that this interpretation implies that *under thermal-equilibrium conditions* Sb preferentially diffuses via vacancies.

Further results of enhanced- or retarded-diffusion studies (for references see [1] and [28]), particularly such concerning the diffusion of *other* substitutional solutes, will be incorporated in the following conclusions.

2.3. Conclusions

The observations reported in Sects. 2.1 and 2.2 show that in Si self-interstitials and vacancies coexist under thermal-equilibrium conditions. Moreover, there is evidence that self-interstitial or vacancy injection does not influence the concentrations C_X (X = I or V) of self-interstitials (I) or vacancies (V) *independently* [28]. Rather in any steady state of self-defect injection C_I and C_V appear to be coupled according to

$$C_I C_V = C_I^{eq} C_V^{eq} \quad , \tag{3}$$

where $C_I^{eq} C_V^{eq}$ is a constant at a given temperature [1]. An example is the influence of surface oxidation on the diffusivity of Sb (Sect. 2.2). Immediately after the onset of oxidation C_I is enhanced above its equilibrium value C_I^{eq} by self-interstitial injection, whereas C_V is not yet affected (i.e., $C_V = C_V^{eq}$). As a result, the diffusion of Sb is enhanced by an additional interstitialcy-diffusion component, though Sb prefers to diffuse via vacancies. After long-time oxidation a steady state according to (3) has been established (i.e., $C_I > C_I^{eq}$ and $C_V < C_V^{eq}$), and — since Sb preferentially diffuses via vacancies — the diffusion of Sb has slowed down.

Thermodynamics tells us that in thermal equilibrium $C_I = C_I^{eq}$ and $C_V = C_V^{eq}$, where C_I^{eq} and C_V^{eq} are *independent* constants at given values of temperature and pressure. A coupling of these quantities via (3) may therefore be considered as a manifestation of the mass-action law of the reactions

$$I + V \rightleftarrows 0 \ , \tag{4}$$

i.e., the mutual recombination of self-interstitials and vacancies and the spontaneous generation of Frenkel pairs. Hence, from the existence of the relationship (3) Frank et al. [1] have concluded that under self-defect injection in the dislocation-free Si bulk a global steady state cannot be attained, but the local dynamical equilibrium (3) can be established via the reactions (4). The occurrence of the reactions (4) in dislocation-free Si has been proposed previouly by Prussin [29] and Sirtl [30].

Concerning the mechanisms of substitutional-dopant diffusion in Si the investigations discussed in Sect. 2.2 have shown that both diffusion via vacancies (Fig. 3) and interstitialcy diffusion (Fig. 4) occur. As discussed in more detail in [1], smallness and Group-III membership of a solute atom favour its interstitialcy-diffusion component, whereas fatness and Group-V membership are advantageous for diffusion via vacancies (Fig. 5). This empirical rule reflects the elastic and the Coulomb interactions between the solutes and the intrinsic point defects acting as diffusion vehicles [1,2]. Among the three solutes considered above the Group-III B atom, which is distinctly smaller than a Si matrix atom, and the relatively fat Group-V Sb atom represent extremes, which follow the above rule. In the case of P the elastic attraction to self-interstitials appears to be stronger than the Coulomb attraction to vacancies, so that P preferentially diffuses via self-interstitials though it belongs to Group V.

The information on the mechanisms of Si self-diffusion extractable from the investigations of enhanced and retarded diffusion of substitutional solutes is scarce and merely qualitative: Both vacancies and self-interstitials are present and mobile in thermal equilibrium, and hence both must contribute to self-diffusion. As already announced in Sect. 1, *quantitative* information on the relative contributions of these mechanisms to Si self-diffusion and on the self-diffusion mechanism in Ge has been obtained from diffusion studies of foreign atoms that can occupy both substitutional and interstitial sites. This will be the subject of the remainder of the present paper.

3. INTERSTITIAL—SUBSTITUTIONAL DIFFUSION OF AMPHOTERIC TRANSITION-METAL SOLUTES

3.1. Indication of the amphoteric nature of Au and Pt in Si

In Fig. 6 Arrhenius plots of the diffusivities in Si single crystals have been put together for a number of elements. There is a large gap of many orders of magnitude between the diffusivities of the so-called fast diffusors Cu, Ni, Li, and Fe and of the slow diffusing self-atoms and elements of Groups III to V. This gap is due to the facts (α) that the fast diffusors migrate via *direct* interstitial mechanisms whereas the slow diffusors undergo *indirect* diffusion via self-interstitials and/or vacancies and (β) that the diffusivity of an *indirectly* diffusing atom is; roughly speaking, C_X^{eq} (X = I or V) times smaller than it would be if it diffused via a *direct* interstitial mechanism with the diffusivity of the diffusion vehicles. Remembering the estimates $2 \times 10^{-8} \leq C_I^{eq}(T_m) \leq 2 \times 10^{-6}$

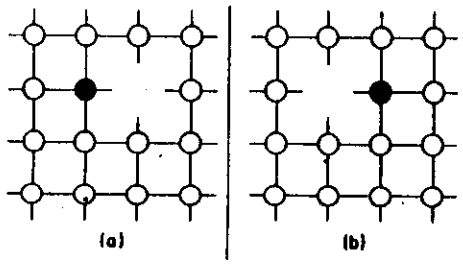

Fig. 3. Vacancy mechanism. The radioactive self-atom in tracer self-diffusion or foreign atom in substitutional-solute diffusion (full circle) moves, by jumping into the vacancy on its right-hand side (a), to the right (b) by one nearest-neighbour distance of the regular lattice atoms.

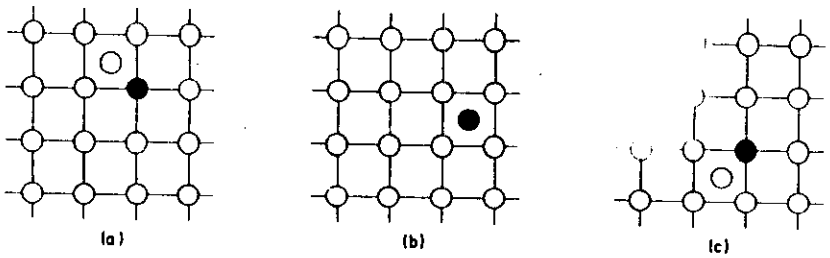

Fig. 4. Interstitialcy mechanism. In (a) a self-interstitial (open circle in the centre of a cell) has approached a self- or substitutional-foreign tracer atom (full circle). In the saddle-point configuration (b) the tracer atom has temporarily become an interstitial. In (c) the tracer atom has re-occupied a regular site by kicking a self-atom into an interstice.

and $C_V^{eq}(T_m) < C_I^{eq}/(T_m)$ (Sect. 1) one realizes that indeed the observed diffusivity gap is compatible with this interpretation. Further evidence for this is the weaker temperature dependence of the diffusivities of the fast diffusors in comparison with that of the slow diffusors. Whereas in direct diffusion the temperature dependence of the diffusivity is determined by the migration enthalpy of the interstitial diffusors, in indirect diffusion the corresponding role is played by the *sum* of the formation and migration enthalpy of the diffusion vehicles.

From the large difference between the diffusivities of directly and indirectly diffusing elements the minor diffusivity differences *within* these two groups have to be distinguished. It is clear that differences in the electronic structure and atomic size may account for the diffusivity differences among the fast interstitial diffusors. In the case of the slow indirect diffusors it is not surprising that the diffusivity of the isoelectronic Ge is very similar to Si self-diffusion. The fact that the diffusivities of the Group-III dopants and P — i.e. the elements diffusing mainly via self-interstitials — are higher than those of the vacancy-preferring Group-V elements reflects that above 1270 K, where such data exist, $D_I C_I^{eq} > D_V C_V^{eq}$, as will be shown in Sect. 4.1 (D_I = diffusivity of self-interstitials). However, since in spite of this the diffusivities of the vacancy-preferring Group-V elements — including Sb whose interstitialcy-diffusion component is very small (Fig. 5) — are still higher than the Si self-diffusivity , $D_V C_V^{eq}$ cannot be *extremely* small in comparison with $D_I C_I^{eq}$. Otherwise the Group-V-element–vacancy attraction could not overcompensate the disadvantage for vacancy diffusors arising from $D_V C_V^{eq} < D_I C_I^{eq}$.

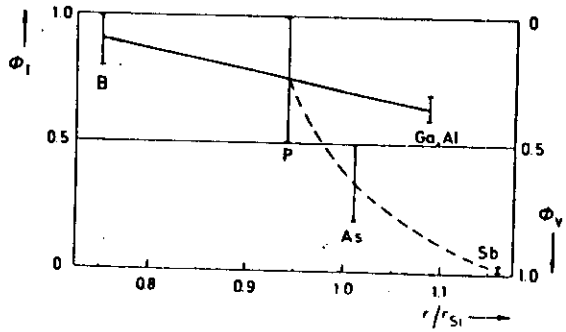

Fig. 5. Fractional contributions Φ_I and Φ_V to the diffusivities of substitutional solutes in Si by the interstitialcy and the vacancy mechanisms, respectively, versus the atomic radii r of the solutes in units of the atomic radius r_{Si} of Si [1].

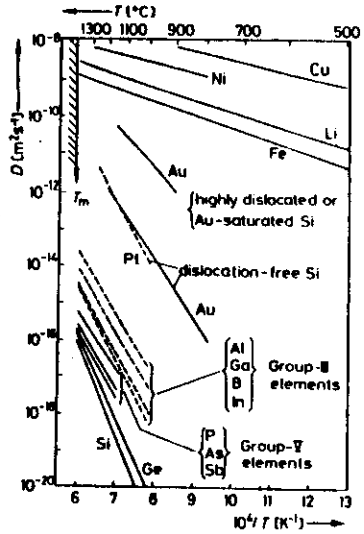

Fig. 6. Survey of the diffusivities of self- and foreign atoms in Si. For references see [1] and, particularly for the diffusivities of Au and Pt, Sect. 3.3.

As seen in Fig. 6, the diffusivities of Au and Pt in Si lie just in the gap between the fast and the slow diffusors. Hence, it is tempting to speculate that these elements might be "somehow intermediate". Extensive diffusion and solubility studies have confirmed this view (Sect. 3.3). They have shown that in silicon Au and Pt are capable of occupying both substitutional and interstitial sites. Though the interstitial solubilities C_I^{eq} of these elements are considerably smaller than their substitutional solubilities C_s^{eq}, their long-range transport occurs almost exclusively via direct interstitial diffusion since their interstitial diffusivities D_I are distinctly larger than their substitutional diffusivities D_s. Cu in Ge, which is a third example of an amphoteric solute in an elemental semiconductor, possesses the same properties (Sect. 3.4).

3.2. Mechanisms of interstitial–substitutional diffusion

During diffusion an amphoteric solute A interchanges between interstitial (A_i) and substitutional sites (A_s). These interchanges require the cooperation of either vacancies according to the *dissociative mechanism* [31]

$$A_i + V \rightleftarrows A_s \tag{5}$$

or self-interstitials according to the *kick-out mechanism* [32]

$$A_i \rightleftarrows A_s + I \,. \tag{6}$$

The two mechanisms are illustrated in Figs. 7a and 7b, respectively.

In a combined theoretical and experimental effort by the present authors and their collaborators (see Acknowledgements) it has been demonstrated that, in agreement with Frank and Turnbull's 30-year-old proposal [31], the diffusion of Cu in Ge involves the

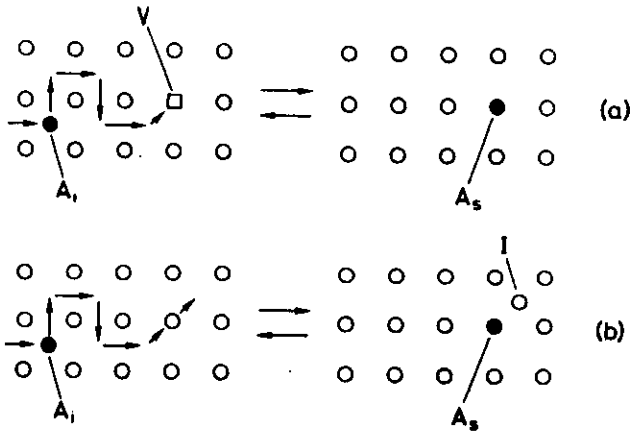

Fig. 7. Mechanisms of interstitial–substitutional diffusion. The foreign atom (full circle) interchanges between interstitial sites, A_i, and substitutional sites, A_s, by either (a) the dissociative mechanism [31] via vacancies, V, or (b) the kick-out mechanism [32] via self-interstitials, I.

dissociative mechanism and that, by contrast, the diffusion of Au or Pt in Si is dominated by the kick-out mechanism. Here the major issues which have led to these conclusions will be summarized. In the following we first will present characteristic predictions of the theories of dissociative and kick-out diffusion, which in Sects. 3.3 and 3.4 will be compared to diffusivity data of Au or Pt in Si and Cu in Ge, respectively. The bearing on self-diffusion in Si and Ge will be discussed in Sect. 4.

The effective diffusion of the substitutional component A_s of an amphoteric solute A in *highly* dislocated or dislocation-*free* specimens may be described by the diffusion equation

$$\partial C_s/\partial t = (\partial/\partial x)(D_s^{\mathrm{eff}}\partial C_s/\partial x) \ , \tag{7}$$

where C_s, x, and t are the concentration of A_s, the space coordinate in the diffusion direction considered, and the time of diffusion, respectively [1,32]. Eq. (7) is valid, irrespective of whether the diffusion occurs via the dissociative or the kick-out mechanism. For *intermediate* dislocation densities, (7) has to be extended by an additional term, which is different for dissociative and kick-out diffusion [1,32]. Theoretical treatments of these intermediate-dislocation-density cases have been given in [33] and [34], respectively.

In the *high-dislocation-density case* the effective diffusion coefficient D_s^{eff} in (7) is the same for dissociative and kick-out diffusion [1,32],

$$D_s^{\mathrm{eff}} \equiv \widetilde{D}_i \equiv D_i C_i^{eq}/C_s^{eq} \ , \tag{8}$$

i. e., a discrimination between these mechanisms by means of studies of amphoteric-solute diffusion in highly dislocated specimens is not possible. In such specimens in the case of the dissociative mechanism (kick-out mechanism) the vacancies (excess self-interstitials) consumed (produced) by the transformation of the A_i atoms to A_s atoms via the reaction (5) (reaction (6)) are immediately replaced (eliminated) by vacancy emission from (self-interstitial absorption at) dislocations. Thus the influx $D_i C_i^{eq}$ of A_i from the

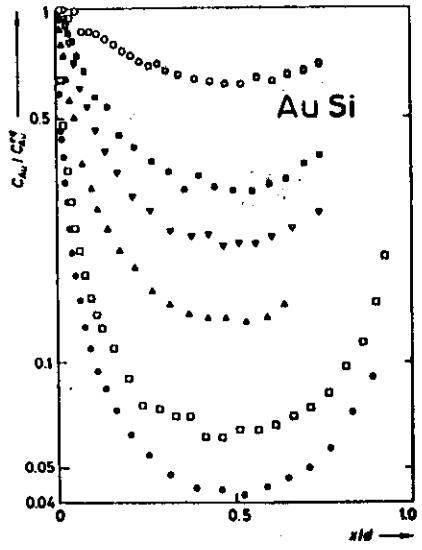

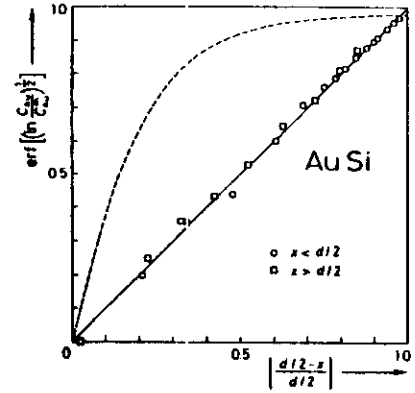

Fig. 8 (left). Penetration profiles of Au in dislocation-free Si wafers measured by means of NAA after annealing at 1273 K for 0.467 h (full circles), 1.03 h (empty squares), 4.27 h (full and empty triangles), 26.8 h (full squares), and 100.6 h (empty circles), respectively [35]. The Au concentration C_{Au} is given in units of the solubility limit C_{Au}^{eq}. In one of the 4.27 h anneals (open triangles) a 300 μm-thick wafer was used; otherwise the wafer thickness was d = 500 μm.
Fig. 9 (right). Au-diffusion profile measured by NAA on a 500 μm-thick, dislocation-free Si wafer after a 1.03 h anneal at 1273 K (empty symbols) [35] compared with the predictions of the kick-out model (solid straight line according to (11)) and the dissociative model (dashed curve according to (7) in [36]).

specimen surface controls the effective influx $D_s^{\mathrm{eff}}C_s^{eq}$ of A_s. This is expressed by (8).

In *dislocation-free specimens* the effective diffusion coefficient D_s^{eff} is different for dissociative and kick-out diffusion [1,32]. In the case of *dissociative diffusion* [1,31,32] the effective influx $D_s^{\mathrm{eff}}C_s^{eq}$ of A_s is controlled by the influx $D_V C_V^{eq}$ of vacancies from the surface, so that

$$D_s^{\mathrm{eff}} \equiv \widetilde{D}_V \equiv D_V C_V^{eq}/C_s^{eq} \ . \tag{9}$$

By contrast, in *kick-out diffusion*, due to the very nature of this mechanism, each regular lattice site which is occupied by a self-atom represents a potential A_s site. Therefore, as long as the specimen is "A_s-empty" ($C_s/C_s^{eq} \ll 1$) the effective influx of A_s is "unlimited" (or, more precisely, limited by the very rapid influx of A_i only), whereas in a specimen "filled up with A_s" ($C_s/C_s^{eq} = 1$) the outflux $D_I C_I^{eq}$ to the surface of the self-interstitials produced via the kick-out reaction (6) controls the effective in-diffusion of A_s. These unique features of kick-out diffusion in a dislocation-free specimen are reflected in the expression for the corresponding effective diffusion coefficient [1,32],

$$D_s^{\mathrm{eff}} \equiv \widetilde{D}_I(C_s^{eq}/C_s)^3 \equiv (D_I C_I^{eq}/C_s^{eq})\ (C_s^{eq}/C_s)^2 . \tag{10}$$

Hence, this effective diffusion coefficient depends on x and t via C_s, in contrast to what

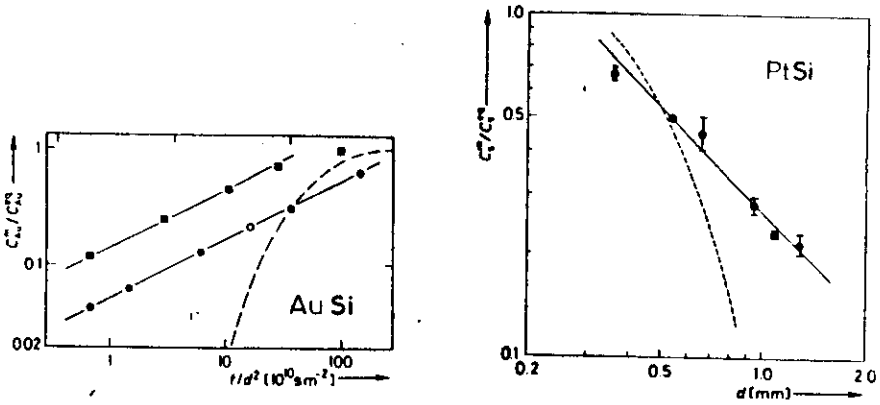

Fig. 10 (left). Increase of the Au concentration C_{Au}^m in the centres of dislocation-free Si wafers as a function of t/d^2 (full circles: 1273 K, d = 500 μm; empty circle: 1273 K, d = 300 μm; full squares: 1371 K, d = 500 μm) [35].
Fig. 11 (right). C_s^m measured by SRT on dislocation-free Si wafers after 3.5 h Pt-diffusion anneals at 1423 K as a function of the wafer thickness d (full circles) [43] compared with the predictions of the kick-out model (solid straight line according to (12)) and the dissociative model (dashed curve according to (7) in [36]).

is true for the diffusion coefficient of either dissociative or kick-out diffusion in highly dislocated specimens or dissociative diffusion in dislocation-free specimens.

A *qualitative* feature which dissociative and kick-out diffusion in dislocation-free specimens have in common is the U shape of the diffusion profiles in wafers. This is caused by the fact that – after a short initial transition during which the A_i concentration C_i reaches its limit C_i^{eq} ($\ll C_s^{eq}$) throughout the wafer – C_s approaches C_s^{eq} most rapidly in the vicinity of the two wafer surfaces, since these constitute the only sources of the vacancies that are necessary for an increase of C_s via (5) or the only sinks for the self-interstitials that have to be eliminated for an increase of C_s via (6), respectively. Fig. 8 demonstrates the U shape of Au-diffusion profiles in dislocation-free Si wafers [35].

The *discrimination* between dissociative and kick-out diffusion requires *quantitative* analyses of diffusion profiles in *dislocation-free* specimens. In the case of the *dissociative diffusion*, in which the effective diffusion coefficient $\tilde{D}_V$ in a dislocation-free medium is independent of x and t, the solution of (7) for a "thick" specimen (eq. (5) in [36]), which is mathematically modelled by the in-diffusion from the surface into a semi-infinite solid, or a wafer of thickness d (eq. (7) in [36]) may be found in standard textbooks on diffusion or conduction of heat [37,38]. (A plate-shaped specimen, as usually used in diffusion studies, is denoted as a "thick" specimen if – *under the diffusion conditions applied* – the two parts of the diffusion profile that arise from atoms penetrating from the opposite surfaces do *not* overlap. Otherwise the specimen is called a wafer or a "thin" specimen.) By contrast, as a result of the C_s dependence of D_s^{eff} according to (10), the quantitative predictions for *kick-out diffusion* in dislocation-free crystals are quite unusual. E.g., as long as C_s does not come very close to C_s^{eq}, kick-out in-diffusion profiles in a dislocation-free wafer may be described by the relationship [32,35]

$$\operatorname{erf}\left[\ln(C_s/C_s^m)^{1/2}\right] = \left|\frac{d/2 - x}{d/2}\right| , \qquad (11)$$

where C_s^m is the value of C_s in the wafer centre $x = d/2$. Since (11) must hold for any temperature and duration of diffusion, its comparison with diffusion profiles found by experiment may serve as a crucial test for kick-out diffusion. Further tests may be based on the prediction [32]

$$C_s^m/C_s^{eq} = (2/d)\,(\pi\tilde{D}_I t)^{1/2} , \qquad (12)$$

which relates the A_s concentration in the centre of a wafer to the diffusion time and the wafer thickness, and on comparisons of diffusion profiles observed in "thick" specimens with the expression predicted for kick-out diffusion profiles in dislocation-free semi-infinite media (eq. (43) in [39]).

3.3. Measurements of the diffusion of gold or platinum in silicon

The diffusion studies of both Au and Pt in Si to be reported in this section have been performed by means of the neutron-activation analysis (NAA) [35,40,41] or the spreading-resistance technique (SRT) [41,42]. (In our investigations of Ge in Cu (Sect. 3.4) SRT [36] has been used.) The two methods are complementary in the sense that the SRT exclusively measures the concentration C_s of the electrically active A_s configuration, whereas the NAA yields the total concentration of the amphoteric solute A, i.e. $C_s + C_i + C_c$, where C_c is the concentration of A contained in clusters. The fact that in all cases to be discussed here identical results have been obtained by both techniques may be taken as evidence that, in agreement with the statement $C_i^{eq} \ll C_s^{eq}$ in Sect. 3.1, C_i is undetectibly small in comparison with C_s and that clustering of A is negligible. Therefore, in the following the theoretical expressions involving C_s (e.g., eqs. (11) and (12) in Sect. 3.2) may be compared to both the NAA and the SRT data.

Fig. 9 is a replot from Fig. 8 of the diffusion profile of Au in a 500 μm-thick, dislocation-free Si wafer measured by NAA after a 1.03 h diffusion anneal at 1273 K [35]. It is seen that the data (open symbols) follow closely the solid straight line expected for kick-out diffusion according to (11). The dashed curve represents an obviously unsuccessful attempt of adjusting the theoretical $C_s(x)$ expression for dissociative diffusion in a dislocation-free wafer (eq. (7) in [36]) to the experimental data.

Fig. 10 is a demonstration that, in accordance with the kick-out diffusion theory [eq. (12)], the Au concentration in the centres of dislocation-free Si wafers, C_{Au}^m, increases proportional to the square root of the diffusion time. In fact, in this double-logarithmic $C_{Au}^m - t/d^2$ plot the C_{Au}^m values measured at the same temperature (circles at 1273 K, squares at 1371 K)[35] lie on the same straight line with the slope 1/2. Since the data taken after 1273 K diffusion anneals comprise measurements on wafers of different thicknesses, the arrangement of these data along a straight line with the slope 1/2 also confirms the $1/d$ dependence of C_s^m predicted by (12) for kick-out diffusion. The failure of the theory of dissociative diffusion (dashed curve according to (7) in [36]) to describe the experimental data is evident.

Fig. 11 presents comparisons of the Pt concentrations C_s^m (full circles) measured by the SRT on dislocation-free Si wafers of various thicknesses after 3.5 h diffusion anneals at 1423 K [43] with the d dependences of C_s^m predicted by the kick-out-diffusion theory (solid line according to (12)) and the dissociative-diffusion theory (dashed curve according to (7) in [36]), respectively. In Fig. 12 the diffusion profile of Pt in a "thick" Si specimen determined with the aid of NAA [43] is compared to the two interstitial–substitutional diffusion theories. From Figs. 11 and 12 it is clear that Pt in Si diffuses via the kick-out mechanism.

The precedingly compiled evidence for the predominance of the kick-out mechanism in the diffusion of both Au and Pt in Si does not exclude a minor contribution by the dissociative mechanism. Such a contribution may be expected, since investigations of the enhanced and retarded substitutional-solute diffusion in Si (Sect. 2) have shown that in Si under thermal-equilibrium conditions self-interstitials and vacancies coexist. In fact,

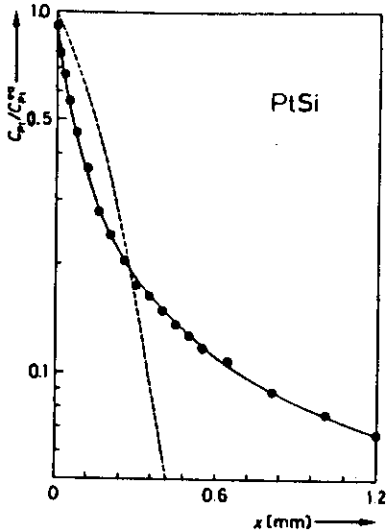

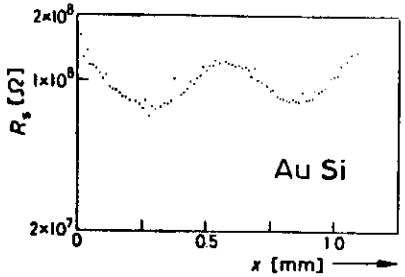

Fig. 12 (left). Pt-diffusion profile measured by NAA on a 4.9 mm-thick, dislocation-free Si specimen after a 0.5 h anneal at 1523 K (full circles) [43] compared with the predictions of the kick-out model (solid curve according to (43) in [39]) and the dissociative model (dashed curve according to (5) in [36]).
Fig. 13 (right). W-shaped spreading-resistance (R_s) Au-diffusion profile measured on a 900 μm-thick, dislocation-free Si wafer after a 0.75 h anneal at 1473 K [41].

Morehead and co-workers [44], who carefully analysed Au-diffusion profiles in dislocation-free Si wafers diffusion-annealed at 1273 K, have found that there is a contribution by the dissociative mechanism to the diffusion of Au in Si. It is almost undetectibly small after short annealing times (t = 0.5 h) but becomes clearly "visible" after long-time annealing (t = 100 h). This is so since, according to (9) and (10), even for $D_V C_V^{eq} = D_I C_I^{eq}$ – which Morehead et al. [44] have estimated for 1273 K from their analysis – kick-out diffusion dominates for $C_s < C_s^{eq}$ and approaches the value of the t-independent contribution by the dissociative mechanism when C_s comes close to C_s^{eq}.

There are several observations which are *in accordance with* the view that Au in Si diffuses mainly via the kick-out mechanism but, in contrast to the Au (or Pt) diffusion profiles in dislocation-free Si discussed above, can *not* be used *to exclude* a major contribution by the dissociative mechanism. Among these findings is the fact (Fig. 6) that in highly dislocated [42] or in dislocation-free, Au-saturated [45] Si the diffusivity of Au is the same, but by one to two powers of ten higher than in the (above considered) dislocation-free Si not saturated with Au. The difference between the Au diffusivities in non-saturated, dislocation-free specimens and highly dislocated specimens is expected, since – according to the discussion in Sect. 3.2 – in the first case the effective diffusivity (10) is limited by the outflux of self-interstitials produced via (6) to the specimen surfaces whereas in the second case, in which self-interstitials can be readily absorbed at dislocations, the effective diffusivity (8) is determined by the A_I influx. In Au-saturated specimens the net rate at which self-interstitials are produced via (6) is equal to zero, so that – like in highly dislocated specimens – the effective diffusivity is controlled by the A_I influx and thus given by (8).

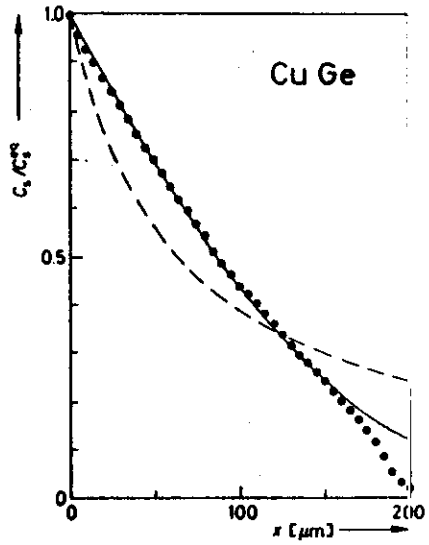

Fig. 14. Cu-diffusion profile measured by SRT on a "thick", dislocation-free Ge specimen after a 1 h anneal at 951 K (full circles) [50] compared with the dissociative model (solid curve according to (5) in [36]) and the kick-out model (dashed curve according to (43) in [39]).

Further phenomena finding a natural explanation in terms of kick-out diffusion are the occurrence of peaks in the Au-diffusion profiles of weakly dislocated [46] and dislocation-free [41] Si wafers at locations where optical microscopy and optical microscopy in combination with transmission electron microscopy reveal the presence of groups of dislocations and interstitial-type dislocation loops, respectively. In both cases [46,41] the dislocation-type defects locally increase the removal rate of the self-interstitials produced via (6), which leads to a locally enhanced rate at which C_s increases towards C_s^{eq}. In the second case [41] the interstitial-type dislocation loops giving rise to anomalous W-shaped Au-diffusion profiles (Fig. 13) are formed of their own as a result of the in-diffusion of Au, presumably by heterogeneous nucleation of the "kicked-out" self-interstitials at small clusters of carbon atoms.

3.4. Measurements of the diffusion of copper in germanium

In the case of Ge, investigations of enhanced or retarded diffusion of substitutional solutes are not available. Therefore, the only reliable information on the self-diffusion mechanism in this material comes from studies of the interstitial–substitutional diffusion of Cu in Ge. The conclusion [47] based on early measurements [48,49] on dislocated Ge that Cu in Ge diffuses via the dissociative mechanism has been fully confirmed by recent SRT studies on dislocation-free specimens by Stolwijk et al. [36,50]. Fig. 14 demonstrates this for a Cu-diffusion profile (full circles) measured on a "thick" Ge specimen after a 1 h diffusion anneal at 951 K [50]. Whereas an erfc-type profile (solid curve), as predicted by the dissociative-diffusion theory (eq. (5) in [36]), well describes the experimental data, a kick-out diffusion profile (dashed curve according to eq. (43) in [39]) cannot be adjusted.

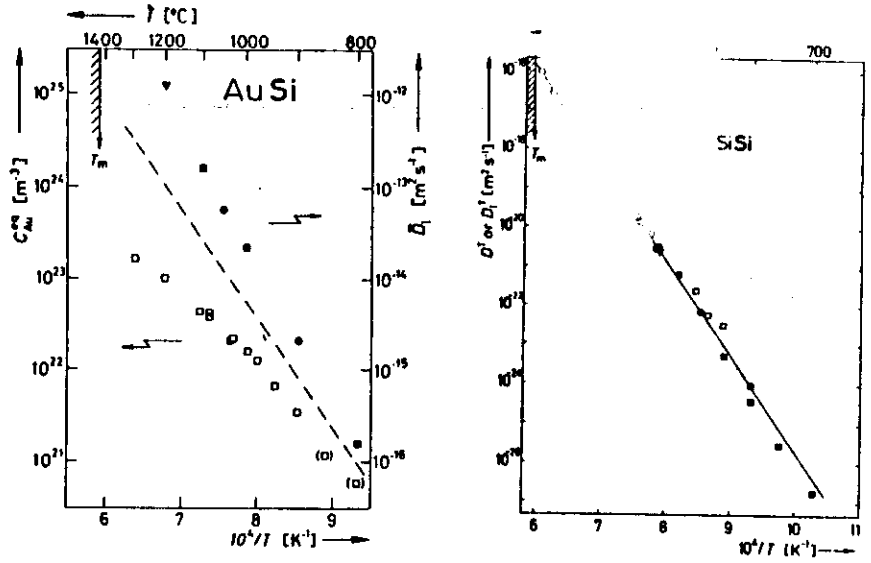

Fig. 15 (left). Arrhenius plots of C_{Au}^{eq} (empty squares) and $\tilde{D}_I$ (full circles: from "thick" specimens, full squares: from "thin" specimens, full triangle: from the d dependence of C_s^m) for Au in dislocation-free Si [40,42,50].
Fig. 16 (right). Arrhenius plots of data on the tracer self-diffusion coefficient D^T (empty circles [51] and empty squares [52]) and its interstitialcy component D_I^T (full symbols) in Si. The D_I^T data originate from studies of Au in Si (full circles [40,42,50]) and Pt in Si (full triangles [43] and full squares [53]). The straight line is a least-squares fit of an Arrhenius law to the D_I^T data from [40,42,50] and [43].

4. SELF-DIFFUSION MECHANISMS IN SILICON AND GERMANIUM

In Si and Ge the concentrations of intrinsic point defects in thermal equilibrium are extremely low, so that contributions to self-diffusion by multiple defects may safely be neglected (Sect. 1). Under these circumstances the tracer self-diffusion coefficient is given by

$$D^T = D_I^T + D_V^T \tag{13}$$

with

$$D_I^T \equiv f_I D_I C_I^{eq} \tag{13a}$$

and

$$D_V^T \equiv f_V D_V C_V^{eq} . \tag{13b}$$

D_I^T is the contribution by single self-interstitials to D^T and f_I the correlation factor for self-diffusion via self-interstitials. With the aid of (9) and (10), eqs. (13a) and (13b) may be re-written as

$$D_I^T = f_I \tilde{D}_I C_s^{eq} \tag{14a}$$

and

$$D_V^T = f_V \tilde{D}_V C_s^{eq} . \tag{14b}$$

Hence, by combining data on the substitutional solubility C_s^{eq} of an amphoteric solute A (which, because of $C_I^{eq} \ll C_s^{eq}$, is practically identical with its total solubility C_A^{eq}) with its kick-out diffusivity $\tilde{D}_I$ or its dissociative diffusivity $\tilde{D}_V$, the contribution to the self-diffusion coefficient by self-interstitials, D_I^T, or by vacancies, D_V^T, may be calculated, respectively. This way has been gone for both Si and Ge.

4.1. Silicon

Fig. 15 shows an Arrhenius plot of the total solubility C_{Au}^{eq} (empty squares) measured on "thin", Au-saturated Si wafers by means of NAA [40,50]. The data points at the two lowest temperatures are put in parantheses since in these cases the solubility limit has not been reached completely, though the diffusion anneals have lasted up to several months. Also included in Fig. 15 are kick-out diffusivities $\tilde{D}_I$ of Au in Si [40,42,50], which have been determined from diffusion profiles measured on "thick" (full circles) or "thin" (full squares) specimens or from the d dependence of C_s^m (full triangle).

In Fig. 16 data on the Si self-diffusion coefficient D^T measured by means of Si-tracer techniques [51,52] (empty symbols) are compared with values of the self-interstitial contribution D_I^T to D^T (full symbols). The D_I^T data represented by the full circles and the full triangles have been calculated from the kick-out-diffusion ($\tilde{D}_I$) and solubility (C_{Au}^{eq}) data on Au in Si shown in Fig. 15 and from corresponding data on Pt in Si [43], respectively, with the aid of (14a) putting $f_I = 1/2$. These two D_I^T-data sets obey the Arrhenius law

$$D_I^T = (3.5\ ^{+1.2}_{-0.9}) \times 10^{-2} \exp[-(4.81 \pm 0.04)\ \mathrm{eV}/kT]\ \mathrm{m^2 s^{-1}} \tag{15}$$

corresponding to the straight line in Fig. 16. The full squares, which represent D_I^T data obtained from capacitance–voltage measurements and deep-level transient spectroscopy measurements of the diffusion of Pt in Si by Mantovani and co-workers [53], lie close to this line. As may be seen from Fig. 16, there are no significant deviations between the D_I^T and the D^T data in the temperature regime above 1270 K. This is supported by a comparison of (15) with the Arrhenius laws

$$D^T = (14.6\ ^{+17}_{-8}) \times 10^{-2} \exp[-(5.02 \pm 0.10)\ \mathrm{eV}/kT]\ \mathrm{m^2 s^{-1}} \tag{16}$$

and

$$D^T = (1.54\ ^{+39}_{-1.5}) \times 10^{-2} \exp[-(4.64 \pm 0.35)\ \mathrm{eV}/kT]\ \mathrm{m^2 s^{-1}} \tag{17}$$

by which the D^T data of Mayer et al. [51] (empty circles), who used the ^{31}Si-radiotracer technique, and of Kalinowski and Seguin [52] (empty squares), who studied the ^{30}Si-tracer diffusion by means of secondary-ion mass spectroscopy, may be described, respectively.

From the preceding comparison between data on D^T and D_I^T as well as from other observations reported in Sects. 2 and 3 we conclude that above about 1270 K Si self-diffusion is dominated by the interstitialcy mechanism. Whether the fact that in Fig. 16 the three D^T-data points of Kalinowski and Seguin [52] (empty squares) below 1270 K lie above the straight line representing (15) is significant and indicates a contribution to D^T by the vacancy mechanism is not clear. Finally we focus attention on the pre-exponential factors in (15) to (17), which – in accordance with the results of the early Si self-diffusion studies – are very large in comparison with the pre-exponential self-diffusivity factors in metals. This supports the proposal by Seeger and Chik [2] that at high temperatures Si self-interstitials are spread out (Sect. 1).

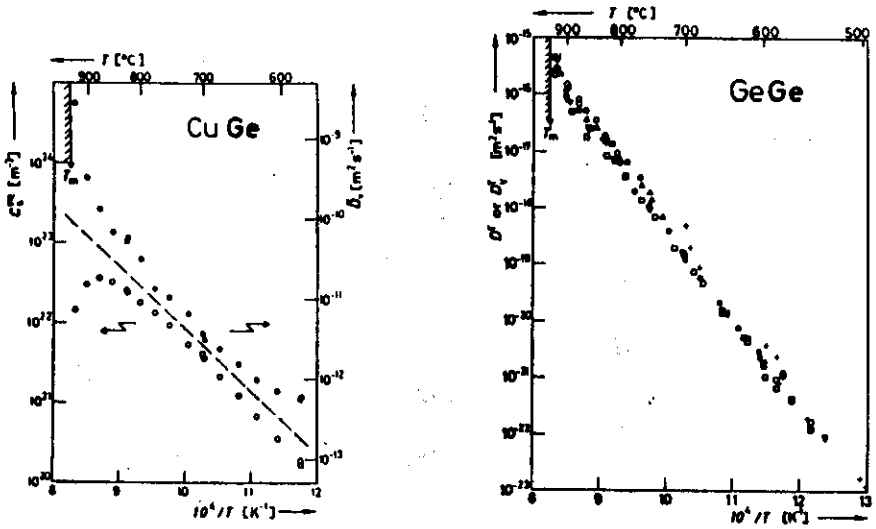

Fig. 17 (left). Arrhenius plots of C_i^{eq} (empty circles) and $\tilde{D}_V$ (full circles) for Cu in dislocation-free Ge [36,50].
Fig. 18 (right). Arrhenius plots of data on the Ge tracer self-diffusion coefficient D^T (○ [54], △ [55], ◇ [56], □ [57], ▽ [58]) and its vacancy component D_V^T. The D_V^T data originate from studies of Cu in dislocated (+ [47-49]) and dislocation-free (● [36,50]) Ge.

4.2. Germanium

The values of the solubility limit C_i^{eq} and the dissociative diffusivity $\tilde{D}_V$ shown in Fig. 17 have been determined by fitting the expressions (5) and (7) in [36], predicted by the theory of dissociative diffusion, to Cu-diffusion profiles measured on "thick" and "thin" dislocation-free Ge specimens [36,50], respectively, by means of the SRT. Using (14b) and the f_V value (0.5) for tracer self-diffusion via monovacancies in diamond structures, the contribution D_V^T by vacancies to the self-diffusion coefficient D^T in Ge has been calculated as a function of temperature from the data in Fig. 17. The D_V^T values obtained in this way are presented in Fig. 18 as full circles. Most surprisingly, they obey the Arrhenius law

$$D_V^T = (2.13 \pm 1.2) \times 10^{-3} \exp[-(3.11 \pm 0.05)\text{eV}/kT] \ \text{m}^2\text{s}^{-1}, \qquad (18)$$

though the $\tilde{D}_V$–$1/T$ and C_i^{eq}–$1/T$ curves are positively and negatively curved, respectively (Fig. 17). At high temperatures C_i^{eq} even becomes retrograde. The crosses in Fig. 18 mark D_V^T values determined from the diffusion of Cu in dislocated Ge [47-49]. All D_V^T data, particularly those deduced from Cu-diffusion studies on dislocation-free Ge [36,50], follow closely the D^T data measured by various authors [54-58] by means of Ge-tracer techniques and included in Fig. 18 as open symbols. The most recent D^T data of Werner et al. [58] covering the widest temperature regime (808 K–1177 K) may be described by

$$D^T = (1.36 \pm 0.15) \times 10^{-3} \exp[-(3.09 \pm 0.02)\text{eV}/kT] \ \text{m}^2\text{s}^{-1}. \qquad (19)$$

A comparison between (18) and (19) confirms the excellent agreement between the D^T and the D_V^T data and leads to the conclusion that at least in the entire temperature regime in which both kinds of data exist Ge self-diffusion occurs via vacancies. The relatively high pre-exponential factors in (18) and (19) indicate that in thermal equilibrium vacancies in Ge may be spread out, as proposed previously by Seeger and Chik [2] (Sect. 1).

5. SUMMARY

In the case of Ge we have arrived at the following simple picture: (a) Self-diffusion occurs via spread-out vacancies. (b) The substitutional solutes of Groups III and V diffuse via the vacancy mechanism. (c) Cu diffuses in Ge via the dissociative mechanism.

In remarkable contrast to Ge, in Si the situation is quite complicated: (A) In thermal equilibrium self-interstitials and vacancies coexist. (B) Above about 1270 K self-diffusion occurs preferentially via spread-out self-interstitials. (C) Both self-interstitials and vacancies contribute to the diffusion of substitutional solutes. Group-III membership and small atomic size of a solute favour its diffusion via self-interstitials, whereas Group-V membership and large atomic size are advantageous for diffusion via vacancies. (D) Au and Pt diffuse in Si preferentially via the kick-out mechanism.

A challenging task for future research is a reliable separation of $D_V C_V^{eq}$ and $D_I C_I^{eq}$ in diffusivities and equilibrium concentrations.

ACKNOWLEDGEMENTS

The authors are very grateful to their collaborators Dr. U. Gösele, Dr. J. Hauber, Ing. J. Hölzl, Dipl.-Phys. B. Kühn, Prof. Dr. H. Mehrer, and Prof. Dr. A. Seeger. The work reported in Sect. 3.3 is part of the research project NT 2582/0 of the Bundesministerium für Forschung und Technologie of the Federal Republic of Germany.

REFERENCES

[1] Frank, W., Gösele, U., Mehrer, H., and Seeger, A., in: Diffusion in Crystalline Solids, Eds. G.E. Murch and A.S. Nowick, Academic Press, Orlando 1984 (p. 63)
[2] Seeger, A., and Chik, K.P.: phys. stat. sol., 1968, 29, 455
[3] Pandey, K.C.: Phys. Rev. Letters, submitted
[4] Seeger, A., and Mehrer, H., in: Vacancies and Interstitials in Metals, Eds. A. Seeger, D. Schumacher, W. Schilling, and J. Diehl, North-Holland, Amsterdam 1970 (p. 1)
[5] Mehrer, H.: J. Nucl. Mater., 1978, 69/70, 38
[6] Peterson, N.L.: J. Nucl. Mater., 1978, 69/70, 3
[7] Trost, W.: Dr. rer. nat. thesis, University of Stuttgart 1986
[8] Differt, K., Seeger, A., and Trost, W.: these proceedings
[9] James, H.M., and Lark-Horovitz, K.: Z. Phys. Chem. (Leipzig), 1951, 198, 107
[10] Blount, E.I.: J. Appl. Phys., 1959, 30, 1218
[11] Shaw, D.: phys. stat. sol. (b), 1975, 72, 11
[12] Van Vechten, J.A., and Thurmond, C.D.: Phys. Rev. B, 1976, 14, 3551
[13] Fair, R.B., in: Semiconductor Silicon 1977, Eds. H.R. Huff and E. Sirtl, Electrochemical Society, Princeton, N.J., 1977 (p. 968)
[14] Bernewitz, L.J., and Mayer, K.R.: phys. stat. sol. (a), 1973, 16, 579
[15] De Kock, A.J.R.: Philips Res. Rep. Suppl., 1973, 4, 1
[16] Föll, H., and Kolbesen, B.O.: Appl. Phys., 1975, 8, 319
[17] Petroff, P.M., and de Kock, A.J.R.: J. Cryst. Growth, 1975, 30, 117
[18] Föll, H., Kolbesen, B.O., and Frank, W.: phys. stat. sol. (a), 1975, 29, K83
[19] Seeger, A., Föll, H., and Frank, W., in: Radiation Effects in Semiconductors 1976, Eds. N.B. Urli and J.W. Corbett, Institute of Physics, Inst. Phys. Conf. Ser. No. 31, Bristol and London 1977 (p. 12)

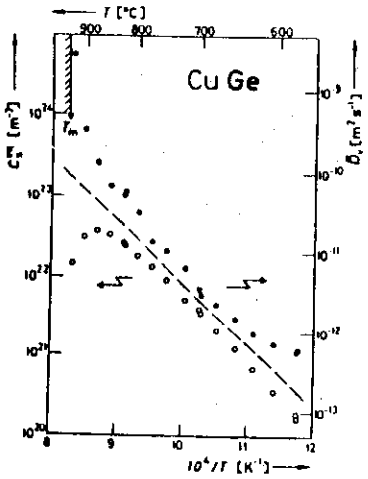

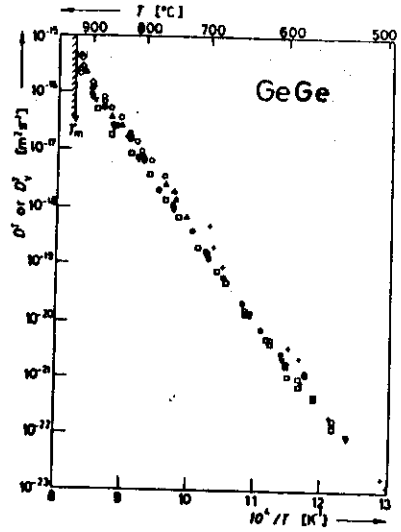

Fig. 17 (left). Arrhenius plots of C_s^{eq} (empty circles) and $\tilde{D}_V$ (full circles) for Cu in dislocation-free Ge [36,50].
Fig. 18 (right). Arrhenius plots of data on the Ge tracer self-diffusion coefficient D^T (○ [54], △ [55], ◇ [56], □ [57], ▽ [58]) and its vacancy component D_V^T. The D_V^T data originate from studies of Cu in dislocated (+ [47-49]) and dislocation-free (●[36,50]) Ge.

4.2. Germanium

The values of the solubility limit C_s^{eq} and the dissociative diffusivity $\tilde{D}_V$ shown in Fig. 17 have been determined by fitting the expressions (5) and (7) in [36], predicted by the theory of dissociative diffusion, to Cu-diffusion profiles measured on "thick" and "thin" dislocation-free Ge specimens [36,50], respectively, by means of the SRT. Using (14b) and the f_V value (0.5) for tracer self-diffusion via monovacancies in diamond structures, the contribution D_V^T by vacancies to the self-diffusion coefficient D^T in Ge has been calculated as a function of temperature from the data in Fig. 17. The D_V^T values obtained in this way are presented in Fig. 18 as full circles. Most surprisingly, they obey the Arrhenius law

$$D_V^T = (2.13 \pm 1.2) \times 10^{-3} \exp[-(3.11 \pm 0.05)\text{eV}/kT] \ \text{m}^2\text{s}^{-1}, \qquad (18)$$

though the $\tilde{D}_V$–$1/T$ and C_s^{eq}–$1/T$ curves are positively and negatively curved, respectively (Fig. 17). At high temperatures C_s^{eq} even becomes retrograde. The crosses in Fig. 18 mark D_V^T values determined from the diffusion of Cu in dislocated Ge [47-49]. All D_V^T data, particularly those deduced from Cu-diffusion studies on dislocation-free Ge [36,50], follow closely the D^T data measured by various authors [54-58] by means of Ge-tracer techniques and included in Fig. 18 as open symbols. The most recent D^T data of Werner et al. [58] covering the widest temperature regime (808 K–1177 K) may be described by

$$D^T = (1.36 \pm 0.15) \times 10^{-3} \exp[-(3.09 \pm 0.02)\text{eV}/kT] \ \text{m}^2\text{s}^{-1}. \qquad (19)$$

A comparison between (18) and (19) confirms the excellent agreement between the D^T and the D_V^T data and leads to the conclusion that at least in the entire temperature regime in which both kinds of data exist Ge self-diffusion occurs via vacancies. The relatively high pre-exponential factors in (18) and (19) indicate that in thermal equilibrium vacancies in Ge may be spread out, as proposed previously by Seeger and Chik [2] (Sect. 1).

5. SUMMARY

In the case of Ge we have arrived at the following simple picture: (a) Self-diffusion occurs via spread-out vacancies. (b) The substitutional solutes of Groups III and V diffuse via the vacancy mechanism. (c) Cu diffuses in Ge via the dissociative mechanism.

In remarkable contrast to Ge, in Si the situation is quite complicated: (A) In thermal equilibrium self-interstitials and vacancies coexist. (B) Above about 1270 K self-diffusion occurs preferentially via spread-out self-interstitials. (C) Both self-interstitials and vacancies contribute to the diffusion of substitutional solutes. Group-III membership and small atomic size of a solute favour its diffusion via self-interstitials, whereas Group-V membership and large atomic size are advantageous for diffusion via vacancies. (D) Au and Pt diffuse in Si preferentially via the kick-out mechanism.

A challenging task for future research is a reliable separation of $D_V C_V^{eq}$ and $D_I C_I^{eq}$ in diffusivities and equilibrium concentrations.

ACKNOWLEDGEMENTS

The authors are very grateful to their collaborators Dr. U. Gösele, Dr. J. Hauber, Ing. J. Hölzl, Dipl.-Phys. B. Kühn, Prof. Dr. H. Mehrer, and Prof. Dr. A. Seeger. The work reported in Sect. 3.3 is part of the research project NT 2582/0 of the Bundesministerium für Forschung und Technologie of the Federal Republic of Germany.

REFERENCES

[1] Frank, W., Gösele, U., Mehrer, H., and Seeger, A., in: Diffusion in Crystalline Solids, Eds. G.E. Murch and A.S. Nowick, Academic Press, Orlando 1984 (p. 63)
[2] Seeger, A., and Chik, K.P.: phys. stat. sol., 1968, 29, 455
[3] Pandey, K.C.: Phys. Rev. Letters, submitted
[4] Seeger, A., and Mehrer, H., in: Vacancies and Interstitials in Metals, Eds. A. Seeger, D. Schumacher, W. Schilling, and J. Diehl, North-Holland, Amsterdam 1976 (p. 1)
[5] Mehrer, H.: J. Nucl. Mater., 1978, 69/70, 38
[6] Peterson, N.L.: J. Nucl. Mater., 1978, 69/70, 3
[7] Trost, W.: Dr. rer. nat. thesis, University of Stuttgart 1986
[8] Differt, K., Seeger, A., and Trost, W.: these proceedings
[9] James, H.M., and Lark-Horovitz, K.: Z. Phys. Chem. (Leipzig), 1951, 198, 107
[10] Blount, E.I.: J. Appl. Phys., 1959, 30, 1218
[11] Shaw, D.: phys. stat. sol. (b), 1975, 72, 11
[12] Van Vechten, J.A., and Thurmond, C.D.: Phys. Rev. B, 1976, 14, 3551
[13] Fair, R.B., in: Semiconductor Silicon 1977, Eds. H.R. Huff and E. Sirtl, Electrochemical Society, Princeton, N.J., 1977 (p. 968)
[14] Bernewitz, L.J., and Mayer, K.R.: phys. stat. sol. (a), 1973, 16, 579
[15] De Kock, A.J.R.: Philips Res. Rep. Suppl., 1973, 4, 1
[16] Föll, H., and Kolbesen, B.O.: Appl. Phys., 1975, 8, 319
[17] Petroff, P.M., and de Kock, A.J.R.: J. Cryst. Growth, 1975, 30, 117
[18] Föll, H., Kolbesen, B.O., and Frank, W.: phys. stat. sol. (a), 1975, 29, K83
[19] Seeger, A., Föll, H., and Frank, W., in: Radiation Effects in Semiconductors 1976, Eds. N.B. Urli and J.W. Corbett, Institute of Physics, Inst. Phys. Conf. Ser. No. 31, Bristol and London 1977 (p. 12)

[20] Föll, H., Gösele, U., and Kolbesen, B.O.: J. Cryst. Growth, 1977, 40, 90
[21] Petroff, P.M., and de Kock, A.J.R.: J. Cryst. Growth, 1976, 36, 4
[22] Van Vechten, J.A.: Phys. Rev. B, 1978, 17, 3197
[23] Frank, W., in: Festkörperprobleme (Advances in Solid State Physics), Vol. 21, Ed. J. Treusch, Vieweg, Braunschweig 1981 (p. 221)
[24] Strunk, H., Gösele, U., and Kolbesen, B.O.: Appl. Phy[illegible]9, 34, 530
[25] Booker, G.R., and Tunstall, N.J.: Phil. Mag., 1966, 13,
[26] Jaccodine, R.J., and Drum, C.M.: Appl. Phys. Letters, 1966, 8, 29
[27] Hu, S.M.: J. Appl. Phys., 1974, 45, 1567
[28] Fahey, P., and Dutton, R.W., in: Semiconductor Silicon 1986, Eds. H.R. Huff, T. Abe, and B.O. Kolbesen, Electrochemical Society, Pennington, N.J., 1986 (p. 571)
[29] Prussin, S.: J. Appl. Phys., 1972, 43, 2850
[30] Sirtl, E., in: Semiconductor Silicon 1977, Eds. H.R. Huff and E. Sirtl, Electrochemical Society, Princeton, N.J., 1977 (p. 4)
[31] Frank, F.C., and Turnbull, D.: Phys. Rev., 1956, 104, 617
[32] Gösele, U., Frank, W., and Seeger, A.: Appl. Phys., 1980, 23, 361
[33] Sturge, M.D.: Proc. Phys. Soc. London, 1959, 73, 297
[34] Seeger, A., and Frank, W.: Appl. Phys. A, 1982, 27, 171
[35] Stolwijk, N.A., Schuster, B., Hölzl, J., Mehrer, H., and Frank, W.: Physica B, 1983, 116, 335
[36] Stolwijk, N.A., Frank, W., Hölzl, J., Pearton, S.J., and Haller, E.E.: J. Appl. Phys., 1985, 57, 5211
[37] Carslaw, H.S., and Jaeger, J.C.: Conduction of Heat in Solids, Oxford University Press (Clarendon), London and New York 1959
[38] Crank, J.: Mathematics of Diffusion, Oxford University Press (Clarendon), London and New York 1975
[39] Seeger, A.: phys. stat. sol. (a), 1980, 61, 521
[40] Stolwijk, N.A., Schuster, B., and Hölzl, J.: Appl. Phys. A., 1984, 33, 133
[41] Hauber, J., Stolwijk, N.A., Tapfer, L., Mehrer, H., and Frank, W.: J. Phys. C, in press
[42] Stolwijk, N.A., Hölzl, J., Frank, W., Weber, E.R., and Mehrer, H.: Appl. Phys. A, 1986, 39, 37
[43] Hauber, J.: Dr. rer. nat. thesis, University of Stuttgart 1986
[44] Morehead, F., Stolwijk, N.A., Meyberg, W., and Gösele, U.: Appl. Phys. Letters, 1983, 42, 690
[45] Kühn, B.: private communication
[46] Stolwijk, N.A., Mehrer, H., Hölzl, J., Hauber, J., and Frank, W.: J. Electrochemical Society, to be submitted
[47] Penning, P.: Phys. Rev., 1958, 110, 586
[48] Tweet, A.G.: Phys. Rev., 1957, 106, 221
[49] Woodbury, H.H., and Tyler, W.W.: Phys. Rev., 1957, 105, 84
[50] Stolwijk, N.A., and Frank, W., in: Proc. 13th Internat. Conf. Defects in Semiconductors, Eds. L.C. Kimerling and J.M. Parsey, Jr., Metallurgical Society of AIME, Warrendale, Pennsylvania, 1985 (p. 285)
[51] Mayer, H.J., Mehrer, H., and Maier, K., in: Radiation Effects in Semiconductors 1976, Eds. N.B. Urli and J.W. Corbett, Institute of Physics, Inst. Phys. Conf. Ser. No. 31, Bristol and London 1977 (p. 186)
[52] Kalinowski L., and Seguin, R.: Appl. Phys. Letters, 1979, 35, 211 and 1980, 36, 171
[53] Mantovani, S., Nava, F., Nobili, C., and Ottaviani, G.: Phys. Rev. B, 1986, 33, 5536
[54] Letaw, H., Jr., Portnoy, W.M., and Slifkin, L.: Phys. Rev., 1956, 102, 636
[55] Widmer, H., and Gunther-Mohr, G.R.: Helv. Physica Acta, 1961, 34, 635
[56] Campell, D.R.: Phys. Rev. B, 1975, 12, 2318
[57] Vogel, G., Hettich, G., and Mehrer, H.: J. Phys. C, 1983, 16, 6197
[58] Werner, M., Mehrer, H., and Hochheimer, H.D.: Phys. Rev. B, 1985, 32, 3930

(4)

Defect and Diffusion Forum 75, 121–147 (1991)

[illegible]ERPLAY OF SOLUTE- AND SELF-DIFFUSION — A KEY [illegible]VEALING DIFFUSION MECHANISMS IN SILICON AND GERMANIUM

W. Frank

Max-Planck-Institut für Metallforschung, Institut für Physik,
and
Universität Stuttgart, Institut für Theoretische und Angewandte Physik,
P. O. Box 800 665, D-7000 Stuttgart 80,
Federal Republic of Germany

ABSTRACT

The paper reviews the key experiments which have led to a comprehensive understanding of the diffusion mechanisms and the thermal-defect scenarios in the elemental semiconductors Si and Ge. It is demonstrated that the analysis of the interplay between solute- and self-diffusion in Si on the one hand and the comparison between Si and Ge on the other hand have played an important role in arriving at the picture described in what follows.

In *silicon* self-interstitials and vacancies coexist under thermal-equilibrium conditions. Above about 1000 °C, self-diffusion is dominated by an interstitialcy mechanism, and (so-called hybrid) elements which occupy both interstitial and substitutional sites (e.g., Au and Pt) diffuse almost exclusively via the kick-out mechanism. In the diffusion of substitutional solutes, small atomic size and Group-III membership (e.g., of B) favour interstitialcy diffusion, whereas large atomic size and Group-V membership (e.g., of Sb) are advantageous for diffusion via vacancies. There are indications that the importance of vacancies for diffusion processes in Si increases at temperatures below 1000 °C.

In *germanium* both self-diffusion and substitutional-solute diffusion take place by means of vacancies; the hybrid Cu undergoes dissociative diffusion.

It is speculated that the existence of thermal-equilibrium self-interstitials in Si is related to the great mass-density increase of Si of about 10% at melting. This idea is supported by a comparison with *ice*, which shows the same density anomaly at melting and, presumably as a result of this, similar diffusion and thermal-defect properties.

1. SILICON

1.1. Classification of diffusers and introductory survey

Fig. 1 shows the Arrhenius plots of the diffusivities in monocrystalline silicon for a selection of elements. Obviously, there is a gap of many orders of magnitude between the diffusivities of the so-called fast diffusers (e.g., Cu, Ni, Li, and Fe) and the diffusivities of the slow diffusing elements of Groups III to V (including the self-diffusivity). This gap is bridged by Au and Pt, which henceforth will be referred to as "hybrids". This notation will turn out to be justified not only by the intermediate values of the diffusivities of these elements, but also by the nature of their diffusion mechanism.

It is undisputed that the fast diffusers in Si migrate via a direct interstitial mechanism, i.e., they hop from interstitial site to interstitial site through the Si lattice (Fig. 2). Here the word "direct" indicates that this diffusion mechanism does not require the cooperation of intrinsic point defects (i.e. vacancies or self-interstitials) as diffusion vehicles. In Sect. 1.2 new experimental results on the diffusion and solubility of Pd in Si will be presented. They demonstrate that Pd is one of the fastest interstitial diffusers in Si.

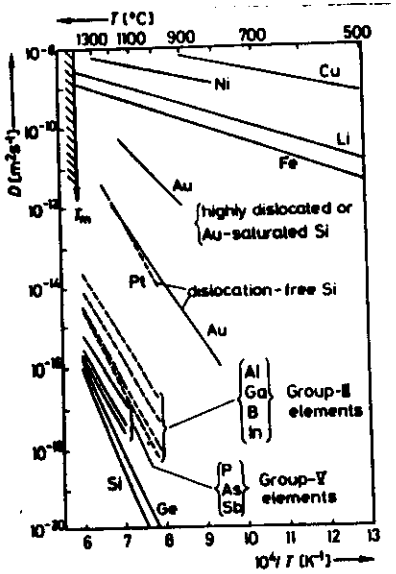

Fig. 1 (left). Survey of the diffusivities of self- and foreign atoms in Si. For references see [1] and, particularly for the diffusivities of Au and Pt, Sects. 1.4, 1.5.2, and 1.5.3.

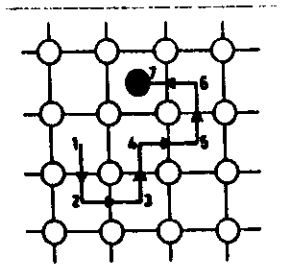

Fig. 2 (right). Direct interstitial mechanism: An interstitial atom (full circle) jumps from interstice 1 to interstice 2, from 2 to 3, etc. Regular lattice atoms are represented by empty circles.

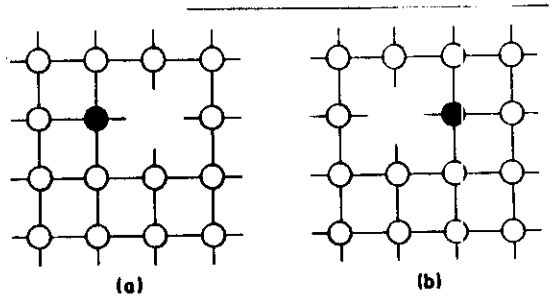

Fig. 3. Vacancy mechanism: A radioactive self-atom in tracer self-diffusion or a foreign atom in substitutional-solute diffusion (full circle) moves, by jumping into the vacancy on its right-hand side (a), to the right (b) by one nearest-neighbour distance of the regular lattice atoms (empty circles).

Although details are still controversial, it is generally accepted that the slow diffusing dopants of Groups III and V undergo indirect diffusion as a result of site exchanges with the randomly migrating intrinsic point defects which are present in thermal equilibrium. Figs. 3 and 4 illustrate the simplest versions of indirect diffusion via vacancies (vacancy mechanism) and self-interstitials (interstitialcy mechanism), respectively. (The reader is expressly warned against mixing up "interstitialcy diffusion" (Fig. 4) with "direct interstitial diffusion" (Fig. 2).) In Sect. 1.3 experiments will be reported in which the influence of the injection of self-interstitials or vacancies on the diffusivities of dopants has been studied. The outcome of these investigations is that in Si vacancies and self-interstitials coexist under thermal-equilibrium conditions and that their fractional contributions to dopant diffusion differ from element to element.

Sect. 1.4 will be devoted to Au and Pt in Si, which show hybrid features with regard to both their lattice locations and their diffusion mechanisms. The realization that these elements predominantly diffuse via the so-called kick-out mechanism, which is a combination of interstitialcy and direct interstitial diffusion, was a milestone in the understanding of diffusion processes in Si. In particular, it led to a quantitative, self-consistent picture of hybrid diffusion and self-diffusion. Sect. 1.5 is to round off this picture.

1.2. Diffusion and solubility of palladium

In our laboratory the diffusion of Pd in float-zone-grown, phosphorus-doped, dislocation-free Si single crystals has recently been investigated by means of neutron activation analysis in combination with serial sectioning [2]. At 1376 K the Pd diffusivity is so high that in a 25 mm long rod-shaped specimen Pd atoms diffuse from one end to the other within about one hour. The erfc-shaped diffusion profiles (Fig. 5) as well as the diffusion enthalpy (0.22 eV) and the pre-exponential factor (2.95×10^{-8} m^2s^{-1}) deduced from the Arrhenius-type temperature dependence of the diffusion coefficient (Fig. 6) clearly indicate that Pd belongs to the fast diffusers in Si that undergo direct interstitial diffusion (Sect 1.1).

Fig. 7 shows the solubility of Pd in Si as a function of the reciprocal temperature. Both its magnitude and the indication of a retrograde behaviour at high temperatures resemble very much the solubility of Au in Si, although Au is incorporated in Si preferentially on substitutional sites (Sect. 1.4).

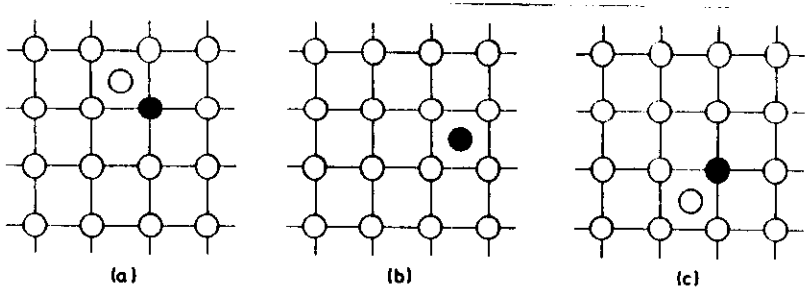

Fig. 4. Interstitialcy mechanism: In (a) a self-interstitial (empty circle in the centre of a lattice cell) has approached a radiotracer self-atom or a substitutional foreign atom (full circle), respectively; in (b) the marked atom has exchanged its original position with the self-interstitial. In this way the marked atom has temporarily become an interstitial, whereas the original self-interstitial has disappeared by occupying a regular lattice site. In (c) the marked atom has re-occupied a regular site by kicking a self-atom into an interstice.

1.3. Intrinsic-point-defect injection, diffusion of substitutional solutes, and the coexistence of vacancies and self-interstitials in thermal equilibrium

Investigations of fast diffusers like Pd (Sect. 1.2) do not yield any information on either the diffusion mechanisms of other atoms or intrinsic point defects in Si. This is different for substitutional dopants, since — as will be discussed in what follows — these solutes diffuse indirectly with the aid of vacancies and self-interstitials via which a coupling among different substitutionally incorporated species and to self-atoms is established.

During the past decade, rapid progress in the understanding of substitutional-solute diffusion has been achieved by studies of the influence of surface oxidation and nitridation of Si on the diffusivities of elements of Groups III and V and on the simultaneous changes of the sizes of precedingly introduced interstitial-type dislocation loops [3—8]. For instance, oxidation (nitridation) is found to make interstitial loops grow (shrink) and to enhance (retard) the diffusivity of B, but to retard (enhance) the diffusivity of Sb. The compatibility of these observations requires (i) that surface oxidation and nitridation lead to an injection of self-interstitials (I) and vacancies (V), respectively, (ii) that self-interstitials and vacancies coexist in Si under thermal-equilibrium conditions, and (iii) that B diffuses preferentially via self-interstitials, whereas Sb prefers vacancies as diffusion vehicles.

The fractional contributions Φ_n of self-interstitials (n = I) and vacancies (n = V) to the diffusivities of substitutional solutes may be obtained from the sort of surface oxidation and nitridation experiments just described. Fig. 8 represents Φ_I (= 1-Φ_V) for the Group-III elements B, Al, Ga and the Group-V elements P, As, Sb as a function of r/r_{Si} (r = atomic radii of the solutes, r_{Si} = atomic radius of Si) [1]. A qualitative understanding of these findings in terms of a combined elastic and electrostatic interaction between the solutes and the diffusion vehicles is straightforward. Solute atoms elastically attract self-interstitials or vacancies depending on whether they are smaller or larger than the Si atoms, respectively. Coulomb attractions exist between

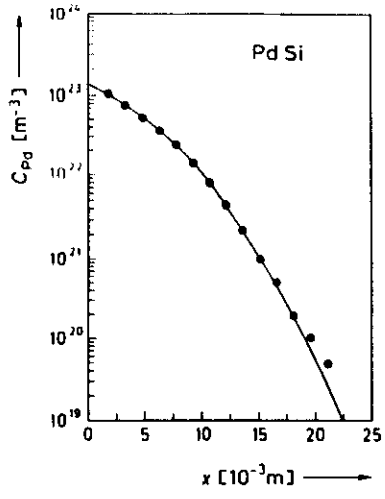

Fig. 5 (left). Penetration profile of Pd in Si measured by means of neutron activation analysis after a 58 min diffusion anneal at 1376 K [2].

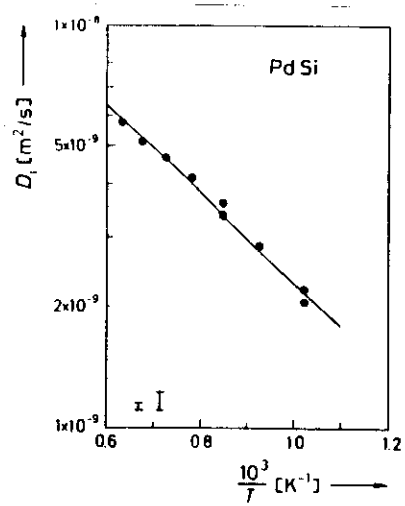

Fig. 6 (right). Diffusivity of Pd in Si [2]. The minimum and maximum error bars are indicated.

the donor solutes and the acceptor-type vacancies[1] as well as between the acceptor solutes and the self-interstitials which — except in highly n-doped Si — behave as donors[2]. As a result, smallness and Group-III membership of a solute favour its diffusion via self-interstitials, whereas largeness and Group-V membership are advantageous for diffusion via vacancies. This simple rule makes immediately comprehensible why B and Sb preferentially diffuse with the aid of self-interstitials and vacancies, respectively. In the case of P, for which Φ_I is close to unity, the elastic attraction of self-interstitials obviously exceeds the Coulomb attraction of vacancies, while in the cases of Ga and Al ($\Phi_I > 0.5$) the Coulomb attraction of self-interstitials must be larger than the elastic attraction of vacancies.

---

[1] Experiments by Watkins et al. [9,10] have revealed quite a complicated level structure of the Si vacancy. However, under most conditions achievable by usual chemical doping the Si vacancy appears as an acceptor whose level is located in the lower part of the energy gap.

[2] According to Blount (tight-binding approximation) [11] and Watkins et al. (atomic-orbital—molecular-orbital cluster model) [12] the Si self-interstitial possesses an acceptor level in the upper half of the band gap and a donor level in the lower half. As a result, it is negatively charged (I^-) in n-type material, electrically neutral (I^0) in intrinsic material, and positively charged (I^+) in p-type material. These theoretical predictions are in accordance with the mechanisms by which substitutional solutes in Si undergo diffusion (Sect. 1.3) and with the dependence of the substitutional-solute diffusion in Si on chemical doping (Sect. 1.5.1).

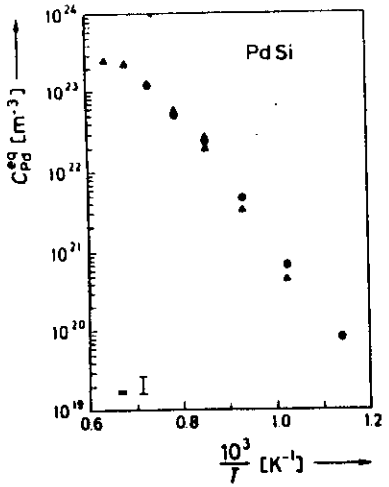

Fig. 7. Solubility limit of Pd in Si [2]. The minimum and maximum error bars are indicated.

The precedingly described experiments have led us to an understanding of the essential features of substitutional-solute diffusion in Si. The picture evolved above is confirmed by observations of the influence of chemical doping on the diffusivities of Group-III and Group-V elements [1]. This point and some refinements of the substitutional-solute diffusion model will be briefly considered in Sect. 1.5.1.

Concerning self-defects in Si, the surface oxidation/nitridation experiments [3–8] have yielded the qualitative result that vacancies and self-interstitials coexist under thermal-equilibrium conditions. Hence, both kinds of defects may contribute to Si self-diffusion. Information on the relative importance of vacancies and self-interstitials as self-diffusion vehicles and values of the interstitialcy component of the tracer self-diffusion coefficient may be deduced from the diffusivities and solubilities of the hybrids Au and Pt (Sect. 1.4).

1.4. The hybrids Au and Pt

1.4.1. Evidence for self-interstitial-controlled kick-out diffusion in dislocation-free specimens

As discussed in Sect. 1.1, the diffusivities of Au and Pt in Si lie just between those of the fast interstitial diffusers and the slow diffusing substitutional solutes. Therefore, it is tempting to speculate that these elements might be "somehow intermediate". Indeed, from extensive neutron-activation-analysis [13–15] and spreading-resistance studies [15,16] of the diffusivities and solubilities of Au and Pt — a large number of which have been performed at our laboratory — the following picture has arisen. The main fraction of a hybrid species, which governs the solubility limit, is present in substitutional solution and thus virtually immobile, whereas the hybrid transport occurs via a small fraction of atoms undergoing fast interstitial diffusion [17]. Hence, a hybrid A may be characterized by the inequalities

$$C_s^{eq} \gg C_i^{eq} \quad \text{and} \quad D_s \ll D_i \qquad (1\text{ a \& b})$$

for its solubilities C_n^{eq} and diffusivities D_n, where n = s and n = i refer to the substitutional configuration A_s and the interstitial configuration A_i, respectively.

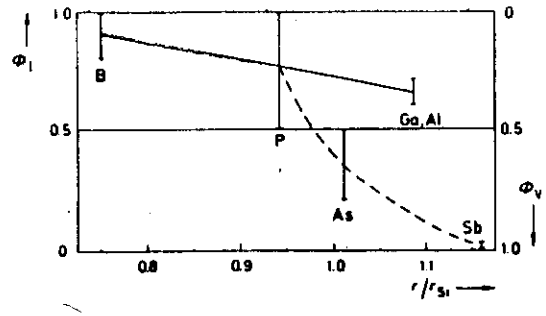

Fig. 8. Fractional contributions Φ_I and Φ_V to the diffusivities of substitutional solutes in Si by the interstitialcy and the vacancy mechanism, respectively, versus the atomic radii r of the solutes in units of the atomic radius r_{Si} of Si [1].

During the so-called substitutional–interstitial diffusion of a hybrid solute, interchanges between interstitial and substitutional sites take place either according to the kick-out mechanism (Fig. 9) [18]

$$A_i \rightleftarrows A_s + I \qquad (2)$$

or the dissociative mechanism (Fig. 10) [19]

$$A_i + V \rightleftarrows A_s\,, \qquad (3)$$

respectively. While Reaction (2) produces self-interstitials, Reaction (3) consumes vacancies. In both cases a quantitative description of the effective diffusion of A_s is possible by means of the diffusion equation [1,18]

$$\partial C_s/\partial t = \partial/\partial x(D_s^{eff}\partial C_s/\partial x) \qquad (4)$$

(C_s = concentration of A_s, x = space coordinate in the diffusion direction considered, t = diffusion time).

In highly dislocated specimens (Sect. 1.5.3) the effective diffusion coefficient D_s^{eff} in (4) is the same for dissociative and kick-out diffusion [1,18],

$$D_s^{eff} \equiv D_i^{*} \equiv D_i C_i^{eq}/C_s^{eq}, \qquad (5)$$

i.e., a discrimination between these mechanisms by means of studies of hybrid diffusion in highly dislocated specimens is not possible.

Here we concentrate on hybrid diffusion in dislocation-free specimens, for which D_s^{eff} is different for dissociative and kick-out diffusion. In the case of dissociative diffusion the effective influx $D_s^{eff}C_s^{eq}$ of A_s is controlled by the influx $D_V C_V^{eq}$ of vacancies from the specimen surface, which allow for the transformation of the very rapidly in-diffusing A_i to A_s according to (3); hence

$$D_s^{eff} \equiv D_V^{*} \equiv D_V C_V^{eq}/C_s^{eq} \qquad (6)$$

(D_V = diffusivity of V, C_V^{eq} = thermal-equilibrium concentration of V) [1,18,19]. By contrast, in kick-out diffusion — due to the very nature of this mechanism — each regular lattice site which is occupied by a self-atom represents a potential A_s site. Therefore, as long as the specimen is "A_s-empty" ($C_s/C_s^{eq} \ll 1$) the effective influx $D_s^{eff}C_s^{eq}$ of A_s is "unlimited" or, more precisely, limited by the very rapid influx of A_i only, whereas in a specimen "filled up with A_s" ($C_s/C_s^{eq} = 1$) the outflux $D_i C_i^{eq}$ to

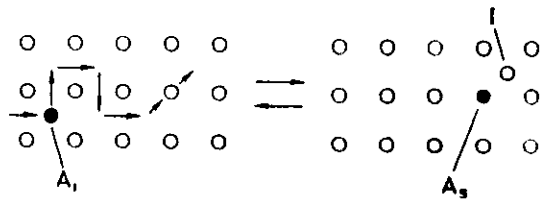

Fig. 9. Kick-out mechanism: Foreign atoms (full circle) interchange between interstitial sites (A_i) and substitutional sites (A_s) in cooperation with self-interstitials (I).

the surface of the self-interstitials produced via the kick-out reaction (2) controls the effective in-diffusion of A_s (D_I = diffusivity of I, C_I^{eq} = thermal-equilibrium concentration of I). These features are reflected in the expression for the corresponding effective diffusion coefficient [1,18],

$$D_s^{eff} \equiv D_I^{\circ}(C_s^{eq}/C_s)^2 \equiv (D_I C_I^{eq}/C_s^{eq})(C_s^{eq}/C_s)^2. \qquad (7)$$

This D_s^{eff} depends on x and t via C_s, in contrast to what is true for the effective diffusion coefficient of either dissociative or kick-out diffusion in highly dislocated specimens or dissociative diffusion in dislocation-free specimens.

Concerning the well-known solutions of (4) for dissociative diffusion in dislocation-free specimens (i.e. for a constant diffusion coefficient (Eq. (6)) we refer to text books on diffusion [20,21]. In the following, we shall compile the unusual and thus, specific predictions of the theory of kick-out diffusion in dislocation-free specimens (which may be deduced from (4) and (7) for various boundary and initial conditions) and compare these to experimental results on the diffusion of Au or Pt in Si and to the corresponding predictions of the dissociative-diffusion theory.

A qualitative explanation [1,13,17,18] of the U-shaped diffusion profiles of Au in dislocation-free, "thin" Si wafers[3] (Fig. 11) is possible in terms of both dissociative and kick-out diffusion. After a short initial transition during which the A_i concentration C_i reaches its solubility limit C_i^{eq} ($\ll C_s^{eq}$) throughout the wafer, C_s approaches C_s^{eq} most rapidly in the vicinity of the two wafer surfaces, since these constitute either the only sources of the vacancies required for the conversion of A_i to A_s via (3) or the only sinks at which the self-interstitials that are generated during an increase of C_s via (2) can be eliminated. However, a quantitative interpretation of the diffusion profiles in Fig. 11 can be achieved exclusively within the framework of the kick-out diffusion theory. This predicts that the diffusion profiles in a "thin", dislocation-free wafer of thickness d obey the relationship [1,18]

$$\mathrm{erf}[(\ln C_s/C_s^m)^{1/2}] = |(d/2-x)/(d/2)|, \qquad (8)$$

irrespective of the temperature and duration of diffusion ($C_s^m \equiv C_s(x = d/2)$). Fig. 12 demonstrates convincingly for the Au diffusion profile measured after a 1.03 h anneal at 1237 K (empty squares in Fig. 11) that the experimental data (open symbols)

[3] A wafer (plate-shaped specimen) is called "thin" when the foreign atoms penetrating from the opposite surfaces interfere in the specimen centre. If this is not the case, a specimen is referred to as "thick".

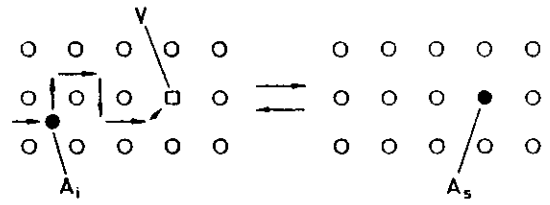

Fig. 10. Dissociative mechanism: Foreign atoms (full circle) interchange between interstitial sites (A_i) and substitutional sites (A_s) in cooperation with vacancies (V).

lie on the solid straight line representing (8), whereas the profile form expected on the basis of dissociative diffusion (dashed line) cannot be adjusted to these data.

Further typical features of kick-out diffusion emerge from the expression for the A_s concentration in the centre of a dislocation-free wafer [1,18],

$$C_s^m/C_s^{eq} = (2/d)(\pi D_I^{\circ} t)^{1/2} \qquad (9)$$

(which ceases to be valid if C_s^m comes close to C_s^{eq}). For Au and Pt Figs. 13 and 14 respectively confirm the dependencies of C_s^m on the diffusion time ($\sim t^{1/2}$) and the wafer thickness ($\sim 1/d$) as stated by Eq. (9) (solid straight lines). By contrast, dissociative diffusion (dashed curves) cannot account for the t and d dependencies of C_s^m found by experiment.

For kick-out diffusion into a dislocation-free, semi-infinite solid, an analytical solution of (4) with (7) is available in a parametric form [24], which is not reproduced here. In Fig. 15 this solution has been adjusted successfully (solid curve) to a diffusion profile of Pt measured by means of neutron activation analysis on a "thick" dislocation-free Si specimen (full circles). On the other hand, an attempt to fit the corresponding solution for dissociative diffusion (dashed curve) to the experimental data has obviously failed.

In summary of Sect. 1.4.1 it is concluded that the diffusion of Au and Pt into Si occurs via the kick-out mechanism and that in dislocation-free specimens the effective diffusivity of the substitutional fraction of these elements (which in the solubility limit is close to 100%) is controlled by the out-diffusion to the specimen surface of the self-interstitials produced in the kick-out reaction (2).

A third hybrid in Si that undergoes kick-out diffusion is Zn. For details on this the reader is referred to [25].

1.4.2. Information on self-diffusion from the diffusivities and solubilities of hybrids

A major objective of this paper is to focus attention on the interplay of foreign-atom diffusion and self-diffusion and on how this can be exploited to improve our understanding of diffusion mechanisms. Having this in mind, the interpretation of the diffusion of Au and Pt in dislocation-free Si as self-interstitial-controlled kick-out diffusion (Sect. 1.4.1) makes us watch out for a quantitative link between the diffusivities of hybrids and the interstitialcy component of the self-diffusion coefficient. Indeed, such a relationship follows from (7) [1,17,26]:

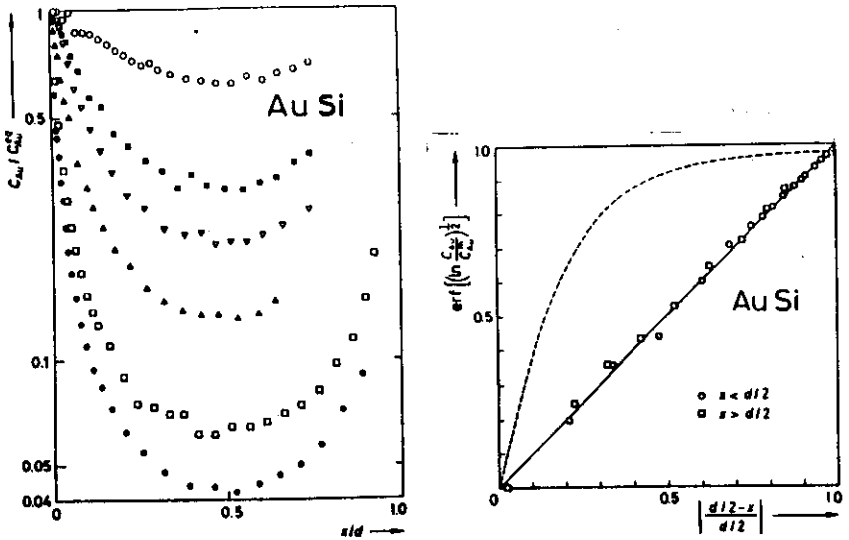

Fig. 11 (left). Penetration profiles of Au in dislocation-free Si wafers measured by means of neutron activation analysis after annealing at 1237 K for 0.467 h (full circles), 1.03 h (empty squares), 4.27 h (full and empty triangles), 26.8 h (full squares), and 100.6 h (empty circles), respectively [13]. The Au concentration C_{Au} is given in units of the solubility limit C_{Au}^{eq}. In one of the 4.27 h anneals (empty triangles) a 300 μm thick wafer was used; otherwise the wafer thicknesses were d = 500 μm.

Fig. 12 (right). Au diffusion profile measured by neutron activation analysis on a 500 μm thick, dislocation-free Si wafer after a 1.03 h anneal at 1237 K (empty symbols) [13] compared with the predictions of the kick-out model (solid straight line according to (8)) and the dissociative model (dashed curve according to (7) in [22]).

$$D_I C_I^{eq} = D_I^{\circ} C_s^{eq}. \tag{10}$$

Choosing 0.5 for the correlation factor f_I, with the aid of Eq. (10) the contribution

$$D_I^T \equiv f_I D_I C_I^{eq} \tag{11}$$

of self-interstitials to the tracer self-diffusion coefficient D^T has been calculated from the effective diffusivities D_I° and the solubilities C_s^{eq} of Au and Pt. In Fig. 16 the D_I^T values obtained in this way are represented by full symbols. They obey the Arrhenius law (solid straight line)

$$D_I^T = \left(3.5\ ^{+1.2}_{-0.9}\right)\times 10^{-4}\exp\left[-(4.81\pm 0.03)\mathrm{eV}/kT\right]\mathrm{m^2 s^{-1}} \tag{12}$$

(k = Boltzmann's constant, T = absolute temperature) over many orders of magnitude and are in good agreement with directly measured values of the tracer self-diffusion coefficient D^T (open symbols), at least above about 1200 K. This strongly suggests that — in the entire temperature regime in which data on both D^T and D_I^T are available — self-diffusion in Si is dominated by an interstitialcy mechanism. The fact

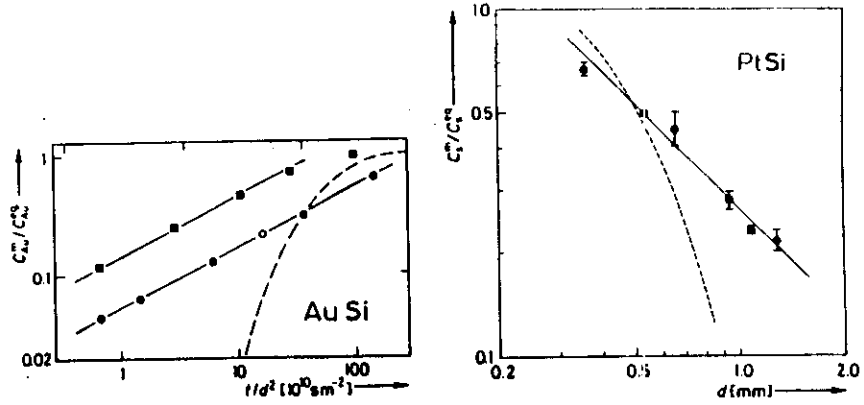

Fig. 13 (left). Increase of the Au concentration C_{Au}^m in the centres of dislocation-free Si wafers as a function of t/d^2 (full circles: 1237 K, d = 500 μm; empty circle: 1237 K, d = 300 μm; full squares: 1371 K, d = 500 μm) [13].

Fig. 14 (right). C_s^m measured by the spreading-resistance technique on dislocation-free Si wafers after 3.5 h Pt diffusion anneals at 1423 K as a function of the wafer thickness d (full circles) [23] compared with the predictions of the kick-out model (solid straight line according to (9)) and the dissociative model (dashed curve according to (7) in [22]).

that below 1200 K the D^T data lie slightly above the Arrhenius line (12), whereas the D_I^T data fall somewhat below it, might indicate the existence of a vacancy contribution to self-diffusion at low temperatures, as proposed by Seeger and Chik [31] already in 1968. Further pieces of evidence for this are the coexistence of vacancies and self-interstitials in thermal equilibrium as demonstrated by the surface oxidation/nitridation experiments reported in Sect. 1.3, the presence of a small contribution to the diffusivity of Au in Si by the dissociative mechanism (Sect. 1.5.2), and a "hidden similarity" to the self-diffusion in Ge (Sects. 3.1 and 3.2.1) which takes place by means of vacancies (Sect. 2.3).

Finally, we call attention to the pre-exponential factor of D_I^T (Eq. (12)), which — in agreement with the results of Si self-diffusion studies (Eqs. (16) and (17) in [17]) — is considerably larger than the pre-exponential factors of the self-diffusion coefficients of "normal" metals. An explanation of this is proposed in Sect. 3.2.1.

1.5. Extensions and refinements

1.5.1. Diffusion of substitutional solutes

In Sect. 1.3 it was shown (i) that the diffusion of substitutional solutes in Si occurs by indirect diffusion mechanisms involving self-interstitials and vacancies and (ii) that smallness and Group-III membership of a solute favour diffusion via self-interstitials, whereas largeness and Group-V membership foster diffusion via vacancies.

The variation of the relative importance of the two kinds of diffusion vehicles from solute to solute, as expressed by Item (ii), can qualitatively be explained in terms

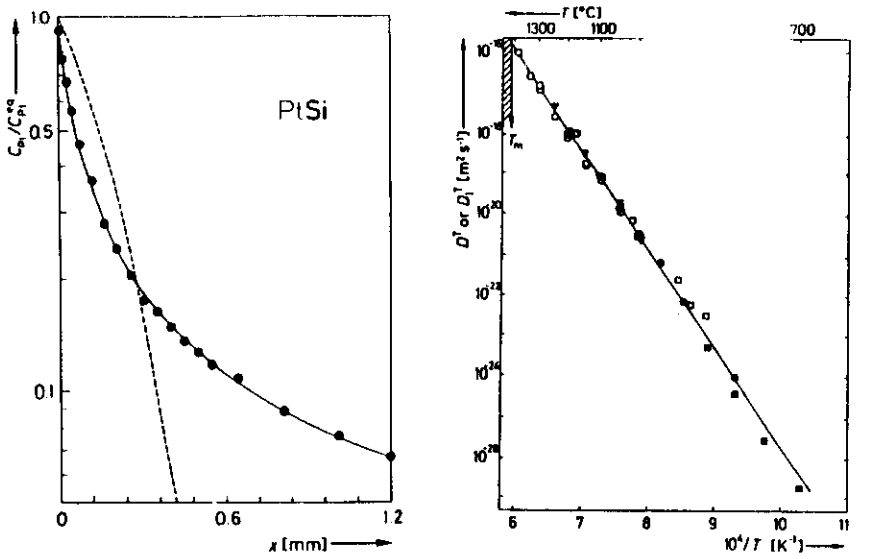

Fig. 15 (left). Pt diffusion profile measured by neutron activation analysis on a 4.9 mm thick, dislocation-free Si specimen after a 0.5 h anneal at 1523 K (full circles) [23] compared with the predictions of the kick-out model (solid curve according to (43) in [24]) and the dissociative model (dashed curve according to (5) in [22]).

Fig. 16 (right). Arrhenius plots of data on the tracer self-diffusion coefficient D^T (empty circles [27] and empty squares [28,29]) and its interstitialcy component D_I^T (full symbols) in Si. The D_I^T data originate from studies of Au in Si (full circles [14,16,26]) and Pt in Si (full triangles [23] and full squares [30]). The straight line is a least-squares fit of an Arrhenius law to the D_I^T data from [14,16,26] and [23].

of a competition of elastic and electrostatic interactions between the solutes and the diffusion vehicles (Sect. 1.3) [1]. An understanding of more subtle features of substitutional-solute diffusion (e.g., the influence of chemical doping or the kink-and-tail shape of phosphorus diffusion profiles) requires that at least two more effects have to be taken into account, which will be discussed briefly in what follows.

Depending on the position of the Fermi level the diffusion vehicles may occur in different electrical charge states. Si self-interstitials are negatively charged in n-type material, electrically neutral in intrinsic material, and positively charged in p-type material [1,32].[2)] By contrast, due to their major acceptor level in the lower half of the band gap, Si vacancies are electrically neutral in p-type material and negatively charged otherwise.[1)] It is obvious that both the thermal-equilibrium concentrations and the diffusivities of intrinsic defects may be charge-dependent. Indeed, in order to understand the influence of chemical doping on the diffusivities of substitutional solutes in Si in terms of the mechanisms proposed in Sect. 1.3 and condensed above to Items (i) and (ii), one has to allow for a doping dependence of the thermal-equilibrium concentrations of self-interstitials and vacancies which is in accordance with the electronic levels of these defects. Details are found in [1].

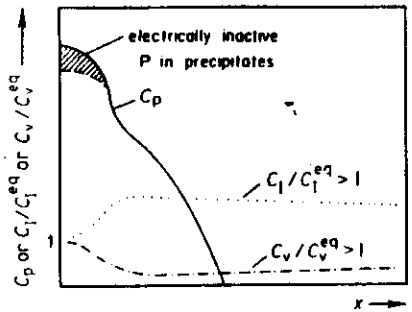

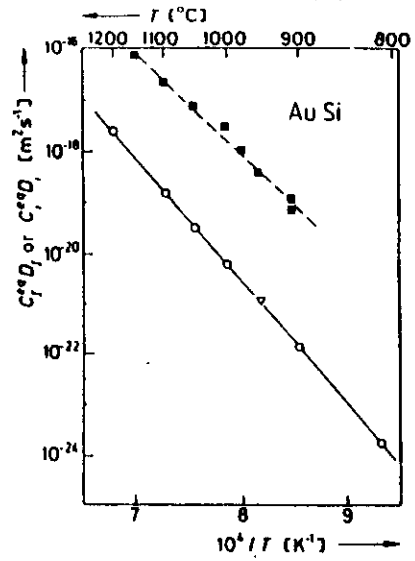

Fig. 17 (left). Schematic plots of the phosphorus concentration C_P and of the normalized concentrations of vacancies, C_V/C_V^{eq}, and self-interstitials, C_I/C_I^{eq}, as functions of the penetration depth x [36].

Fig. 18 (right). Arrhenius plots of the diffusion fluxes of self-interstitials, $D_IC_I^{eq}$ (solid line), and interstitial Au atoms, $D_IC_I^{eq}$ (dashed line) [16]. The data result from measurements of the Au diffusion in dislocation-free (empty symbols) and highly dislocated (full squares) Si, respectively.

A complete understanding of all features of substitutional-solute diffusion in Si is not possible in terms of indirect diffusion via the vacancy (Fig. 3) and the interstitialcy (Fig. 4) mechanisms alone. An example is the in-diffusion of phosphorus driven by a high P concentration at the specimen surface [33–36]. In this case the P diffusion profile possesses a kink-and-tail shape, which is schematically shown in Fig. 17. Gösele and Tan [36] have proposed that phosphorus interstitials penetrate from the specimen surface by direct diffusion (Fig. 2) and, some distance below the surface, convert to substitutional P plus self-interstitials (Reaction (2)). In the depth in which this conversion takes place, a supersaturation of self-interstitials is built up (Fig. 17). Due to $\Phi_I \approx 1$ for P, this gives rise to enhanced P diffusion by both the interstitialcy mechanism (Fig. 4) and the kick-out mechanism (Fig. 9). The result is a tail in the diffusion profile.

The preceding explanation is supported by the observation that in "buried layers" of Sb the diffusion of Sb is retarded under surface areas covered by P in high concentration [37,38]. In those regions the P-induced supersaturation of self-interstitials leads to an undersaturation of vacancies according to the mass-action law

$$C_IC_V = C_I^{eq}C_V^{eq} , \qquad (13)$$

which has been found to be fulfilled in surface oxidation/nitridation experiments [8]. It is clear that $C_V/C_V^{eq} < 1$ results in a retardation of the diffusion of Sb, for

which $\Phi_V \approx 1$.

There are several extensions of the Gösele–Tan model of P diffusion, the most general one being that of Morehead and Lever [39]. These authors assume that — in addition to I and V — P_i (P interstitials or pairs of I and substitutional P) and PV (substitutional-P–V pairs) are mobile defects which are involved in the diffusion of P, that all mobile species are present in concentrations which are very small in comparison with that of immobile substitutional P, and that a steady-state solution with respect to the sum of fluxes of the mobile species is established. This model indeed produces a kink-and-tail profile for the substitutional phosphorus.

1.5.2. A dissociative admixture in the diffusion of Au

In Sect. 1.4.1 evidence has been presented that in dislocation-free Si the hybrids Au and Pt diffuse by the kick-out mechanism. Stimulated by the coexistence of self-interstitials and vacancies in thermal equilibrium (Sect. 1.3) Morehead and co-workers [40] analyzed Au diffusion profiles measured at 1273 K in terms of a diffusion model which comprises both kick-out and dissociative diffusion. They came to the conclusion that — although at this temperature $D_V C_V^{eq} = D_I C_I^{eq}$ — the dissociative contribution is negligibly small, except for very long diffusion times (≈ 100 h) at which it amounts to about 10%. This result can be rationalized as follows. According to Eqs. (6) and (7) the effective diffusion coefficient for combined kick-out and dissociative diffusion is given by

$$D_s^{eff} = D_V^{*} + D_I^{*}(C_s^{eq}/C_s)^2 \quad , \tag{14}$$

which for $D_V C_V^{eq} = D_I C_I^{eq}$ reduces to

$$D_s^{eff} = D_V^{*}[1 + (C_s^{eq}/C_s)^2] \quad . \tag{15}$$

In (15) the second term in brackets arises from kick-out diffusion. Therefore, in in-diffusion experiments kick-out diffusion dominates over dissociative diffusion at small diffusion times at which $C_s < C_s^{eq}$ is fulfilled, even if the contributions by the vacancy mechanism and the interstitialcy mechanism to self-diffusion are comparable. The physical reason for this is that at the beginning of an in-diffusion experiment ($C_s \ll C_s^{eq}$) almost each regular lattice site is available for being occupied by a substitutional Au atom via a kick-out reaction (2), whereas the rate of dissociative diffusion is limited by the (comparatively small number of) vacancies present in thermal equilibrium.

1.5.3. Gold-interstitial-controlled kick-out diffusion and related subjects

The in-diffusion of hybrid solutes, say Au atoms, into Si via the kick-out mechanism occurs in three steps: (A) Au_i atoms penetrate into Si and diffuse rapidly over large distances, (B) the Au_i atoms are transformed to Au_s atoms according to Reaction (2), by which I are produced in supersaturation; (C) this supersaturation decays by interstitialcy self-diffusion to sinks. So far we have dealt with kick-out diffusion in dislocation-free high-purity specimens, in which the densities of internal sinks for I are extremely small. In such specimens, Step (C) is slowest and thus rate-controlling, since the kicked-out self-interstitials have to diffuse over large distances to the specimen surfaces in order to be annihilated. By contrast, in heavily dislocated and/or impure specimens the high internal densities of I sinks enforce C_I values close to C_I^{eq}, irrespective of the self-interstitial kicking-out rate, so that Step (A) becomes rate-controlling. Under these circumstances, D_s^{eff} is independent of x and t (Eq. (5)), which explains why in-diffusion profiles of Au in "thick", highly dislocated specimens are erfc-shaped [1,18]. From such profiles the Au_i flux $D_I C_I^{eq}$ has been extracted [16]. In Fig. 18 it is compared to the self-interstitial flux $D_I C_I^{eq}$ taken from corresponding measurements on dislocation-free specimens. Since at all temperatures at which data are available $D_i C_i^{eq}$ is considerably larger than $D_I C_I^{eq}$, the prerequisite $D_I^{*} > D_I^{*}(C_s^{eq}/C_s)^2$ for the occurrence of profiles which are characteristic of self-interstitial-controlled kick-out diffusion is fulfilled in all pure, dislocation-free specimens, except for $C_s/C_s^{eq} \ll 1$.

According to the preceding discussion, Au_i-controlled kick-out diffusion takes place either in specimens with high densities of internal sinks for self-interstitials (i.e. in highly dislocated and/or impure Si), in which the self-interstitials kicked out by Au_i atoms can disappear instantaneously, or in I-sink-free (i.e. dislocation-free high-purity) specimens as long as these are almost "Au_s-empty" ($C_s/C_s^{eq} \ll 1$), so that a supersaturation of self-interstitials blocking further $Au_i \rightarrow Au_s$ transitions via (2) does not yet exist. An example of the latter case has been detected by Hauber et al. [15], who measured penetration profiles of Au in dislocation-free Si wafers of different thickness which had been diffusion-annealed for equal periods of time at 1473 K. He found the time dependence predicted by (9), except for his thickest wafer on which too low a value of C_s^m was measured. In this case C_s^m/C_s^{eq} was equal to 0.07, and the deviation from (9) — which is based on the assumption of self-interstitial-controlled kick-out diffusion — reflects that in "gold-empty" specimens kick-out diffusion is Au_i-controlled even in the absence of internal sinks.

A further example of Au_i-limited kick-out diffusion is realized in so-called isoconcentration experiments, in which the in-diffusion of radioactive ^{198}Au into dislocation-free specimens saturated with ^{197}Au is investigated [16]. In this case C_s, C_i, and C_I possess their equilibrium values already at the onset of the in-diffusion of ^{198}Au. As a consequence, the penetration of $^{198}Au_i$ atoms does not induce a further shift of Reaction (2) to its right-hand side, i.e., a supersaturation of I impeding the in-diffusion process is not built up. Therefore, in isoconcentration experiments the chain of reactions required for kick-out diffusion is controlled by the influx of $^{198}Au_i$ atoms, and the effective diffusion coefficient is given by (5). This has been confirmed in recent experiments by Kühn [41].

Interesting phenomena occur when Au diffuses into specimens consisting of a large fraction of I-sink-free volume in which small regions with a high I-sink density are embedded. Then the rate of increase of C_s in the small high-sink-density regions is Au_i-controlled and thus considerably higher than in the surrounding sink-free volume in which the diffusion is I-controlled. As a result, in an intermediate stage of such an in-diffusion process (which precedes the final state in which C_s has reached its solubility limit C_s^{eq} in the entire specimen) Au_s has accumulated preferentially in the high-sink-density regions, i.e., these regions have become "decorated" with gold. In accordance with this picture, spreading-resistance profiles measured on moderately dislocated Si specimens (5×10^8 dislocations/m^2) after Au diffusion annealing at 1273 K show peaks (indicating high local concentrations of Au_s) at locations where bundles of dislocations are observed by means of an etch pit technique [42].

An example of gold decoration leading to far-reaching conclusions is the W-shaped spreading-resistance profiles measured on FZ-Si wafers after Au diffusion annealing (Fig. 19, top). The mechanism by which such profiles are formed is as follows [15]. In the diffusion of Au into a dislocation-free wafer, a supersaturation of self-interstitials is produced via Reaction (2). If the wafer contains a small amount of impurities (e.g., some carbon), which can act as nuclei for "heterogeneous precipitation" of self-interstitials, then this precipitation happens most likely in the specimen centre, since at this location — due to its maximum separation from the surfaces — the I supersaturation is highest. While the so-produced self-interstitial clusters grow, their efficiency as sinks for I becomes larger, and thus in the wafer centre the production rate of Au_s via (2) is enhanced in an avalanche-like manner.

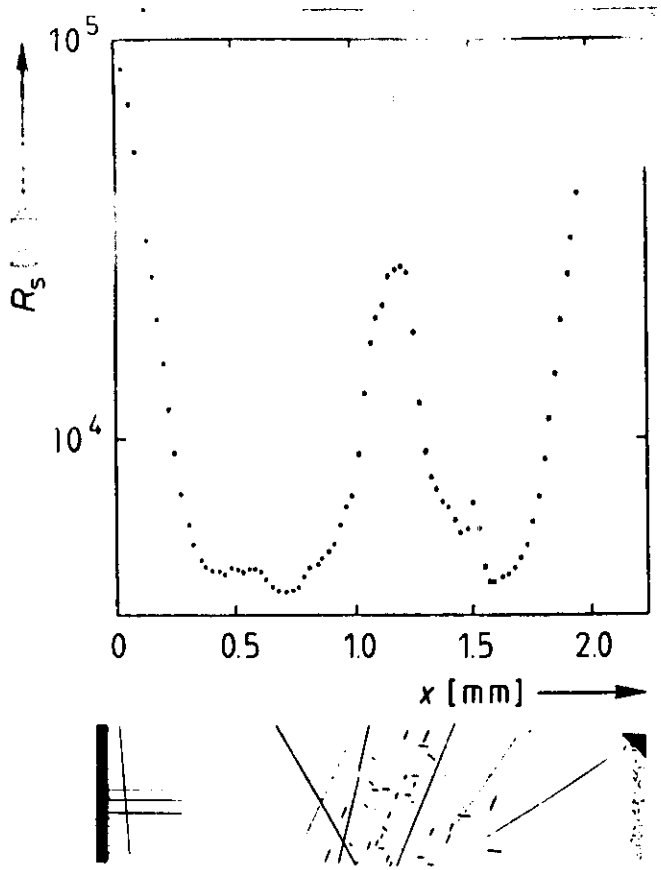

Fig. 19. W-shaped spreading-resistance profile (top) measured on a Si specimen after a 45 min Au diffusion anneal at 1473 K [15]. The peak in this profile is located at the depth at which the optical micrograph (bottom) [15] of the plane across which the profile has been measured shows many stacking faults (short strokes). The long straight lines are scratches.

The preceding explanation of the formation of W profiles is confirmed by the following observations. In the centres of wafers showing W-shaped profiles, dislocation loops are produced *during* the in-diffusion of Au. This was demonstrated by taking optical micrographs of bevel planes running from one wafer surface to the other. These planes were produced by lapping. They were etched before their investigation in the microscope. Faulted dislocation loops in the central part of a wafer, which pierce the micrographed plane (Fig 19, bottom), were *exclusively* observed *after* Au diffusion annealing. From electron microscopy the nature of these loops was found to be interstitial-type [15].

It is important to note that the interstitial nature of the dislocation loops produced concomitantly with W-shaped Au diffusion profiles is in accordance with kick-out diffusion, but — taken alone — does not exclude dissociative diffusion. If Au in Si diffused by the dissociative mechanism, according to Eq. (3) in V-source-poor crystals the in-diffusion of Au would generate an undersaturation of vacancies. In the presence of nuclei for I precipitates this V undersaturation could act as a driving force for the growth of interstitial-type dislocation loops by vacancy emission. Hence, in order to exclude this possibility one has also to take into account the characteristic features of kick-out diffusion found in Au or Pt diffusion experiments on pure dislocation-free Si, in particular the extraordinary "thin"-wafer diffusion profiles (Eq. (8) and Fig. 12) together with their time evolution and their dependence on the wafer thickness (Eq. (9) and Figs. 13 and 14) as well as the shape of diffusion profiles in "thick" specimens ([26] and Fig. 15).

According to the preceding discussion, the specific U shape (8) of hybrid diffusion profiles in dislocation-free high-purity Si wafers allows us to discriminate between kick-out diffusion and dissociative diffusion in favour of the kick-out mechanism, whereas the interstitial nature of the Au-diffusion-induced dislocation loops in wafers with W-shaped profiles is in accordance with both kick-out and dissociative diffusion. Interestingly enough, one might invoke an alternative mechanism to kick-out diffusion by replacing Reaction (2) by

$$A_s V \rightleftharpoons A_s + V \,. \tag{16}$$

In this mechanism the transport of A atoms would occur by fast diffusing substitutional-A-atom—vacancy pairs (A_sV), which break up in sessile A_s atoms plus mobile vacancies. Obviously, in dislocation-free high-purity specimens this mechanism would be controlled by the diffusion to the specimen surface of the vacancies produced by Reaction (16), and thus — in analogy to (7) — in such specimens the effective diffusion coefficient of A_s would be given by

$$D_s^{\text{eff}} \equiv D_V^{*}(C_s^{eq}/C_s)^2 \equiv (D_V C_V^{eq}/C_s^{eq})(C_s^{eq}/C_s)^2 . \tag{17}$$

Since this D_s^{eff} depends on C_s in the same way as the D_s^{eff} for I-controlled kick-out diffusion (Eq. (7)), there would be no way to distinguish between kick-out diffusion and the diffusion mechanism involving Reaction (16) on the basis of the shapes of the diffusion profiles observed. However, for the diffusion of Au in Si the A_sV-pair mechanism may safely be excluded, since the dislocation loops found in wafers showing W-shaped profiles would have to result from the condensation of vacancies and therefore be of vacancy type if this mechanism were operative.

1.5.4. Simultaneous diffusion of Au and other elements

In conclusion of the discussion of hybrid diffusion in Si, attention is drawn to two recent observations which spectacularly demonstrate the interplay between the kick-out diffusion of Au and co-diffusing elements.

Czaputa et al. [43], who studied the in-diffusion of Au into Rh-doped dislocation-free Si, report that doping with Rh enhances the introduction rate of Au_s considerably. They convincingly explain this finding as follows. Au_i atoms can become substitutional not only by Reaction (2), but also by replacing substitutional Rh according to

$$Au_i + Rh_s \rightarrow Au_s + Rh_i \,. \tag{18}$$

Provided that Rh interstitials diffuse faster than self-interstitials, the in-diffusion of Au in Rh-doped Si is Rh_i-controlled and faster than the I-controlled in-diffusion of Au in dislocation- and Rh-free Si.

An and collaborators [44] found an enhancement of the diffusion of B in those parts of their Si specimens which lay under surface areas on which Au had been deposited. The explanation is straightforward: Au interstitials penetrating from the surface produce a self-interstitial supersaturation via Reaction (2). As a result, the interstitialcy diffusion of B is enhanced. This mechanism is a variant on the classical emitter push effect [45], in which Au has taken over the role originally played by P.

2. GERMANIUM

2.1. General remarks

Many investigators have measured the tracer self-diffusion coefficient D^T of Ge [46–50]. Even the recent data of Werner and collaborators [50], which cover the widest temperature regime so far investigated (808 K — 1177 K), may be well described by a simple Arrhenius law:

$$D^T = (1.36 \pm 0.15) \times 10^{-3} \exp[-(3.09 \pm 0.02)\text{eV}/kT]\,\text{m}^2\text{s}^{-1}. \qquad (19)$$

Already in 1968 Seeger and Chik [31] argued that this observation may be accounted for in terms of an indirect self-diffusion mechanism involving one type of intrinsic defects, presumably monovacancies. Further experimental results put together by Frank et al. [1] confirmed this interpretation.

Like in the case of Si, the most reliable information on the self-diffusion mechanism in Ge comes from studies of interstitial–substitutional diffusion. An appropriate candidate for such investigations is Cu, which is a hybrid solute in Ge obeying (1a) and (1b). In Sect. 2.2 spreading-resistance data on the diffusion of Cu in Ge will be reported and compared with the predictions of the theories of kick-out and dissociative diffusion. The implications of this analysis with regard to the mechanism of self-diffusion in Ge will be considered in Sect. 2.3.

2.2. Evidence for dissociative diffusion of Cu

The full circles in Fig. 20 mark a penetration profile of Cu in a "thick", dislocation-free, high-purity Ge specimen. The solid curve represents a fit of the diffusion profile which is predicted by the dissociative-diffusion model for a V-source-free medium and the appropriate boundary condition. From the good quality of this fit and from the failure to adjust a kick-out diffusion profile to these data (dashed curve) it is concluded that Cu diffuses in Ge by the dissociative mechanism. More details, in particular an explanation of the great-depth deviation of the experimental data from the theoretical dissociative-diffusion profile, were given elsewhere [22].

2.3. Information on self-diffusion from the diffusivity and solubility of Cu

From Eq. (6) defining the dissociative diffusivity D_V^* in V-source-free specimens, one realizes that the contribution D_V^T of monovacancies to the self-diffusion coefficient in Ge,

$$D_V^T \equiv f_V D_V C_V^{eq}, \qquad (20)$$

may be calculated from the correlation factor f_V for tracer self-diffusion via monovacancies (which in diamond structures is equal to 0.5) and from the diffusivity D_V^* and the substitutional solubility C_s^{eq} of Cu in dislocation-free high-purity Ge

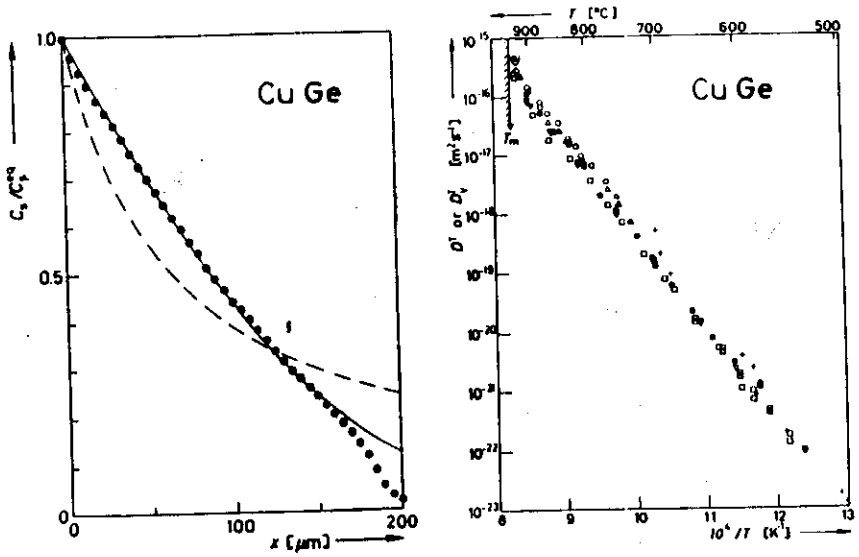

Fig. 20 (left). Cu diffusion profile measured by the spreading-resistance technique on a "thick", dislocation-free Ge specimen after a 1 h anneal at 951 K (full circles) [26] compared with the dissociative model (solid curve according to (5) in [22]) and the kick-out model (dashed curve according to (43) in [24]).

Fig. 21 (right). Arrhenius plots of data on the Ge tracer self-diffusion coefficient D^T (empty symbols [46–50]) and its vacancy component D_V^T. The D_V^T data originate from studies of Cu in dislocated (crosses [51–53]) and dislocation-free (full circles [22,26]) Ge.

[22,26]. Fig. 21 shows D_V^T values calculated in this way (full circles) as well as measured values of the Ge tracer self-diffusion coefficient D^T (empty symbols). The crosses mark D_V^T values deduced from data on the diffusivity of Cu in Ge with intermediate dislocation density [51–53]. These D_V^T values are less reliable than those derived from Cu diffusivity data on dislocation-free Ge, since their calculation requires the knowledge of the (only inaccurately known) dislocation density [1,18]. The coincidence of the data on D_V^T, describable by

$$D_V^T = (2.13 \pm 1.2) \times 10^{-3} \exp[-(3.11 \pm 0.05)\text{eV}/kT]\ \text{m}^2\text{s}^{-1}, \qquad (21)$$

and D^T (Eq. (19)) over many orders of magnitude makes us conclude that Ge self-diffusion takes place exclusively by monovacancies.

A striking feature of (19) and (21) is the magnitude of the pre-exponential factor. On the one hand, it is clearly greater than the pre-exponential factors of the self-diffusion coefficients of "normal" metals; on the other hand, it lies about an order of magnitude below the corresponding quantity for Si (Eq. (12)). We will return to this point in Sect. 3.2.2.

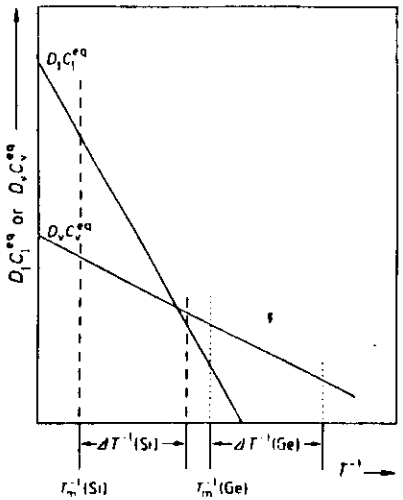

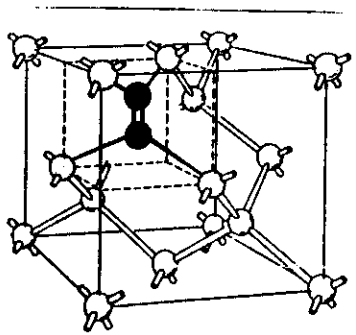

Fig. 22 (left). Schematic diagram illustrating the dominance of self-interstitials in Si and vacancies in Ge under thermal-equilibrium conditions.

Fig. 23 (right). Electrically neutral low-temperature configuration of the self-interstitial in Si [55].

2.4. Diffusion of substitutional solutes

The influence of doping by elements of Group III or V on Ge self-diffusion is in accordance with the conclusion of Sect. 2.3 that self-diffusion in Ge occurs via monovacancies [1]. (The Ge self-diffusion coefficient is enhanced by n doping and decreased by p doping. This is expected if vacancies in Ge possess an acceptor level in the lower half of the band gap and if the doping dependence of the self-diffusivity arises from the dependence of the vacancy formation enthalpy on the position of the Fermi level.) The fact that the diffusivities of Group-III and Group-V elements in Ge show the same doping dependence as the Ge self-diffusion coefficient is therefore not surprising, but may be taken as an indication that these solutes diffuse in Ge via the vacancy mechanism, too. In fact, this view is confirmed further by the observations that the diffusivities of the Group-III elements are very similar to the self-diffusion coefficient (exceeding it by not more than an order of magnitude at the melting temperature), whereas the diffusivities of the Group-V elements are considerably larger (by two orders of magnitude or more) than the self-diffusion coefficient: For Group-V donors, the probability to find acceptor-type vacancies on nearest-neighbour sites and thus to be able to perform diffusional jumps is enhanced by Coulomb attraction, whereas for the Group-III acceptors this enhancement effect does not exist.

3. SILICON VERSUS GERMANIUM

3.1. The "hidden similarity"

Many properties of the two elemental semiconductors Si and Ge are very similar. Therefore, at first sight it is surprising that — according to Sects. 1 and 2 — the two elements seem to differ radically with respect to the thermal-equilibrium defects and the mechanisms of diffusion. In the following, evidence for the view will be presented that in Si and Ge the basic thermal-defect and diffusion scenarios are qualitatively the same, but that in the two materials quantitatively different aspects are revealed in the temperature intervals respectively accessible by experiments.

In order to put the above idea in concrete terms, let us consider Fig. 22. This is a schematic logarithmic plot of the thermal-equilibrium fluxes of vacancies, $D_V C_V^{eq}$, and self-interstitials, $D_I C_I^{eq}$, as functions of T^{-1}, where the scales of both coordinates are different for Si and Ge. ΔT^{-1}(Si) and ΔT^{-1}(Ge) represent the temperature intervals which have been covered in diffusion experiments on Si and Ge, respectively. One recognizes that in Si self-interstitials are the dominant thermal-equilibrium defects (compare $D^T \approx D_I^T$ (Sect. 1.4.2)), except at the low-temperature end of ΔT^{-1}(Si) (corresponding to about 1000 °C (Sect. 1.5.2)) where $D_V C_V^{eq}$ and $D_I C_I^{eq}$ become comparable. By contrast, in Ge the self-interstitial contribution is negligibly small in the entire ΔT^{-1}(Ge) regime in comparison to the vacancy contribution.

The concept developed above and illustrated in Fig. 22 may be reduced to an extremely simple statement: The essential differences between the thermal-defect and diffusion scenarios of Si and Ge arise from the fact that, by contrast to Ge, Si does not melt before $D_I C_I^{eq}$ exceeds $D_V C_V^{eq}$. In Sect. 3.2 it will be argued that this property is related to the pronounced mass-density anomaly of Si at melting.

3.2. Extended atomic defects at high temperatures

3.2.1. "Liquid" self-interstitials

As already pointed out in Sect. 1.4.2, the pre-exponential factor of the self-diffusion coefficient of Si (henceforth called $D_{I,0}^T$) is extraordinarily large. According to Seeger and Chik [31,54] such a large $D_{I,0}^T$ value would be incomprehensible if the carriers of Si self-diffusion were normal point defects or small point-defect agglomerates. Therefore, these authors proposed that under high-temperature equilibrium conditions Si self-interstitials are "extended", i.e., that the extra atom representing a self-interstitial is spread out over, say, 10 atomic volumes. This extended defect configuration may be realized by many microscopically different states. Therefore, it possesses a large configurational entropy. Its number of potential diffusion paths is very great, too. Hence, both its formation entropy S_I^F and its migration entropy S_I^M are large.

In order to account for the $D_{I,0}^T$ value found for Si, $S_I^F + S_I^M$, which enters $D_{I,0}^T$ exponentially [1], must amount to about $13k$. On the other hand, from internal-friction measurements Frank [55] has concluded that Si self-interstitials frozen in at temperatures below 600 K are present in dumbbell configurations whose crystallographic orientations depend on the electrical charge state. Thus, at low and intermediate temperatures the self-interstitials in Si are real "point" defects. Fig. 23 shows the electrically neutral <100> dumbbell interstitial I^0. For this defect, at 570 K the migration enthalpy H_I^M is 1.5 eV, and S_I^F and S_I^M are of the order of magnitude of $1k$.

The preceding conclusions concerning the self-interstitial configurations in different temperature regimes can be reconciled if — proceeding from intermediate to

high temperatures — the interstitials gradually lose their dumbbell configurations and finally become spread out over several atomic volumes [32]. This picture is confirmed by the fact that, allowing for a linear temperature dependence of both the migration enthalpy H_I^M and the formation enthalpy H_I^F and taking into account the thermodynamic relationship

$$T(\partial S/\partial T)_p = (\partial H/\partial T)_p \qquad (22)$$

between enthalpies (H) and entropies (S) valid for experiments performed at constant pressure p, Seeger et al. [56] succeeded in fitting the self-diffusion data of Mayer et al. [27] by a quasi-straight Arrhenius line. In doing so, they used the above-mentioned values of H_I^M, S_I^F, and S_I^M, which characterize the "point" defect I^0 at 570 K, and obtained $H_I^F = 3$eV, $H_I^M = 2$eV, $S_I^F = 6k$, and $S_I^M = 7k$ for I^0 at 1658 K, i.e. values of S_I^F and S_I^M which are in accordance with an extended hightemperature interstitial configuration.[4]

From an atomistic point of view the change of the geometrical configuration of I^0 with increasing temperature may be described as follows [32]. In the low-temperature configuration (Fig. 23) the electrons forming the bonds between the two atoms of the dumbbell are well localized in the centre of gravity of the defect. When the temperature is raised, these electrons occupy excited states and thus become more and more delocalized. As a consequence, the dumbbell relaxes and spreads out. The concomitant increase of its formation entropy leads to a decrease of its Gibbs free energy of formation, G_I^F, according to

$$G_I^F = H_I^F - TS_I^F \,.^{[5]} \qquad (23)$$

The spreading out of the dumbbell I^0 at high temperatures not only results in a decrease of its G_I^F, but also in a reduction of its Gibbs free energy of migration, G_I^M. As mentioned above, the extended configuration possesses a greater number of diffusion paths than the dumbbell and thus a larger S_I^M. On the other hand, H_I^M is larger, too, if I^0 is extended, since then more bonds have to be broken when it migrates. Since bond breaking becomes less important when the temperature is raised, at high temperatures spreading out of the dumbbell makes G_I^M decrease.

The precedingly discussed reduction of G_I^F and G_I^M resulting from the spreading out of the self-interstitials at high temperatures can only occur in covalent structures which show a mass-density anomaly at melting. Covalency is required since the spreading-out mechanism involves electronic states localized at the self-interstitials. A density increase at melting is needed because of the following reason. If the smearing out of a point-like interstitial resulted in a disordered spot of lower average density, the surrounding crystalline matrix would be compressed

[4] At high temperatures the Fermi level approaches the centre of the forbidden gap. Hence, according to the Blount's model I^0 dominates at high temperatures [11]. Therefore, the influence of I^+ and I^- has been neglected in the self-diffusion-data analysis of Seeger et al. [56]. Because of the same reason, in the subsequent atomistic view, I^0 will be considered exclusively, though the conclusions will be valid irrespective of the charge state of the interstitial.

[5] Note that at low temperatures a spreading out of the I^0 dumbbell would result in an increase of G_I^F: In this case the electrons are well localized in covalent bonds, so that a spreading out of the dumbbell would require the breaking of strong electronic bonds and thus lead to such a large increase of H_I^F that this could not be overcompensated by the second term on the right-hand side of Eq. (23).

elastically, i.e., the smearing out would result in an enhancement of H_I^F which could not be overcompensated by the concomitant increase of S_I^F. By contrast, in materials whose densities increase at melting (e.g., Si or Ge), the smearing out of an interstitial at high temperatures leads to a disordered spot of higher density. In such crystals the compressive strain existing around a point-like interstitial and thus its contribution to H_I^F can be reduced by smearing out the defect. Hence, under these circumstances G_I^F may be lowered by "local pre-melting" of the environment of the point-like interstitial. Le Chatelier's principle tells us that this "liquidation" *does* take place. Therefore, Seeger and Chik [31,54] postulated that under thermal-equilibrium conditions the self-interstitials in Si are extended and may be considered as "liquid droplets" embedded in a crystalline matrix of lower density.

The starting point of the preceding discussion has been the huge $D_{I,O}^T$ value of Si. Now its explanation is obvious. It is due to the large value of $S_I^F+S_I^M$ of the liquid-droplet-like Si self-interstitials, which, in turn, is related to the density anomaly of Si at melting. Ge possesses a less pronounced density anomaly, so that $S_I^F+S_I^M$ and thus $D_{I,O}^T$ are smaller. As a consequence, on suitably normalized scales the temperature at which $D_IC_I^{eq}$ exceeds $D_VC_V^{eq}$ is higher in Ge than in Si (Fig. 22). Presumably, in Ge this temperature would lie even above the temperature of melting. This may explain why in Ge an influence of self-interstitials on diffusion processes has not been observed.

3.2.2. "Amorphous" vacancies

In Sect. 2.3 it has been concluded that self-diffusion in Ge takes place via monovacancies. Hence, as already realized by Seeger an Chik [31,54], the unusually large pre-exponential factor of the Ge self-diffusion coefficient (Eqs. (19) and (21)) reflects a large value of the sum of the entropies for the formation and migration of vacancies and thus indicates that under high-temperature thermal-equilibrium conditions monovacancies in Ge are spread out over about 5 atomic volumes. This phenomenon is a consequence of Le Chatelier's principle, according to which "the state of least constraint" around a vacancy can be achieved by a local phase transition to a state of lower mass density, i.e. to the amorphous phase. This "amorphization" of the vacancies is restricted to high temperatures at which — as a result of the excitation and delocalization of the valence electrons — the concomitant stretching and distortion of bonds lead to an increase of the vacancy formation enthalpy that is small enough to be overcompensated by the increase of the vacancy formation entropy.

4. ICE

In Sects. 3.1 and 3.2.1 the dominance of self-interstitials in Si under thermal-equilibrium conditions at temperatures above about 1000°C has been related to the large mass-density increase of almost 10% that Si undergoes at melting. In the light of this interpretation the corresponding density increase of 5% in the case of Ge must be considered to be too small for the occurrence of thermal self-interstitials in a detectable concentration. On the other hand, it is commonly known that at ambient pressure H_2O shows a solid–liquid phase transition at 0°C in which its density increases by about 10%. This fact leads us to the challenging question whether — like in Si that melts with the same increase of density — the thermal-equilibrium defects dominating in ice at "high" temperatures (i.e. just below 0°C) are of interstitial type. In the following, studies on ice will be reported which confirm this expectation.

A group of Japanese investigators [57–63] have demonstrated by means of high-power X-ray topography that all the concentric dislocation loops formed in nearly perfect ice single crystals during crystal growth at temperatures above −50°C are of interstitial nature. Since these loops, which represent the analogue to the A-type swirl

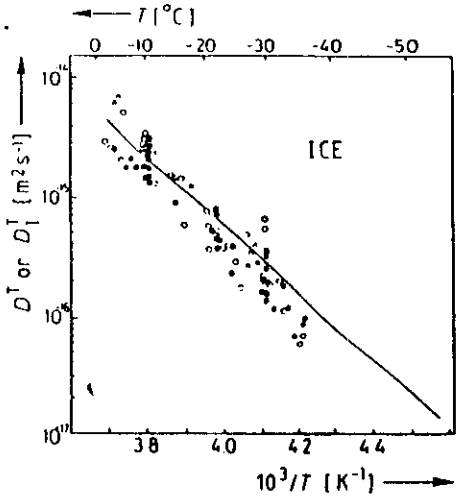

Fig. 24. Comparison of values of the self-diffusion coefficient D^T in ice measured by means of ^3H tracers (open circles: parallel to c axis, full circles: perpendicular to c axis) and ^{18}O tracers (triangles) with the self-interstitial contribution D_I^T (straight line) to D^T calculated from (24) and (25) according to (26) [61].

defects in dislocation-free Si single crystals [32], are generated by cooling-induced agglomeration of the point-defect species dominating in thermal equilibrium, this species must be of interstitial type. By measuring the size and number density of the loops in dependence of the temperature T from which the crystals have been cooled [58] and of the hydrostatic pressure p applied in some of the experiments [63], the following expression for the thermal-equilibrium concentration of self-interstitials in ice at temperatures above -30 °C has been established:

$$C_I^{eq} = (1/2)\exp(S_I^F/k)\exp[-(H_I^F+pV_I^F)/kT)] \quad . \qquad (24)$$

In Eq. (24), in which the factor 1/2 means the ratio of the numbers of interstitial sites available for H_2O molecules and regular lattice sites in the ice lattice, the quantities S_I^F, H_I^F, and the self-interstitial formation volume V_I^F possess the values $4.9k$, 0.4eV, and -0.8Ω, respectively (Ω = molecular volume). On the one hand, the large formation entropy indicates that the interstitial molecules are not well localized; on the other hand, the lattice dilatation due to an extra molecule on an interstitial site, $\Omega+V_I^F = 0.2\Omega$, is quite small. Both features are compatible with the picture of a fairly extended interstitial environment of enhanced density, but with minute displacements of the atoms from their regular lattice sites.

From in-situ X-ray topography investigations of the growth of the interstitial-type dislocation loops upon cooling, the diffusion coefficient D_I of self-interstitials in ice has been found to obey the relationship

$$D_I = 1.8\times10^{-6}\exp(-0.16\text{eV}/kT) \ \text{m}^2\text{s}^{-1} \qquad (25)$$

in the temperature regime -50 °C — -20 °C [61].

With aid of Fig. 24, which has been published by Goto et al. [61], it is

demonstrated convincingly that, at least above -40 °C, self-diffusion in ice takes place via interstitial H_2O molecules. In this figure the straight line shows the self-interstitial contribution D_I^T to the self-diffusion coefficient as calculated from Eqs. (24) and (25) according to

$$D_I^T = D_I C_I^{eq} \quad . \qquad (26)$$

The open/solid circles and the triangles represent the diffusivities of ^3H parallel/perpendicular to the c axis and of ^{18}O, respectively. Since both the ^3H and ^{18}O data follow the straight line representing (26), Goto and collaborators [61] have correctly concluded that, in the temperature regime considered, the carriers of self-diffusion in ice are interstitial H_2O molecules migrating as units. Since, in contrast to the interstitialcy self-diffusion mechanism in Si, this is a direct interstitial mechanism, it is justified that in Eq. (26) the correlation factor has been assumed to be equal to unity.

There appears to be a remarkable difference between the thermal-equilibrium structures of the self-interstitials in Si and ice. Consider a Gedankenexperiment in which an interstitial defect is produced by introduction of a marked extra atom (molecule) into the host lattice. In Si a liquid-like droplet of enhanced density is formed, within which the chemical bonds dangle to and fro between different neighbouring atoms and within which the marked atom does not play a special rôle. The droplet diffuses in the spread-out state, and after some diffusional displacements the marked atom will have been left behind on a regular Si lattice site. By contrast, after introduction of a marked extra H_2O molecule into ice the identity of this molecule remains preserved. Around it, a nearly perfect lattice region of enhanced density, but with distorted bonds and altered bond lengths is created. This region is not really liquid-like as a self-interstitial droplet in Si. In the diffusion of the ice interstitial, the extra molecule jumps onto a neighbouring interstitial site as a unit. Doing so it is followed by its cloud of enhanced density. Note that for such an interstitial H_2O molecule the number of alternative equivalent jump paths is equal to the number of interstitial nearest-neighbour sites in the ice lattice, i.e., this number is small compared with the jump possibilities of a self-interstitial droplet in Si. This picture is in accordance with the comparatively small migration entropy of the ice interstitial, as reflected by the "normal" value of the pre-exponential factor in (25).

After having elaborated on the subtle differences between the "high"-temperature configurations of the self-interstitials in Si and ice, in conclusion attention is drawn to a striking analogy between the two substances showing up at "low" temperatures. In the preceding sections, several indications have been presented which point to a dominance of the vacancies in thermal-equilibrium experiments on Si at temperatures below about 1000 °C. In the following, observations will be reported which show that the same is true for ice below about -50 °C.

Whereas cooling of ice in the temperature regime above -50 °C leads to the formation of interstitial-type prismatic dislocation loops whose diameters may reach several millimeters [58], cooling down to lower temperatures results in the appearance of minute dislocation loops of approximately 50 μm in diameter [59]. The large interstitial-type loops shrink or grow when the ice crystals are warmed up or cooled down, respectively, within the temperature regime above -50 °C [59]. In this way these loops contribute to the increase or decrease of the equilibrium concentration of the self-interstitials, which are the dominating defect species above -50 °C. By contrast, the minute loops grow or shrink when above -50 °C the temperature is raised or lowered, respectively [59]. This demonstrates that these small loops are of vacancy type: They contribute to the increase or decrease of the self-interstitial concentration by growing under interstitial emission or shrinking under interstitial absorption. Since the nucleation of the small, vacancy-type loops takes place during cooling to temperatures below -50 °C, it is concluded that the thermal-equilibrium defects dominating in ice in this temperature regime are vacancies.

ACKNOWLEDGEMENT

The author is very grateful to his collaborators, who have contributed in many ways to this work, as well as to the editors of these proceedings for their patience with regard to the delay in the submission of the manuscript.

REFERENCES

[1] Frank, W., Gösele, U., Mehrer, H., and Seeger, A., in: Diffusion in Crystalline Solids, Eds. G. E. Murch and A. S. Nowick, Academic Press, Orlando 1984 (p. 63)
[2] Kauffmann, V., Zerenner, Th., Mauritz, E., Horváth, J., and Frank, W.: to be published
[3] Booker, G. R., and Tunstall, N. J.: Phil. Mag., 1966, 13, 71
[4] Jaccodine, R. J., and Drum, C. M.: Appl. Phys. Letters, 1966, 8, 29
[5] Hu, S. M.: J. Appl. Phys., 1974, 45, 1567
[6] Mizuo, S., and Higuchi, H.: Jpn. J. Appl. Phys., 1981, 20, 739
[7] Fahey, P. M., and Dutton, R. W., in: Semiconductor Silicon 1986, Eds. H. R. Huff, T. Abe, and B. O. Kolbesen, Electrochemical Society, Pennington, N.J., 1986 (p. 571)
[8] Fahey, P. M., Griffin, P. B., and Plummer, J. D.: Rev. Mod. Phys., 1989, 61, 289
[9] Watkins, G. D., Troxell, J. D., and Chatterjee, A. P . : Inst. Phys. Conf. Ser., 1979, 46, 16
[10] Watkins, G. D., in: Defects in Semiconductors, Eds. J. Narayan and T. Y. Tan, North-Holland, New York 1981 (p. 21)
[11] Blount, E. I.: J. Appl. Phys., 1959, 30, 1218
[12] Watkins, G. D., Messmer, R. P., Weigel, C., Peak, D., and Corbett, J. W.: Phys. Rev. Letters, 1971, 27, 1573
[13] Stolwijk, N. A., Schuster, B., Hölzl, J., Mehrer, H., and Frank, W.: Physica B, 1983, 116, 335
[14] Stolwijk, N. A., Schuster, B., and Hölzl, J.: Appl. Phys. A, 1984, 33, 133
[15] Hauber, J., Stolwijk, N. A., Tapfer, L., Mehrer, H., and Frank, W.: J. Phys. C, 1986, 19, 5817
[16] Stolwijk, N. A., Hölzl, J., Frank, W., Weber, E. R., and Mehrer, H.: Appl. Phys. A, 1986, 39, 37
[17] Frank, W., and Stolwijk, N. A.: Mater. Sci. Forum, 1987, 15–18, 369
[18] Gösele, U., Frank, W., and Seeger, A.: Appl. Phys. A, 1980, 23, 361
[19] Frank, F. C., and Turnbull, D.: Phys. Rev., 1956, 104, 617
[20] Carslaw, H. S., and Jaeger, J. C.: Conduction of Heat in Solids, Oxford University Press (Clarendon), London and New York 1959
[21] Crank, J.: Mathematics of Diffusion, Oxford University Press (Clarendon), London and New York 1975
[22] Stolwijk, N. A., Frank, W., Hölzl, J., Pearton, S. J., and Haller, E. E.: J. Appl. Phys., 1985, 57, 5211
[23] Hauber, J., Frank, W. and Stolwijk, N. A.: Mater. Sci. Forum, 1989, 38–41, 707
[24] Seeger, A.: phys. stat. sol. (a), 1980, 61, 521
[25] Stolwijk, N. A., Perret, M., and Mehrer, H.: Defect and Diffusion Forum, 1988, 59, 79
[26] Stolwijk, N. A., and Frank, W., in: Proc. 13th Internat. Conf. Defects in Semiconductors, Eds. L. C. Kimerling and J. M. Parsey, Jr., Metallurgical Society of AIME, Warrendale, Pennsylvania, 1985 (p. 285)
[27] Mayer, H. J., Mehrer, H., and Maier, K.: Inst. Phys. Conf. Ser., 1977, 31, 186
[28] Kalinowski, L., and Seguin, R.: Appl. Phys. Letters, 1979, 35, 211
[29] Kalinowski, L., and Seguin, R.: Appl. Phys. Letters, 1980, 36, 171

[30] Mantovani, S., Nava, F., Nobili, C., and Ottaviani, G.: Phys. Rev. B, 1986, 33, 5536
[31] Seeger, A., and Chik, K. P.: phys. stat. sol., 1968, 29, 455
[32] Frank, W., in: Advances in Solid State Physics, Vol. 21, Ed. J. Treusch, Vieweg, Braunschweig 1981 (p. 221)
[33] Peart, R. F., and Newman, C. R.: Inst. Phys. Conf. Ser., 1973, 16, 170
[34] Yoshida, M., Arai, E., Nakamura, H., and Terunuma, Y.: J. Appl. Phys., 1974, 45, 1498
[35] Fair, R. B., and Tsai, J. C. C.: J. Electrochem. Soc., 1977, 124, 1107
[36] Gösele, U., and Tan, T. Y.: Defect and Diffusion Forum, 1988, 59, 1
[37] Fahey, P. M., Dutton, R. W., and Hu, S. M.: Appl. Phys. Letters, 1984, 48, 151
[38] Tsai, J. C. C., Schimmel, D. G., Fair, R. B., und Mazara, W.: J. Electrochem. Soc., 1987, 134, 1508
[39] Morehead, F. F., and Lever, R. F.: to be published
[40] Morehead, F. F., Stolwijk, N. A., Meyberg, W., and Gösele, U.: Appl. Phys. Letters, 1983, 42, 690
[41] Kühn, B.: personal communication
[42] Stolwijk, N. A., Hölzl, J., Frank, W., Hauber, J., and Mehrer, H.: phys. stat. sol. (a), 1987, 104, 225
[43] Czaputa, R., Krassnitzer, S., and Feichtinger, H.: Mater. Sci. Engin. B, 1989, 4, 133
[44] An, D. K., Madl, K., Barna, A., Battistic, G., and Gyulai, J.: phys. stat. sol. (a), 1989, 116, 561
[45] Strunk, H., Gösele, U., and Kolbesen, B. O.: Appl. Phys. Letters, 1979, 34, 530
[46] Letaw, H., Jr., Portnoy, W. M., and Slifkin, L.: Phys. Rev., 1956, 102, 636
[47] Widmer, H., and Gunther-Mohr, G. R.: Helv. Physica Acta, 1961, 34, 635
[48] Campell, D. R.: Phys. Rev. B, 1975, 12, 2318
[49] Vogel, G., Hettich, G., and Mehrer, H.: J. Phys. C, 1983, 16, 6197
[50] Werner, M., Mehrer, H., and Hochheimer, H. D.: Phys. Rev. B, 1985, 32, 3930
[51] Penning, P.: Phys. Rev., 1958, 110, 586
[52] Tweet, A. G.: Phys. Rev., 1957, 106, 221
[53] Woodbury, H. H., and Tyler, W. W.: Phys. Rev., 1957, 105, 84
[54] Seeger, A.: Rad. Effects, 1971, 9, 15
[55] Frank, W.: Rad. Effects, 1974, 21, 119
[56] Seeger, A., Föll, H., and Frank, W.: Inst. Phys. Conf. Ser., 1977, 31, 12
[57] Hondoh, T., Itoh, T., and Higashi, A.: Jpn. J. Appl. Phys., 1981, 20, L 737
[58] Goto, K., Hondoh, T., and Higashi, A., in: Point Defects and Defect Interactions in Metals, Eds. J. Takamura, M. Doyama, and M. Kiritani, University Press of Tokyo, Tokyo 1982 (p. 174)
[59] Hondoh, T., Itoh, T., and Higashi, A., in: Point Defects and Defect Interactions in Metals, Eds. J. Takamura, M. Doyama, and M. Kiritani, University Press of Tokyo, Tokyo 1982 (p. 599)
[60] Hondoh, T., Itoh, T., Amakai, S., Goto, K., and Higashi, A.: J. Phys. Chem., 1983, 87, 4040
[61] Goto, K., Hondoh, T., and Higashi, A.: Jpn. J. Appl. Phys., 1986, 25, 351
[62] Hondoh, T., Azuma, K., and Higashi, A.: J. Physique, 1987, 48, C1-183
[63] Goto, K., Hondoh, T., and Higashi, A.: J. Physique, 1987, 48, C1-653

Reviews available directly from the publisher
Photocopying permitted by license only

UNIFIED ANALYS[IS] OF [DIF]FUSION AND RELAXATION PRO[CESSES] IN AMORPHOUS METALL[IC ALL]OYS

H. KRONMÜ[LLER] W. FRANK

Max-Planck-Institut für Me[tallfor]schung, Institut für Physik,

and

Universität Stuttgart, Institut für Theoretische und Angewandte Physik, P.O. Box 800 665, D-7000 Stuttgart 80, Federal Republic of Germany

(Received August 4, 1988)

Self-diffusion data on amorphous metallic alloys determined in long-time radio-tracer experiments and activation-enthalpy spectra deduced from short-time structural relaxation studies on such materials are reviewed and analyzed in terms of current random transition rate models. It is shown that the seeming discrepancy between the self-diffusion enthalpies and the comparatively small enthalpies obtained from measurements of the magnetic after-effect arises from the existence of activation-enthalpy spectra. Whereas the short-time experiments reveal the small-activation-enthalpy parts of these spectra, the long-time self-diffusion experiments are controlled by the larger activation enthalpies. Assuming that the activation-enthalpy distributions are Gaussian, their characteristic parameters have been determined by comparing the two types of measurements. It is shown that the Arrhenius-type diffusion coefficients found by experiment are compatible with half-widths of the activation-enthalpy spectra of about 0.3 eV. Based on an analysis of the pre-exponential factors and other typical properties of the diffusion coefficients, potential mechanisms of the diffusion in amorphous alloys are proposed.

Key words: diffusion, relaxation, metallic glasses, radio-tracer technique, enthalpies, Arrhenius plots.

1 INTRODUCTION

A characteristic feature of amorphous metallic alloys is the occurrence of structural-relaxation phenomena in their mechanical, magnetic, and electronic properties as well as in the self-diffusion of their components. Although these effects have been studied for many years, a coherent model of structural relaxations in amorphous alloys does not yet exist.

Structural relaxation of an amorphous alloy leads from a less stable to a more stable—but still metastable—amorphous state. It has been shown by several authors that it is reasonable to distinguish between so-called reversible and irreversible relaxation phenomena.[1-5] In this context "reversible" means that within a certain regime of thermodynamic variables, say, pressure p and temperature T, the amorphous structure passes thermodynamic quasi-equilibrium states, i.e., it is fully determined by these variables of state. Thus, reversible relaxation requires that the Gibbs-free-energy barriers between the initial and the final quasi-equilibrium state of such a process are far lower than the barriers separating these states from the "true" equilibrium states of the crystalline structure. Under these conditions, which usually prevail in amorphous metallic alloys after the elimination of irreversible structural relaxations by suitable thermal treatments, it is possible to study reversible structural relaxation processes due to diffusion processes within quite a wide temperature range.

A variety of physical properties and processes are related to diffusion, e.g., the annealing out of the specific heat,[6,7] the formation of induced anisotropies,[8,9] magnetic after-effects,[10-14] the recovery of characteristic properties of the magnetic hysteresis loops,[15-18] and the annealing out of mechanical properties such as the internal friction or elastic moduli.[19,20] Hence, a prerequisite for a fundamental understanding of these structural relaxation phenomena is the knowledge of the mechanisms of diffusion in amorphous alloys and their thermodynamic parameters.

Unfortunately, the majority of experimental data on diffusion in amorphous alloys taken during the past years scatter so much that they cannot be used to deduce reliable information on the temperature dependence of the diffusion coefficients, let alone to find out the diffusion mechanisms in amorphous alloys.[21,22] One reason for this is that in most cases the applied techniques were indirect (e.g., Rutherford back-scattering of α-particles,[23] Auger electron spectroscopy,[24] growth of crystalline phases[25]) or at least not precise enough (radio-tracer techniques involving conventional specimen sectioning[26-29]) to determine diffusion coefficients with a higher than half-an-order-of-magnitude accuracy. Moreover, in most investigations it has either been overlooked or not taken into account that in as-quenched amorphous alloys the diffusivities are initially enhanced due to the presence of quenched-in excess free volume and drop drastically when this is eliminated in irreversible relaxation processes in the course of diffusion annealing.

The above-mentioned difficulties in determining diffusion coefficients in amorphous materials have recently been overcome by combining the radio-tracer technique with ion-beam sputtering for serial sectioning of the specimens and by significantly improving the smoothness of the specimen surfaces due to an elaborated preparation technique.[28-32] In this way a specimen sectioning precision of about ± 1 nm has been achieved. With these powerful tools it has been possible to show for a series of amorphous alloys that, in "relaxed" specimens in which the excess free volume had been eliminated by suitable pre-annealing treatments, the tracer self-diffusion coefficients D_R^T obey Arrhenius laws,

$$D_R^T(T) = D_0^T \exp(-H_R^T/kT), \tag{1}$$

within the temperature regimes of 200°C to 500°C covered in these experiments. In Eq. (1), H_R^T denotes an effective diffusion enthalpy, and k means Boltzmann's constant. The pre-exponential factor D_0^T may be expressed in terms of an effective diffusion entropy, S_R^T, via

$$D_0^T = D_{00}^T \exp(S_R^T/k), \tag{2}$$

where D_{00}^T is the "entropy-free" factor of D_0^T. The superscript "T" stands for "tracer self-diffusion"; the subscript "R" is a reminder that the corresponding diffusion parameters refer to amorphous quasi-equilibrium states reached after irreversible relaxation.

Magnetic after-effect measurements and studies of induced anisotropies are alternatives to diffusion experiments by which thermally activated processes in amorphous metallic alloys have been analyzed with quite a high precision. In a series of papers[8-18] it has been shown that both the time and temperature dependences of these relaxation phenomena can be described fairly well by spectra of activation enthalpies. The centres of gravity of these activation-enthalpy distributions in general lie between 0.5 and 1.0 eV below the corresponding self-diffusion enthalpies H_R^T. In the following we shall demonstrate that this seeming

discrepancy results from the different time scales used in relaxation and diffusion measurements and that the results of both types of experiments may be reconciled within a unified model for the diffusion of atoms in a network of randomly distributed barrier heights. In this context it is of interest to note that the famous model of atomic two-level systems represents a subgroup of local diffusional processes within the spectrum of thermally activated jumps to neighbouring positions.

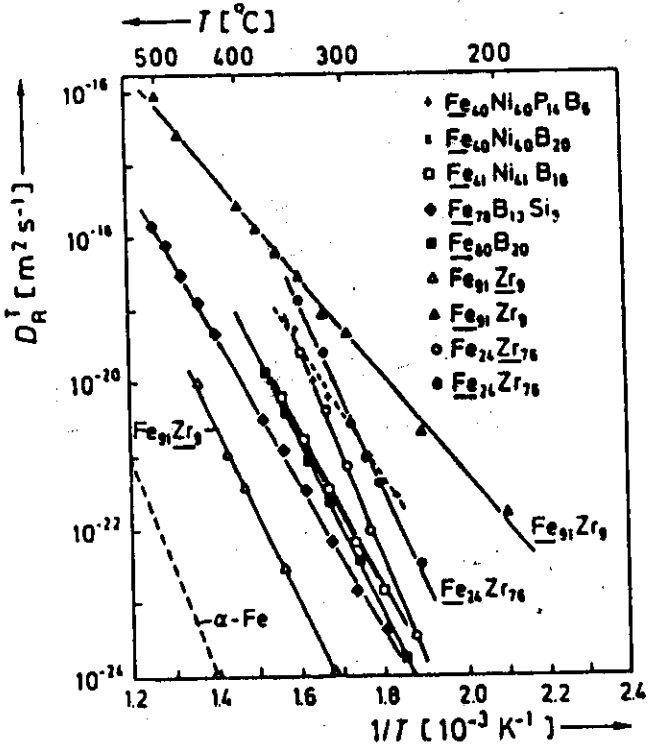

FIGURE 1 Arrhenius plots of radio-tracer self-diffusion coefficients D_R^T in relaxed amorphous alloys.[21-32,48] The diffusing elements are underlined. For comparison the self-diffusion coefficient of α-Fe has been included.

2 BRIEF REVIEW OF EXPERIMENTAL RESULTS

2.1 *Long-Range Diffusion*

Figure 1 shows the temperature dependences of the self-diffusion coefficients of the transition metals Fe and Zr in a series of pre-annealed Fe-, (Fe,Ni)-, and (Fe,Zr)-base amorphous alloys as measured by the radio-tracer technique in combination

with ion-beam sputtering.[28-32] The diffusion profiles extend over 100 to 1000 nm, i.e., in these experiments the diffusing tracer atoms perform a large number of jumps. The most surprising conclusions which may be drawn from these data are as follows:

a) In as-quenched amorphous metallic alloys the tracer self-diffusivities D^T decrease during thermal annealing as a result of irreversible structural relaxations within the amorphous state according to

$$D^T(t, T) = \delta D^T(t, T) + D_R^T(T), \tag{3}$$

where the diffusivity enhancement δD^T in the unrelaxed state drops to zero during annealing.

b) The diffusivities D_R^T in relaxed amorphous alloys obey Arrhenius laws, i.e., within the experimental error bars their temperature dependences may be described by relationships of the form (1) in the temperature regimes investigated.

c) In the relaxed amorphous state a temperature change from T_1 to T_2 (not leading to crystallization) gives rise to a delay-free change in D^T from $D_R^T(T_1)$ to $D_R^T(T_2)$ in all cases in which this effect has been looked for. This phenomenon has been demonstrated systematically and most convincingly for ^{59}Fe in $Fe_{91}Zr_9$.

d) The D_R^T values are larger by five to ten orders of magnitude than the self-diffusivities obtained by extrapolation of the data measured on crystalline iron, nickel, cobalt, or zirconium to the low temperatures at which the D_R^T values have been measured.

e) The tracer self-diffusion enthalpies H_R^T of transition metals in most amorphous metallic alloys lie in the range 1.5 to 2.5 eV and are thus distinctly smaller than those in crystalline Fe, Co, or Ni (~3 eV). An exception is ^{95}Zr in $Fe_{24}Zr_{76}$ ($H_R^T = 3.2$ eV). In this system the pre-exponential factor of the diffusion coefficient is 10^{10} times larger than in typical crystalline metals.

f) The pre-exponential factors D_0^T in various amorphous alloys range from three orders of magnitude below to ten orders of magnitude above 10^{-4} m²/s, which is typical of the pre-exponential factors of the bulk self-diffusion coefficients in crystalline metals.

g) According to Figure 2, there is a clear tendency that, the larger the diffusion enthalpy H_R^T, the larger is D_0^T. This feature may approximately be described by the relationship

$$\log_{10}[D_0^T(\mathrm{m}^2\,\mathrm{s})] = 8(H_R^T - 2.4\ eV)(eV)^{-1}. \tag{4}$$

h) In a given Fe-Zr alloy, H_R^T and D_0^T are larger for the diffusion of the larger ^{95}Zr tracers than for the diffusion of the smaller ^{59}Fe tracers (Figures 2 and 3).

i) For a given tracer, ^{95}Zr or ^{59}Fe, H_R^T and D_0^T are larger in the less open Zr-rich $Fe_{24}Zr_{76}$ structure than in the more open Fe-rich $Fe_{91}Zr_9$ structure (Figures 2 and 3).

2.2 *Short-Range Diffusion*

Whereas in diffusion experiments the tracer atoms perform long-range migrations, magnetic after-effect measurements monitor local rearrangements of mobile atomic

discrepancy results from the different time scales used in relaxation and diffusion measurements and that the results of both types of experiments may be reconciled within a unified model for the diffusion of atoms in a network of randomly distributed barrier heights. In this context it is of interest to note that the famous model of atomic two-level systems represents a subgroup of local diffusional processes within the spectrum of thermally activated jumps to neighbouring positions.

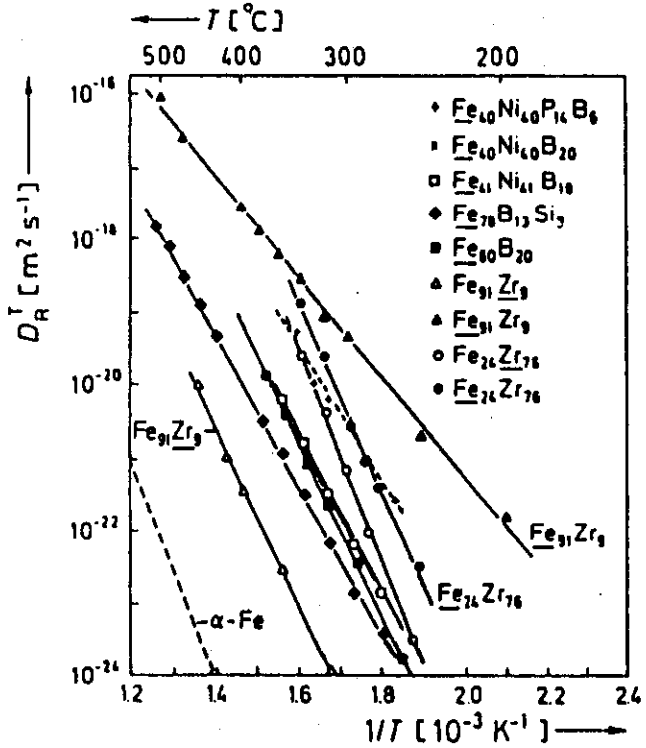

FIGURE 1 Arrhenius plots of radio-tracer self-diffusion coefficients D_R^T in relaxed amorphous alloys.[27-31,48] The diffusing elements are underlined. For comparison the self-diffusion coefficient of α-Fe has been included.

2 BRIEF REVIEW OF EXPERIMENTAL RESULTS

2.1 *Long-Range Diffusion*

Figure 1 shows the temperature dependences of the self-diffusion coefficients of the transition metals Fe and Zr in a series of pre-annealed Fe-, (Fe,Ni)-, and (Fe,Zr)-base amorphous alloys as measured by the radio-tracer technique in combination with ion-beam sputtering.[28-32] The diffusion profiles extend over 100 to 1000 nm, i.e., in these experiments the diffusing tracer atoms perform a large number of jumps. The most surprising conclusions which may be drawn from these data are as follows:

a) In as-quenched amorphous metallic alloys the tracer self-diffusivities D^T decrease during thermal annealing as a result of irreversible structural relaxations within the amorphous state according to

$$D^T(t, T) = \delta D^T(t, T) + D_R^T(T), \tag{3}$$

where the diffusivity enhancement δD^T in the unrelaxed state drops to zero during annealing.

b) The diffusivities D_R^T in relaxed amorphous alloys obey Arrhenius laws, i.e., within the experimental error bars their temperature dependences may be described by relationships of the form (1) in the temperature regimes investigated.

c) In the relaxed amorphous state a temperature change from T_1 to T_2 (not leading to crystallization) gives rise to a delay-free change in D^T from $D_R^T(T_1)$ to $D_R^T(T_2)$ in all cases in which this effect has been looked for. This phenomenon has been demonstrated systematically and most convincingly for ^{59}Fe in $Fe_{91}Zr_9$.

d) The D_R^T values are larger by five to ten orders of magnitude than the self-diffusivities obtained by extrapolation of the data measured on crystalline iron, nickel, cobalt, or zirconium to the low temperatures at which the D_R^T values have been measured.

e) The tracer self-diffusion enthalpies H_R^T of transition metals in most amorphous metallic alloys lie in the range 1.5 to 2.5 eV and are thus distinctly smaller than those in crystalline Fe, Co, or Ni (~3 eV). An exception is ^{95}Zr in $Fe_{24}Zr_{76}$ ($H_R^T = 3.2$ eV). In this system the pre-exponential factor of the diffusion coefficient is 10^{10} times larger than in typical crystalline metals.

f) The pre-exponential factors D_0^T in various amorphous alloys range from three orders of magnitude below to ten orders of magnitude above 10^{-4} m²/s, which is typical of the pre-exponential factors of the bulk self-diffusion coefficients in crystalline metals.

g) According to Figure 2, there is a clear tendency that, the larger the diffusion enthalpy H_R^T, the larger is D_0^T. This feature may approximately be described by the relationship

$$\log_{10}[D_0^T(m^{-2}\,s)] = 8(H_R^T - 2.4\ eV)(eV)^{-1}. \tag{4}$$

h) In a given Fe–Zr alloy, H_R^T and D_0^T are larger for the diffusion of the larger ^{95}Zr tracers than for the diffusion of the smaller ^{59}Fe tracers (Figures 2 and 3).

i) For a given tracer, ^{95}Zr or ^{59}Fe, H_R^T and D_0^T are larger in the less open Zr-rich $Fe_{24}Zr_{76}$ structure than in the more open Fe-rich $Fe_{91}Zr_9$ structure (Figures 2 and 3).

2.2 *Short-Range Diffusion*

Whereas in diffusion experiments the tracer atoms perform long-range migrations, magnetic after-effect measurements monitor local rearrangements of mobile atomic

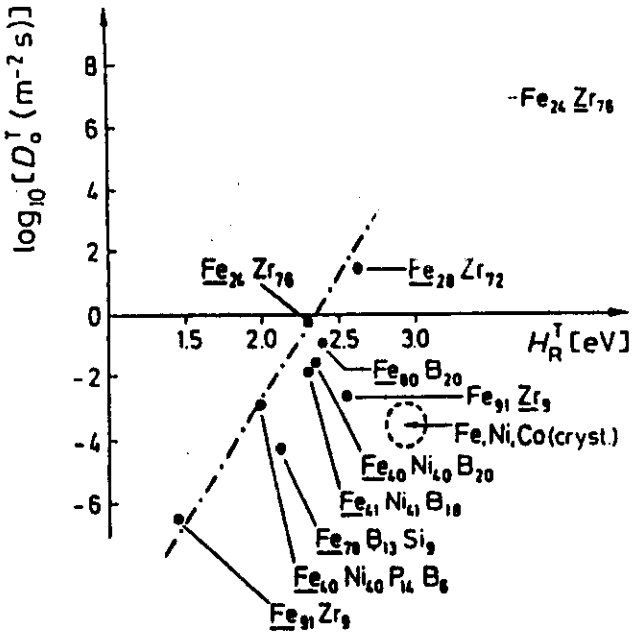

FIGURE 2 Empirical relationship [Eq. (4)] between the pre-exponential factors D_0^T and the activation enthalpies H_R^T of the Arrhenius laws (1) found for the self-diffusion coefficients D_R^T in relaxed amorphous alloys (see Figure 1). The significance of such a relationship has been considered by Dotdale and Brook.[48]

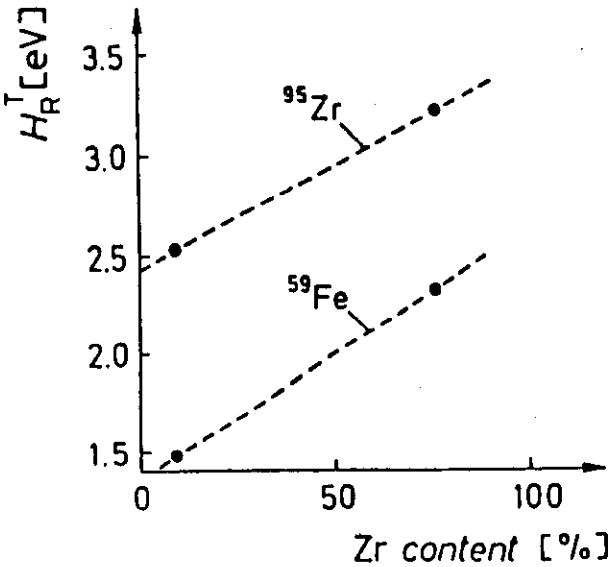

FIGURE 3 Self-diffusion enthalpies H_R^T of ^{95}Zr and ^{59}Fe radio-tracers in relaxed amorphous Fe–Zr alloys as a function of the Zr content.

units only. In fact, usually magnetic after-effect studies are performed at lower temperatures than diffusion measurements. This explains why in magnetic after-effect studies short-range atomic displacements are observed that may be characterized by spectra of relaxation times or of activation enthalpies, in contrast to what is true for diffusion experiments. Figures 4a and 5a show the relaxation spectra of the reciprocal susceptibility, briefly called reluctivity, $r(t) = 1/\chi(t)$, of amorphous $Fe_{..}B_{..}$[33] and $Fe_{77,3}B_{13,6}Si_{9,1}$,[34] respectively, together with the histograms for the activation enthalpies (Figures 4b and 5b). These were deduced under the assumption that the relaxation consists of superposed exponential relaxation processes according to

$$r(t) = r_0 + r_\infty \int [1 - \exp(-t\nu)]p(\nu)\mathrm{d}\nu\,, \tag{5}$$

where $r_\infty - r_0$ denotes the total relaxation amplitude and $p(\nu)$ the probability distribution function of relaxation frequencies ν. In Figures 4a and 5a the relaxation amplitudes measured within the time interval $t_1 \leqslant t \leqslant t_2$,

$$\Delta r(t_1, t_2, T) = \frac{r(t_2, T) - r(t_1, T)}{r(t_1, T)}\,, \tag{6}$$

are plotted versus the temperature of measurement. For an interpretation of the measured relaxation amplitudes it is advantageous to consider the distribution function $p(\nu)$ as a function of activation enthalpies H by assuming the validity of the Arrhenius-type relationship $\nu = \nu_0 \exp(-H/kT)$ [ν_0 = attempt frequency including an entropy factor].

The magnetic after-effect measurements lead to the following results, which may be contrasted with those of the long-range diffusion experiments:

j) Magnetic relaxation processes are characterized by spectra of activation enthalpies.

k) The activation enthalpy of largest probability is smaller by 0.5 to 0.9 eV than the tracer self-diffusion enthalpy of comparable alloys (Table I).

l) The half-widths of the spectra of activation enthalpies are of the order of 0.5 eV.

m) All spectra possess a low energy tail, which recently has been shown to result from tunnelling processes of two-level systems.[35]

n) Like the self-diffusion enthalpy in Fe–Zr alloys, the effective activation enthalpy governing magnetic relaxations increases with increasing diameter of the diffusing atom.

3 DISCUSSION

3.1 *Temperature Dependence of the Diffusion Coefficients and its Interpretation*

Diffusion in disordered media has been the subject of many papers and reviews.[36-42] Several models have been proposed in order to describe the effect of disorder on the diffusion of atoms. For simplicity in this section we exclusively consider so-called direct diffusion mechanisms, in which the tracer atoms perform

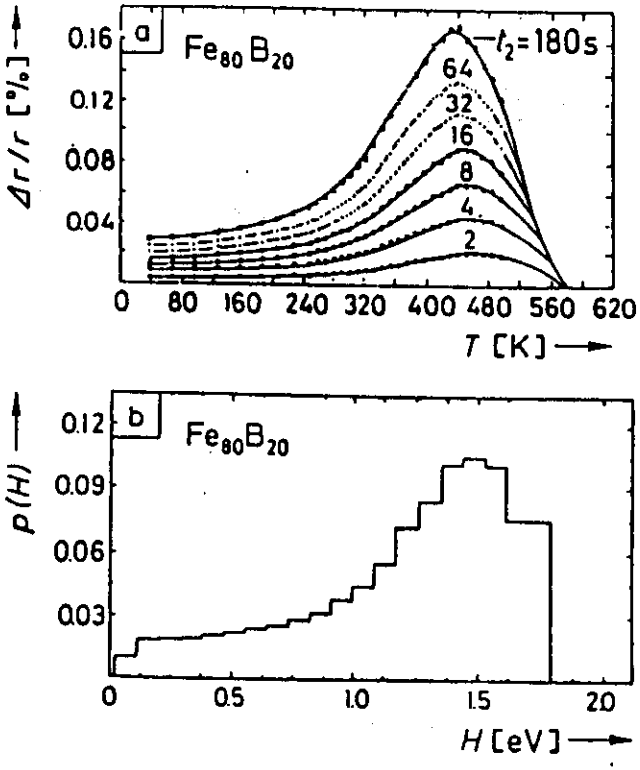

FIGURE 4 Magnetic after-effect spectrum (a) and the corresponding spectrum of activation enthalpies (b) measured on amorphous $Fe_{80}B_{20}$ by Rettenmeier.[33]

TABLE I
Parameters deduced from short-time and long-time experiments on amorphous $Fe_{80}B_{20}$ and $Fe_{78}B_{13}Si_9$

Quantity	$Fe_{80}B_{20}$	$Fe_{78}B_{13}Si_9$
H'_{s0} [eV]	1.5	1.49
H'_{s0} [eV]	2.40	2.09
T' [K]	440	520
T' [K]	600	650
H_0 [eV]	2.05	1.76
H_∞ [eV]	0.14	0.13

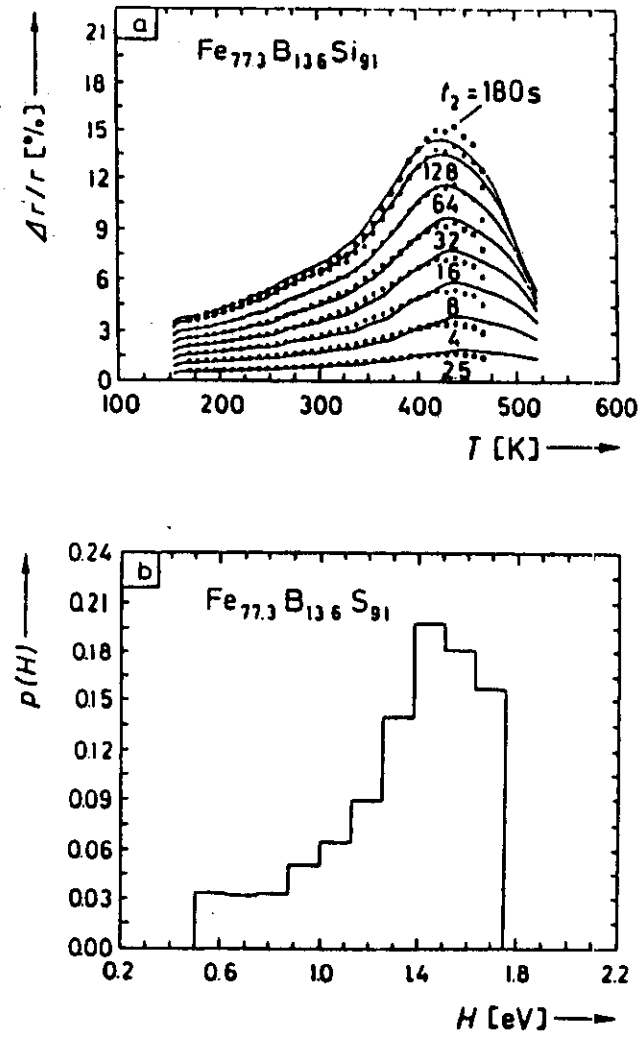

FIGURE 5 Magnetic after-effect spectrum (a) and the corresponding spectrum of activation enthalpies (b) measured on $Fe_{77.3}B_{13.6}Si_{9.1}$ by Rössle.[34]

random walks without the aid of diffusion vehicles. (In crystalline solids, vacancies or self-interstitials can play the role of diffusion vehicles.) An extension to indirect diffusion mechanisms involving diffusion vehicles is straightforward (Section 3.2.3.1.2).

The most significant models for the diffusion in disordered media are the following:

1) Random transition rate models which consider either random barriers assigned to random chemical bonds or random jump rates attributed to atomic transitions between random neighbouring sites.[36-41]

2) Models with randomly distributed sites to which trapping efficiencies characterized by potential wells of different depths are ascribed.[36]

3) Multiple range hopping models in which spectra of particle jump distances are permitted.[42]

A common feature of all the models described above is the use of master equations for determining the probability $p_i(t)$ to find a randomly walking atom at a time t on a given site i. In the random transition rate models it is usually assumed that the jump frequency ν_{ij} from a site i to a neighbouring site j is related via a Boltzmann-type equation,

$$\nu_{ij} = \nu_{ij,0} \exp(-H_{ij}/kT), \tag{7}$$

to the barrier H_{ij} that has to be surmounted in this transition, where $\nu_{ij,0}$ denotes a pre-exponential factor including an entropy term. In the present treatment of direct diffusion H_{ij} means the activation enthalpy for the jump of a tracer atom from site i to site j. In the case of indirect diffusion, two cases have to be distinguished. If the concentration of diffusion vehicles is not the quasi-equilibrium concentration, H_{ij} means the migration enthalpy of the diffusion vehicles. If the vehicles are present in their quasi-equilibrium concentration, H_{ij} is composed of the formation enthalpy of the diffusion vehicles and of the barrier height (= local migration enthalpy) which the vehicles have to overcome in a transition from i to j. In general, ν_{ij} and H_{ij} are characterized by distribution functions. In accordance with experimental results reported in Section 2.1 this treatment leads to diffusion coefficients that obey a conventional Arrhenius-type temperature dependence in the temperature regimes investigated. By contrast, multiple range hopping models predict an $\exp[-A/T^{1/4}]$-law,[43] where A is T-independent. Therefore, it is concluded that the multiple range hopping mechanism is not realized in the diffusion in amorphous alloys. It thus appears to be justified to assume that the elementary diffusion jump distance is of the order of magnitude of the mean nearest-neighbour separation of atoms, which henceforth will be denoted as a.

Within the framework of the random transition rate models, explicit solutions for the mean square displacement of the diffusing atoms have been derived in the one-dimensional case. From effective medium theories it follows that in a first-order approximation these results remain valid in the three-dimensional case, too.[41,42] In the short-time limit, for the mean square displacement $\langle x^2 \rangle$ the following result obtains:[36,39,40]

$$\langle x^2(t) \rangle = 2a^2 \langle \nu_{ij} \rangle t \left[1 - \frac{1}{2} \Delta_1 \langle \nu_{ij} \rangle t + \dots \right], \tag{8}$$

where $\langle \nu_{ij} \rangle$ denotes the average over all individual jump frequencies,

$$\langle \nu_{ij} \rangle = \int \nu_{ij} p_\nu(\nu_{ij}) \, d\nu_{ij}. \tag{9}$$

Here we have introduced a distribution function $p_\nu(\nu_{ij})$ of the jump frequencies. The parameter Δ_1 is related to the second moment. It is defined by the following combination of averages over ν_{ij}:

$$\Delta_1 = 2 \frac{\langle (\nu_{ij} - \langle \nu_{ij} \rangle)^2 \rangle}{\langle \nu_{ij} \rangle^2}. \tag{10}$$

The long-time behaviour of $\langle x^2 \rangle$ may be written as[36,37]

$$\langle x^2(t) \rangle = 2a^2 \frac{1}{\left\langle \frac{1}{\nu_{ij}} \right\rangle} t \left[1 + \frac{2}{\pi^{1/2}} \theta_1 \left(\frac{1}{\left\langle \frac{1}{\nu_{ij}} \right\rangle} t \right)^{-1/2} + \dots \right]. \tag{11}$$

In contrast to Eq. (8), which is a function of $\langle \nu_{ij} \rangle$, in Eq. (11) the average

$$\left\langle \frac{1}{\nu_{ij}} \right\rangle = \int \frac{1}{\nu_{ij}} p_\nu(\nu_{ij}) d\nu_{ij} \tag{12}$$

controls the mean square displacement. The parameter θ_1 is defined as

$$\theta_1 = \frac{1}{2} \left\langle \left(\frac{1}{\nu_{ij}} - \left\langle \frac{1}{\nu_{ij}} \right\rangle \right)^2 \right\rangle \left\langle \frac{1}{\nu_{ij}} \right\rangle^{-2}. \tag{13}$$

The appearance of different averages in the short-time and the long-time approximations has a simple physical origin. As illustrated in Figure 6, at short times, diffusion may set in *independently* at different locations and proceeds fastest where the jump frequencies are largest and the activation enthalpies are smallest. Thus, in the early stage, diffusion is dominated by the large jump frequencies (small activation enthalpies), i.e., the average $\langle \nu_{ij} \rangle$. At long times, diffusion becomes long-range. The arrival rate of an atom at a location far from its original site is mainly controlled by the smallest jump frequencies (largest activation enthalpies) in the required series of jump events, in which each event is *dependent* on the preceding ones. Therefore, the long-time behaviour is governed by the average $\langle 1/\nu_{ij} \rangle$, which suppresses the high frequencies.

For a comparison with the experimentally found temperature dependences of the diffusion coefficients, Eq. (7) has been inserted in the expressions (8) and (11) for $\langle x^2(t) \rangle$. The distribution $p_\nu(\nu_{ij})$ is assumed to be related to a distribution of activation enthalpies. Decomposing, according to

$$H_{ij} = H_0 + \delta H_{ij}, \tag{14}$$

the activation enthalpies in their volume average $H_0 = \langle H_{ij} \rangle$ and in activation-enthalpy fluctuations δH_{ij}, we may reasonably well describe the distribution function of these fluctuations by the Gaussian

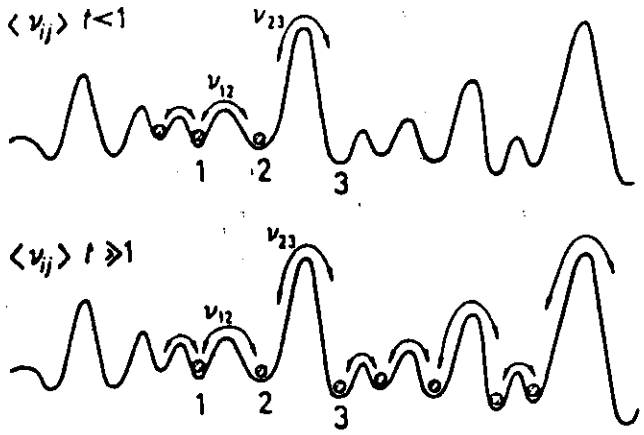

FIGURE 6 Schematic illustration of the diffusion of a tracer atom in a potential with a random distribution of barrier heights for short ($\langle\nu_\nu\rangle t < 1$) and long ($\langle\nu_\nu\rangle t \gg 1$) diffusion times, respectively.

$$p_H(\delta H_\nu) = \frac{1}{(2\pi)^{1/2} H_m} \exp(-\delta H_\nu^2/2H_m^2) \tag{15}$$

with the variance H_m^2. Assuming that the fluctuations of the pre-exponential factors $\nu_{\nu,0}$ and of the activation enthalpies H_ν are uncorrelated, the averages $\langle x^2(t)\rangle$ defined by Eqs. (8) and (11) are evaluated in what follows.

(i) *Short-time approximation* $\langle\nu_\nu\rangle t < 1$:

$$\langle\nu_\nu\rangle = \frac{\langle\nu_{\nu,0}\rangle}{(2\pi)^{1/2} H_m} \exp(-H_0/kT) \int_{-H_0}^{\infty} \exp(-\delta H_\nu/kT)\exp(-\delta H_\nu^2/2H_m^2)\,d\delta H_\nu. \tag{16}$$

In Eq. (16) negative activation enthalpies are excluded by choosing $\delta H_\nu = -H_0$ as the lower bound of the fluctuations. Substituting $U = \delta H_\nu/2^{1/2}H_m + H_m/2^{1/2}kT$ the lower boundary becomes $U_{min} = -H_0/2^{1/2}H_m + H_m/2^{1/2}kT$, and Eq. (16) takes the form

$$\begin{aligned}\langle\nu_\nu\rangle &= \frac{\langle\nu_{\nu,0}\rangle}{\pi^{1/2}} \exp(-H_0/kT)\exp[H_m^2/2(kT)^2]\int_{U_{min}}^{\infty} \exp(-U^2)\,dU \\ &= \frac{\langle\nu_{\nu,0}\rangle}{2} \exp(-H_0/kT)\exp[H_m^2/2(kT)^2] \\ &\times \left\{1 - \mathrm{sgn}(U_{min})\,\mathrm{erf}\left(\left|\frac{H_m}{2^{1/2}kT} - \frac{H_0}{2^{1/2}H_m}\right|\right)\right\}.\end{aligned} \tag{17}$$

(ii) *Long-time approximation* $\langle 1/\nu_\nu\rangle^{-1} t \gg 1$:

$$\left\langle\frac{1}{\nu_\nu}\right\rangle = \left\langle\frac{1}{\nu_{\nu,0}}\right\rangle \frac{\exp(H_0/kT)}{(2\pi)^{1/2} H_m} \int_{-H_0}^{\infty} \exp(\delta H_\nu/kT)\exp(-\delta H_\nu^2/2H_m^2)\,d\delta H_\nu. \tag{18}$$

Substituting $U = \delta H_\nu/2^{1/2}H_m - H_m/2^{1/2}kT$ the lower boundary takes the form $U_{min} = -(H_0/2^{1/2}H_m + H_m/2^{1/2}kT)$, and Eq. (18) yields

$$\begin{aligned}\left\langle\frac{1}{\nu_\nu}\right\rangle &= \left\langle\frac{1}{\nu_{\nu,0}}\right\rangle \frac{\exp(H_0/kT)}{\pi^{1/2}} \exp[H_m^2/2(kT)^2]\int_{U_{min}}^{\infty} \exp(-U^2)\,dU \\ &= \left\langle\frac{1}{\nu_{\nu,0}}\right\rangle \frac{1}{2} \exp(+H_0/kT)\exp[H_m^2/2(kT)^2]\left[1 + \mathrm{erf}\left(\frac{H_m}{2^{1/2}kT} + \frac{H_0}{2^{1/2}kT}\right)\right].\end{aligned} \tag{19}$$

The integrands in Eqs. (16) and (18) obviously play the role of weighting factors, according to which a given activation enthalpy H_ν contributes to the short-time and the long-time averages, respectively. Figure 7 represents the Gaussian distribution function $p_H(\delta H_\nu)$ as well as these weighting factors, g_ν^s and g_ν^l, for Fe in amorphous $Fe_{78}B_{13}Si_9$ in the short-time and long-time approximation, respectively.

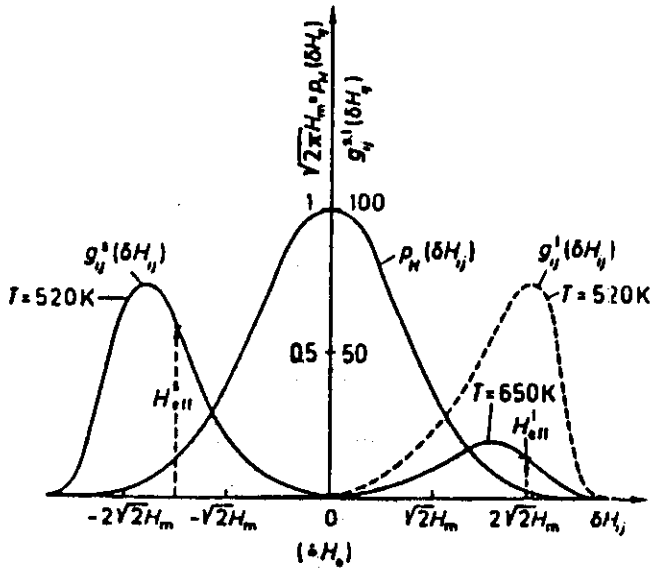

FIGURE 7 Gaussian distribution $p_H(\delta H_\nu)$ of the activation-enthalpy fluctuations and the weighting factors $g_\nu^s = \exp(-\delta H_\nu/kT)\exp(-\delta H_\nu^2/2H_m^2)$ and $g_\nu^l = \exp(\delta H_\nu/kT)\exp(-\delta H_\nu^2/2H_m^2)$ for short-time (at 520 K) and long-time (at 520 K and 650 K) diffusion processes in amorphous $Fe_{78}Si_{13}B_9$.

Now it is straightforward to write down short-time and long-time approximations of the diffusion coefficient in a disordered medium. Using the definition $D = \langle x^2 \rangle / 2t$ of the diffusion coefficient one finds from (8) and (17) for short times

$$D^s = \frac{1}{2} a^2 \langle \nu_{s,n} \rangle \exp(-H_0/kT) \exp[H_m^2/2(kT)^2] \times \left\{ 1 - \mathrm{sgn}(U_{mm}) \, \mathrm{erf}\left(\left| \frac{H_m}{2^{1/2} kT} - \frac{H_0}{2^{1/2} H_m} \right| \right) \right\} \left\{ 1 - \frac{1}{2} \Delta_1(\nu_s) t + \ldots \right\} \tag{20}$$

and from (11) and (19) for long times

$$D^l = 2a^2 \frac{1}{\left\langle \frac{1}{\nu_{l,n}} \right\rangle} \exp(-H_0/kT) \exp[-H_m^2/2(kT)^2] \frac{1 + \frac{2}{\pi^{1/2}} \theta_1 \left(\frac{1}{\langle 1/\nu_s \rangle} t \right)^{-1/2} + \ldots}{1 + \mathrm{erf}\left(\frac{H_m}{2^{1/2} kT} + \frac{H_0}{2^{1/2} H_m} \right)}. \tag{21}$$

In the extreme limits $t \to 0$ and $t \to \infty$ one may neglect the contributions by the second moments Δ_1 and θ_1. Since in the realistic case of $H_0/2H_m > 1$ the error functions in (20) and (21) become approximately equal to unity, under these circumstances Eqs. (20) and (21) reduce to

$$D^s(T) = a^2 \langle \nu_{s,n} \rangle \exp(-H_0/kT) \exp[H_m^2/2(kT)^2] \tag{22}$$

and

$$D^l(T) = a^2 \frac{1}{\left\langle \frac{1}{\nu_{l,n}} \right\rangle} \exp(-H_0/kT) \exp[-H_m^2/2(kT)^2], \tag{23}$$

respectively.

Usually the temperature dependences of diffusion coefficients are displayed in Arrhenius plots. According to Eqs. (22) and (23), in disordered media such plots must be describable by either

$$\ln D^s(T) = \ln D_0^s - \frac{H_0}{kT} + \frac{H_m^2}{2(kT)^2} \tag{24}$$

or

$$\ln D^l(T) = \ln D_0^l - \frac{H_0}{kT} - \frac{H_m^2}{2(kT)^2}, \tag{25}$$

depending on whether the applied experimental technique monitors the short-time or the long-time stage of the diffusion process. In (24) and (25) D_0^s and D_0^l are abbreviations for the pre-exponential factors in the expressions (22) and (23). In Figures 8 and 9 the temperature dependences of the quantities $\ln(D^s/D_0^s)$ and $\ln(D^l/D_0^l)$ are illustrated for different parameters H_0 and H_m. These Arrhenius plots are curved lines, i.e., the preceding random transition rate treatment predicts that at very short and at very long times, diffusion in amorphous alloys is governed by temperature-dependent effective activation enthalpies, viz.,

$$H_{sa}^s = -\frac{\mathrm{d}}{\mathrm{d}(1/kT)} (\ln D^s) = H_0 - \frac{H_m^2}{kT}, \tag{26}$$

$$H_{sa}^l = -\frac{\mathrm{d}}{\mathrm{d}(1/kT)} (\ln D^l) = H_0 + \frac{H_m^2}{kT}. \tag{27}$$

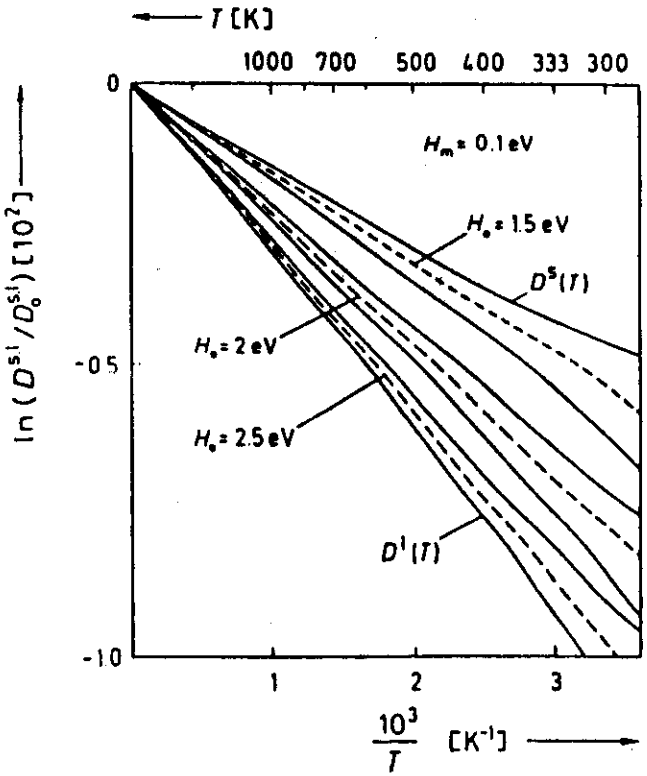

FIGURE 8 Arrhenius plots of the short-time approximation $D^s(T)$ [Eq. (24); positively curved full lines] and the long-time approximation $D^l(T)$ [Eq. (25); negatively curved full lines] of the diffusion coefficient in a disordered medium for $H_m = 0.1$ eV and different values of H_0. The dashed straight lines represent the cases $H_m = 0$.

However, within the temperature intervals in which diffusion coefficients in amorphous alloys have been measured (200°C to 500°C) the curves in Figures 8 and 9 approximately represent straight lines. These correspond to effective activation enthalpies H^{s}_{eff} and H^{l}_{eff} which are smaller or larger than H_0 for short-time or long-time experiments, respectively. Correspondingly the pre-exponential factors determined from experimentally found quasi-straight Arrhenius lines yield a lower or upper bound in the case of short-time or long-time experiments, respectively. If diffusion coefficients or relaxation times are determined within a fixed time interval as a function of temperature, at high temperatures the long-time approximation applies, whereas at low temperatures the short-time approximation is valid, i.e., the diffusion coefficients in amorphous alloys approach D^{l} for $T \to \infty$ and D^{s} for $T \to 0$. This leads to the cross-over behaviour of $D(T)$ illustrated in Figure 10.

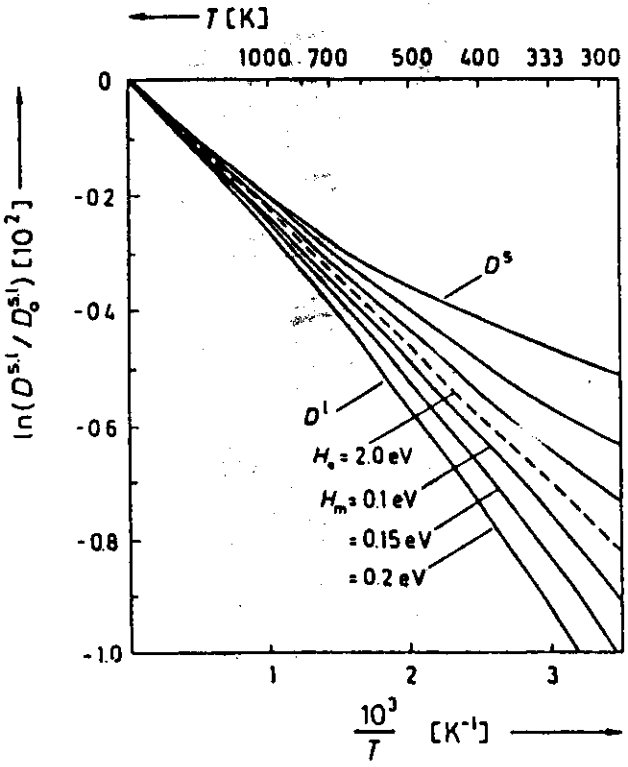

FIGURE 9 Arrhenius plots of the short-time approximation $D^{s}(T)$ [Eq. (24); positively curved full lines] and the long-time approximation $D^{l}(T)$ [Eq. (25); negatively curved full lines] of the diffusion coefficient in a disordered medium for $H_0 = 2.0$ eV and different values of H_m. The dashed straight line represents the case $H_m = 0$.

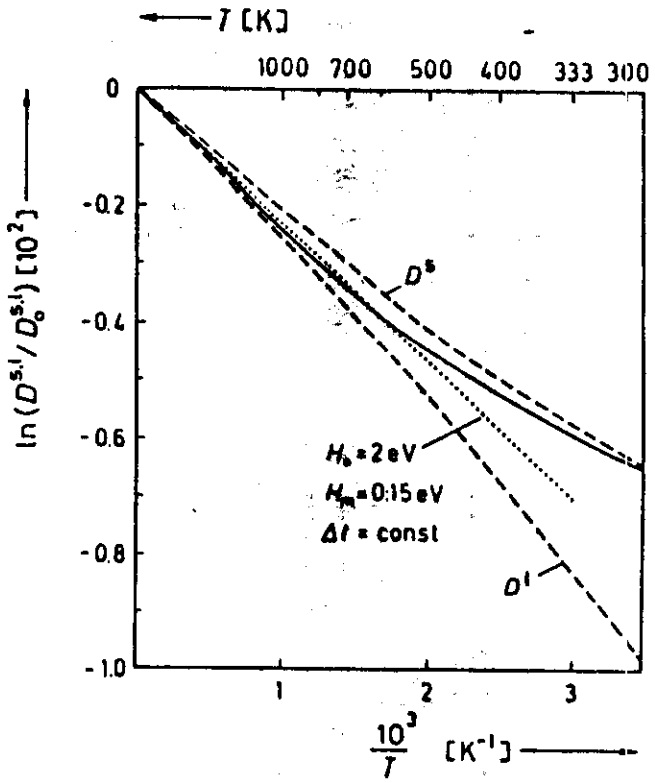

FIGURE 10 Crossing-over of the diffusion coefficient (full curve) from $D^{s}(T)$ at low temperatures to $D^{l}(T)$ at high temperatures in the case of a fixed interval of measuring time. The dotted straight line indicates the case $H_m = 0$.

The difference between the long-time and the short-time behaviour of D may be exploited to determine the parameters H_0 and H_m by combining data from diffusion measurements (long-time approximation) and magnetic-after-effect measurements (short-time approximation). From Eqs. (26) and (27) the following relations between the effective activation enthalpies H^{l}_{eff} and H^{s}_{eff} measured at a temperature T^{l} and at a temperature T^{s} in a long-time and in a short-time experiment, respectively, may be derived:

$$H^{l}_{eff} - H^{s}_{eff} = H_m^2 \left(\frac{1}{kT^{s}} + \frac{1}{kT^{l}} \right), \tag{28}$$

$$H^{l}_{eff} + H^{s}_{eff} = 2H_0 + H_m^2 \left(\frac{1}{kT^{l}} - \frac{1}{kT^{s}} \right). \tag{29}$$

By these relations H_0 and H_m may be deduced from experimental results in an easy way. For $Fe_{78}B_{13}Si_9$ and $Fe_{80}B_{20}$ such measurements are available. Table I shows the

numerical results of their evaluation. In Fig[ure] [11] and 12 ($Fe_{78}B_{13}Si_9$) experimental values of the ^{59}Fe tracer self[-diffusion] coefficients $D_R^T(T)$ [open circles] are compared to the temperature depen[dence] [solid lines] calculated with the aid of Eq. (25) and the H_0 and H_m va[lues] [in] Table I. The agreement between $D_R^T(T)$ and $D^I(T)$ is excellent. Th[is] [demonstrates] that, within the temperature ranges in which D_R^T has been measu[red] considerable fluctuations of the diffusion barriers ($H_m = 0.14$ eV in $Fe_{80}B_{20}$, [0].13 eV in $Fe_{78}Si_9B_{13}$) do not give rise to detectable curvatures in the Arr[henius] lines.

An important result of the preceding discussion [is] the tracer self-diffusion enthalpies H_R^T in relaxed amorphous alloys deduced from the seemingly straight

Arrhenius lines of experimentally determined $D_R^T(T)$ data are average values of H_{eff}^I [Eq. (27)] over the temperature intervals covered in the diffusion studies. In a corresponding way the experimentally found pre-exponential factors D_0^I of D_R^I have the meaning of temperature averages that are larger than $D_0^I = a^2(1/\nu_{y,0})^{-1}$ [Eqs. (23) and (25)] since the temperature average of H_{eff}^I is larger than H_0 (Figure 9). Indeed from the (dashed) straight lines belonging to the activation enthalpies H_0 (Figures 11 and 12) one finds $D_0^I = 1.8 \times 10^{-4}$ m²/s and $D_0^I = 5.4 \times 10^{-6}$ m²/s for ^{59}Fe in $Fe_{80}B_{20}$ and $Fe_{78}Si_9B_{13}$, respectively. These values are by factors of about 10^{-3} and 10^{-4} smaller than the corresponding values for D_0^T derived from the (full) quasi-straight lines through the experimental D_R^T data. A similar evaluation of

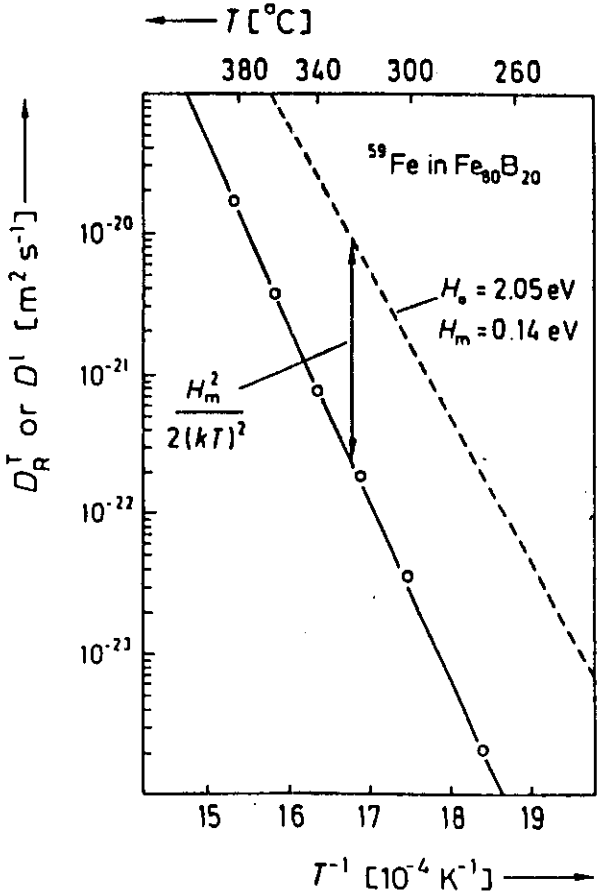

FIGURE 11 Comparison of experimental D_R^T values for the ^{59}Fe diffusion in amorphous $Fe_{80}B_{20}$ (O) with the theoretical expression (25) for $D^I(T)$ [full curve]. The fitting parameters are $H_0 = 2.05$ eV, $D_0^I = 1.8 \times 10^{-4}$ m²/s, and $H_m = 0.14$ eV. The dashed straight line represents the corresponding Arrhenius law to which $D^I(T)$ degenerates for $H_m = 0$.

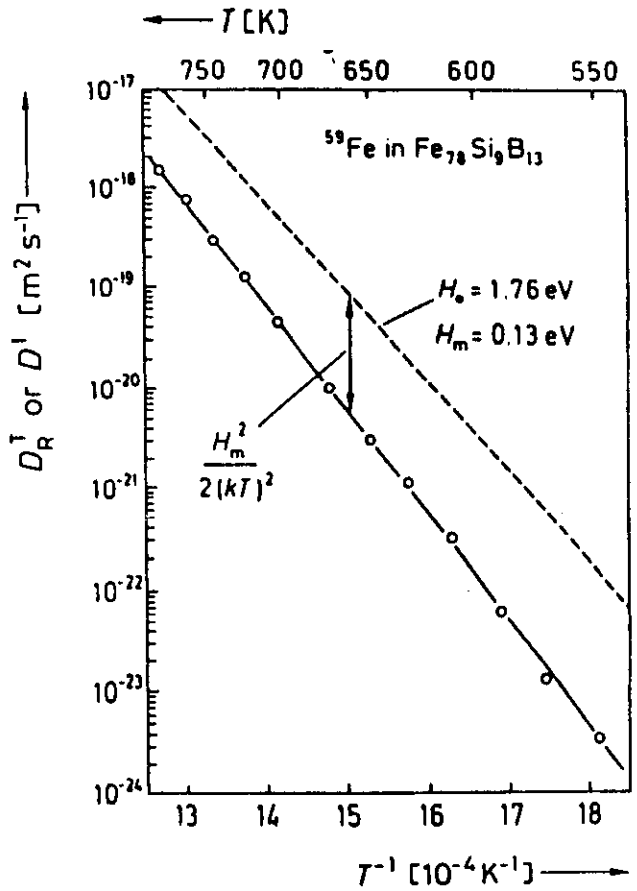

FIGURE 12 Comparison of experimental D_R^T values for the ^{59}Fe diffusion in amorphous $Fe_{78}Si_9B_{13}$ (O) with the theoretical expression (25) for $D^I(T)$ [full curve]. The fitting parameters are $H_0 = 1.76$ eV, $D_0^I = 5.4 \times 10^{-6}$ m²/s, and $H_m = 0.13$ eV. The dashed straight line represents the corresponding Arrhenius law to which $D^I(T)$ degenerates for $H_m = 0$.

diffusion data on ^{59}Fe in $Fe_{91}Zr_9$ ($D_0^T = 3 \times 10^{-7}$ m²/s) and ^{95}Zr in $Fe_{24}Zr_{76}$ ($D_0^T = 7 \times 10^{-6}$ m²/s) yields $D_0^1 \approx 10^{-8}$ m²/s for $H_m = 0.09$ eV and $D_0^1 \approx 10^{-2}$ m²/s for $H_m \approx 0.2$ eV, respectively, provided in these cases the ratio H_m/H_{eff}^1 is close to that for ^{59}Fe in $Fe_{78}Si_9B_{13}$.

From the preceding paragraph it is obvious that the D_0^1 values have a more direct physical meaning than the quantities D_0^T obtainable from experimental D_k^1 data by the extrapolation $1/T \to 0$. However, it should be noted that in the derivation of D_0^1 the existence of a distribution of the migration entropies S_ν entering the pre-exponential frequency factors

$$\nu_{\nu,0} = \tilde{\nu}_{\nu,0} \exp(S_\nu/k) \tag{30}$$

($\tilde{\nu}_{\nu,0}$ = attempt frequencies) has not yet been taken into account explicitly. This deficiency will be removed in Section 3.2.3.1.1, where $D_0^1 \equiv a^2(1/\nu_{\nu,0})^{-1}$ will be considered in more detail.

3.2 *Diffusion Mechanisms*

3.2.1 *Diffusivity enhancement in the unrelaxed amorphous state* As discussed in detail by Frank *et al.*,[44] the diffusivity enhancements δD^T in unrelaxed amorphous alloys represent contributions of indirect tracer diffusion via quasi-vacancies, which are usually denoted as free volume. This interpretation is in accordance with the fact that the decrease of δD^T during irreversible relaxation is accompanied by the elimination of excess free volume.

3.2.2 *Nature of small activation-enthalpy barriers observed in short-time experiments on relaxed specimens* From the interpretation of the diffusivity enhancement in the unrelaxed amorphous state given in Section 3.2.1 a tentative explanation of observation (k) [Section 2.2] emerges. After the elimination of the excess free volume, a remainder of inhomogeneously distributed free volume is retained. It is clear that—irrespective of the specific nature of the diffusion mechanism in the relaxed amorphous state—within islands of retained free volume, atomic rearrangements can take place with lower activation enthalpies than in the denser surrounding. These local low-enthalpy barriers will be detected in short-time experiments. By contrast, long-range diffusion observed in tracer diffusion studies on relaxed samples is controlled by the higher activation enthalpy barriers in the more closely packed material around free-volume islands.

3.2.3 *Long-range diffusion in the relaxed amorphous state* In Section 3.1, for the sake of simplicity it has been assumed that in pre-annealed amorphous alloys, diffusion occurs via a direct diffusion mechanism. This assumption will be critically tested in the following.

3.2.3.1 Pre-exponential Factors D_0^T—A model of tracer self-diffusion in relaxed amorphous alloys must explain the tremendous variation of D_0^T from alloy to alloy as well as from tracer to tracer, say, from ^{59}Fe to ^{95}Zr.

3.2.3.1.1 Direct diffusion mechanisms—In order to derive an explicit expression of D_0^1, Eq. (7) is replaced by

$$\nu_\nu = \tilde{\nu}_{\nu,0} \exp(-G_\nu/kT), \tag{31}$$

where $G_\nu = H_\nu - TS_\nu$ is the Gibbs free energy barrier between the sites i and j. A statistical treatment analogous to that in Section 3.1 leads to

$$D^1(T) = a^2 \frac{1}{\left(\frac{1}{\tilde{\nu}_{\nu,0}}\right)} \exp(-G_0/kT) \exp\left[-\frac{G_m^2}{2(kT)^2}\right]. \tag{32}$$

In Eq. (32) G_0 and G_m^2 mean the average (G_ν) and the variance of the Gaussian distribution of G_ν, respectively. After decomposing G_0 and G_m^2 in their enthalpy and entropy components and assuming that a correlation between enthalpy and entropy fluctuations does not exist, one finds

$$D_0^1 = a^2(1/\tilde{\nu}_{\nu,0})^{-1} \exp\left(\frac{S_{eff}^1}{k}\right) \tag{33}$$

with

$$S_{eff}^1 = S_0 - S_m^2/2k. \tag{34}$$

Here S_0 and S_m^2 mean the average and the variance of the distribution of S_ν, respectively.

According to Eqs. (33) and (34) our view of the physical meaning of D_0^1 has to be modified. It remains true that the entropy S_k^T extracted from a D_0^1 value that has been determined by extrapolating experimental $D_k^1(T)$ data in an Arrhenius plot to $1/T \to 0$ is a temperature average which is larger than S_{eff}^1 defined by Eq. (34). However, S_{eff}^1 is smaller than the average $S_0 \equiv \langle S_\nu \rangle$. Hence, an S_k^T value deduced from a D_0^1 value is not necessarily larger than S_0, but may come close to it. Therefore, S_k^T will approximately be identified with S_0 in the following.

From the preceding considerations the following recipe for estimating S_0 emerges. Identify D_0^1 formally with D_0^1. Then use Eq. (33) to calculate "S_{eff}^1". This is close to S_0. In doing so, three typical D_0^T values are considered which stand for different groups of tracer-amorphous-alloy systems. Group I ($D_0^T \approx 3 \times 10^{-7}$ m²/s) is represented by the diffusion of Fe in $Fe_{91}Zr_9$, group II ($D_0^T \approx 10^{-4}$ m²/s) by Fe in various Fe-Ni-B alloys, and group III ($D_0^T \approx 7 \times 10^{-6}$ m²/s) by Zr in $Fe_{24}Zr_{76}$. Using $a^2 = 6 \times 10^{-20}$ m² and $(1/\tilde{\nu}_{\nu,0})^{-1} = 10^{13}$ s^{-1}, S_0 is found to be about $-0.6\,k$, $5.2\,k$, or $30.2\,k$ for group I, II, or III, respectively. Note that in the case of the direct diffusion mechanisms discussed here these S_0 values mean average tracer migration entropies. (It is obvious that the corresponding is true for H_0. Therefore, in the following in similar cases the physical meaning will be mentioned for entropy-type parameters only.)

3.2.3.1.2 Indirect diffusion mechanisms—*Case A.* If the diffusion vehicles are present in a temperature-dependent quasi-equilibrium concentration, one readily finds

$$D_0^1 = f_i a^2(1/\tilde{\nu}_{\nu,0})^{-1} \exp(S_{eff}^1/k), \tag{35}$$

where S_{eff}^1 is given by Eq. (34). In this case, S_0 values estimated as described in the preceding section, represent sums of the average migration and formation entropies of the diffusion vehicles. The mean attempt frequency $(1/\tilde{\nu}_{\nu,0})^{-1}$ refers to the diffusion vehicles, too. f_i is the so-called correlation factor; by definition, it lies in

diffusion data on ^{59}Fe in $Fe_{91}Zr_9$ ($D_0^T = 3 \times 10^{-7}$ m²/s) and ^{95}Zr in $Fe_{24}Zr_{76}$ ($D_0^T = 7 \times 10^{-6}$ m²/s) yields $D_0^1 = 10^{-8}$ m²/s for $H_m = 0.09$ eV and $D_0^1 = 10^{-2}$ m²/s for $H_m = 0.2$ eV, respectively, provided in these cases the ratio H_m/H_{eff}^1 is close to that for ^{59}Fe in $Fe_{78}Si_9B_{13}$.

From the preceding paragraph it is obvious that the D_0^1 values have a more direct physical meaning than the quantities D_0^T obtainable from experimental D_R^1 data by the extrapolation $1/T \to 0$. However, it should be noted that in the derivation of D_0^1 the existence of a distribution of the migration entropies S_v entering the pre-exponential frequency factors

$$\nu_{v,0} = \tilde{\nu}_{v,0} \exp(S_v/k) \tag{30}$$

($\tilde{\nu}_{v,0}$ = attempt frequencies) has not yet been taken into account explicitly. This deficiency will be removed in Section 3.2.3.1.1, where $D_0^1 \equiv a^2(1/\nu_{v,0})^{-1}$ will be considered in more detail.

3.2 *Diffusion Mechanisms*

3.2.1 *Diffusivity enhancement in the unrelaxed amorphous state* As discussed in detail by Frank *et al.*,[44] the diffusivity enhancements δD^T in unrelaxed amorphous alloys represent contributions of indirect tracer diffusion via quasi-vacancies, which are usually denoted as free volume. This interpretation is in accordance with the fact that the decrease of δD^T during irreversible relaxation is accompanied by the elimination of excess free volume.

3.2.2 *Nature of small activation-enthalpy barriers observed in short-time experiments on relaxed specimens* From the interpretation of the diffusivity enhancement in the unrelaxed amorphous state given in Section 3.2.1 a tentative explanation of observation (k) [Section 2.2] emerges. After the elimination of the excess free volume, a remainder of inhomogeneously distributed free volume is retained. It is clear that—irrespective of the specific nature of the diffusion mechanism in the relaxed amorphous state—within islands of retained free volume, atomic rearrangements can take place with lower activation enthalpies than in the denser surrounding. These local low-enthalpy barriers will be detected in short-time experiments. By contrast, long-range diffusion observed in tracer diffusion studies on relaxed samples is controlled by the higher activation enthalpy barriers in the more closely packed material around free-volume islands.

3.2.3 *Long-range diffusion in the relaxed amorphous state* In Section 3.1, for the sake of simplicity it has been assumed that in pre-annealed amorphous alloys, diffusion occurs via a direct diffusion mechanism. This assumption will be critically tested in the following.

3.2.3.1 Pre-exponential Factors D_0^T—A model of tracer self-diffusion in relaxed amorphous alloys must explain the tremendous variation of D_0^T from alloy to alloy as well as from tracer to tracer, say, from ^{59}Fe to ^{95}Zr.

3.2.3.1.1 Direct diffusion mechanisms—In order to derive an explicit expression of D_0^1, Eq. (7) is replaced by

$$\nu_v = \tilde{\nu}_{v,0} \exp(-G_v/kT), \tag{31}$$

where $G_v \equiv H_v - TS_v$ is the Gibbs free energy barrier between the sites i and j. A statistical treatment analogous to that in Section 3.1 leads to

$$D^1(T) = a^2 \frac{1}{\left\langle \frac{1}{\tilde{\nu}_{v,0}} \right\rangle} \exp(-G_0/kT) \exp\left[-\frac{G_m^2}{2(kT)^2}\right]. \tag{32}$$

In Eq. (32) G_0 and G_m^2 mean the average $\langle G_v \rangle$ and the variance of the Gaussian distribution of G_v, respectively. After decomposing G_0 and G_m^2 in their enthalpy and entropy components and assuming that a correlation between enthalpy and entropy fluctuations does not exist, one finds

$$D_0^1 = a^2(1/\tilde{\nu}_{v,0})^{-1} \exp\left(\frac{S_{eff}^1}{k}\right) \tag{33}$$

with

$$S_{eff}^1 = S_0 - S_m^2/2k. \tag{34}$$

Here S_0 and S_m^2 mean the average and the variance of the distribution of S_v, respectively.

According to Eqs. (33) and (34) our view of the physical meaning of D_0^1 has to be modified. It remains true that the entropy S_R^T extracted from a D_0^1 value that has been determined by extrapolating experimental $D_R^1(T)$ data in an Arrhenius plot to $1/T \to 0$ is a temperature average which is larger than S_{eff}^1 defined by Eq. (34). However, S_{eff}^1 is smaller than the average $S_0 \equiv \langle S_v \rangle$. Hence, an S_R^T value deduced from a D_0^1 value is not necessarily larger than S_0, but may come close to it. Therefore, S_R^T will approximately be identified with S_0 in the following.

From the preceding considerations the following recipe for estimating S_0 emerges. Identify D_0^1 formally with D_0^1. Then use Eq. (33) to calculate "S_{eff}^1". This is close to S_0. In doing so, three typical D_0^1 values are considered which stand for different groups of tracer-amorphous-alloy systems. Group I ($D_0^T \approx 3 \times 10^{-7}$ m²/s) is represented by the diffusion of Fe in $Fe_{91}Zr_9$, group II ($D_0^T \approx 10^{-4}$ m²/s) by Fe in various Fe–Ni–B alloys, and group III ($D_0^T \approx 7 \times 10^{-6}$ m²/s) by ^{95}Zr in $Fe_{24}Zr_{76}$. Using $a^2 = 6 \times 10^{-20}$ m² and $(1/\tilde{\nu}_{v,0})^{-1} = 10^{13}$ s^{-1}, S_0 is found to be about $-0.6\,k$, $5.2\,k$, or $30.2\,k$ for group I, II, or III, respectively. Note that in the case of the direct diffusion mechanisms discussed here these S_0 values mean average tracer migration entropies. (It is obvious that the corresponding is true for H_0. Therefore, in the following in similar cases the physical meaning will be mentioned for entropy-type parameters only.)

3.2.3.1.2 Indirect diffusion mechanisms—*Case A.* If the diffusion vehicles are present in a temperature-dependent quasi-equilibrium concentration, one readily finds

$$D_0^1 = f_c a^2(1/\tilde{\nu}_{v,0})^{-1} \exp(S_{eff}^1/k), \tag{35}$$

where S_{eff}^1 is given by Eq. (34). In this case, S_0 values estimated as described in the preceding section, represent sums of the average migration and formation entropies of the diffusion vehicles. The mean attempt frequency $(1/\tilde{\nu}_{v,0})^{-1}$ refers to the diffusion vehicles, too. f_c is the so-called correlation factor; by definition, it lies in

the range $0 \leq f_v \leq 1$. Using $f_v = 0$ [illegible] and the same [illegible] diffusion for the other quantities, the estimated values of [illegible] larger by $0.7\,k$ than in the case of direct diffusion for all the three groups of systems considered.

Case B. If the diffusion vehicles are present in a temperature-independent non-equilibrium concentration C_v, the pre-exponential factor of D^1 is given by

$$D_0^1 = f_v C_v a^2 (1/\bar{\nu}_{4,0})^{-1} \exp(S_{em}^1/k), \tag{36}$$

where S_{em}^1 is defined by Eq. (34). In this case, S_0 values derived from experimental D_0^1 values with the aid of Eq. (36) and the formal identifications $D_0^1 \equiv D_0^1$ and $S_0 \equiv S_{em}^1$ (Section 3.2.3.1.1) have the meaning of average migration entropies of the diffusion vehicles. For the groups I, II, and III one finds $S_0 = 4.7\,k$, $10.5\,k$, and $35.5\,k$, respectively. In these estimates $C_v = 10^{-2}$ (corresponding to a density increase of about 1% during the crystallization of amorphous alloys) has been used in order to model indirect diffusion via quasi-vacancies present in a temperature-independent non-equilibrium concentration.

3.2.3.2 Cut Down of the Potential Self-diffusion Mechanisms of Transition Metals in Amorphous Metallic Alloys—As already indicated by the title of this section, we shall exclude the diffusion of "small" atoms (e.g., H, B, Si, C) in amorphous metallic alloys from the subsequent discussion. Cahn's[43] proposal that such atoms diffuse by an interstitial-like direct diffusion mechanism appears plausible. However, in spite of the alleged support of this mechanism by diffusivity—T_g/T scaling plots (T_g = glass temperature),[44] additional confirmation is desirable.

Concerning the diffusion of "large" atoms in amorphous structures, Cahn[43] introduced the idea that the largest voids present in the amorphous structure are involved. This is an indirect diffusion mechanism that resembles the self-diffusion via vacancies in crystalline metals. Cahn claims that Buschow's[47] prediction that the formation enthalpy of holes in binary metallic glasses increases linearly with the glass temperature supports this picture. It remains unclear, however, how this mechanism might account for the recent observations listed in Section 2.1.

In what follows the attempt will be made to narrow down the potential diffusion mechanisms with the aid of the check list of the experimental findings (a) to (i) (Section 2.1). Doing so, one has to keep in mind that the following major decisions have to be made before a specific model of diffusion can be proposed: 1) Are there different diffusion mechanisms for different transition metal tracers and different amorphous alloys? 2) Does, in a given system, the same mechanism dominate in the entire temperature regime investigated? 3) Does diffusion occur directly or indirectly?—If it takes place via an indirect mechanism, 4) does this involve vacancy-like or interstitial-like quasi-defects and 5) are these present in thermal quasi-equilibrium or in a temperature-independent concentration?

The answer to the second of the above-mentioned questions is most straightforward. The fact that in each amorphous alloy the diffusivities of both Fe and Zr tracers obey (quasi-)Arrhenius laws in the entire temperature regimes investigated [observation (b)] strongly suggests that in a given system the same diffusion mechanism operates at all accessible temperatures.

The fact that in most amorphous alloys the self-diffusion enthalpies are small in comparison with those in comparable crystalline metals [observation (e)] is at variance with interstitialcy-like indirect diffusion involving quasi-interstitials in thermal equilibrium since the formation enthalpy of quasi-interstitials is expected

to be distinctly [illegible] than that of [illegible] govern self-diffusion in

[illegible] facts that are present in a non-equilibrium concentration [illegible] studies on electron irradiated [illegible] recovery below room temperature, crystallization [illegible] migration. Hence, the [illegible] say, 1 eV. This fact cannot be reconciled with interstitials present in a non-equilibrium concentration, since diffusion enthalpy (1.5 to 2.5 eV) should be identical with the migration enthalpy of the quasi-interstitials.

After the preceding discussion, indirect diffusion mechanisms involving vacancy-like quasi-defects and direct diffusion mechanisms are left over as potential self-diffusion mechanisms of transition metal atoms in relaxed amorphous alloys. In the following the discussion branches off in the cases "Fe or Zr diffusion in Fe-Zr alloys" and "Fe diffusion in Fe-base or (Fe, Ni)-base metal-metalloid alloys".

3.2.3.3 Self-diffusion in Fe–Zr Alloys—The self-diffusion in Fe-Zr alloys[28,29,48] plays an outstanding role in the discussion of diffusion mechanisms in amorphous alloys because of the following reasons: (A) It is these amorphous alloys on which the most systematic diffusion studies have been performed, particularly as far as the width of the alloy composition regime is concerned. (B) Within this series of systems an enormous variation of the pre-exponential factors D_0^1 takes place (Figure 2), corresponding to a variation of the self-diffusion entropy over about $30\,k$ (Section 3.2.3.1). (C) For Fe in $Fe_{91}Zr_9$ it has been demonstrated unambiguously that a temperature change from T_1 to T_2 within the *relaxed* amorphous state gives rise to a *delay-free* change in D^1 from $D_R^1(T_1)$ to $D_R^1(T_2)$ [item (c) in Section 2.1].

Let us begin with the discussion of (C). At the temperatures at which diffusion anneals on amorphous alloys are performed, changes in the quasi-vacancy concentrations occur on time scales that allow us to monitor the kinetics by which the new concentrations are established. This may be seen from the gradual decrease of D^1, while, by irreversible structural relaxations, excess free volume (= supersaturation of quasi-vacancies) is eliminated (Section 3.2.1). Hence, if diffusion in the relaxed amorphous state took place by indirect diffusion via quasi-vacancies in thermal equilibrium, after a temperature change within the relaxed state the establishing of the new quasi-vacancy equilibrium concentration should be reflected by a gradual (and thus observable) change of D^T from $D_R^1(T_1)$ to $D_R^1(T_2)$. At least for the diffusion of Fe in $Fe_{91}Zr_9$ this is not the case [see (C)]. On the basis of this observation the mechanism of indirect diffusion via thermal quasi-vacancies is excluded for the Fe-Zr alloys.

In the following a self-diffusion mechanism for Fe-Zr alloys will be proposed which accounts for the special features of these alloys. The mechanism will be presented in terms of direct diffusion. This description is based on the picture that the remainder of (a temperature-independent concentration of) free volume left over after irreversible structural relaxations is inherent to the relaxed amorphous quasi-equilibrium state. Without this minimum of free volume the material would have to become crystalline. An alternative view would be to ascribe the lower density of the relaxed amorphous state in comparison to the crystalline state to a temperature-independent non-equilibrium concentration of quasi-vacancies. Then

the diffusion mechanisms in Fe–Zr alloys to be proposed below should consequently be translated into terms of indirect diffusion via quasi-vacancies present in a temperature-independent non-equilibrium concentration. This concept has not been adopted since it appears to be inconsistent to endow a quasi-equilibrium state with an inevitable non-equilibrium concentration of quasi-vacancies. Obviously, as far as the physical content is concerned, in the present case the distinction between direct diffusion and indirect diffusion via a non-equilibrium concentration of quasi-vacancies is semantic.

First we consider group-I systems. Fe in $Fe_{91}Zr_9$ is the most extreme representative so far investigated. It possesses the smallest D_0^I value, which in terms of a direct diffusion mechanism corresponds to a negative tracer migration entropy ($S_0 = -0.6\ k$) [Section 3.2.3.1.1], as well as the smallest value of H_R^I ($= 1.5$ eV). We propose that diffusional jumps of the small Fe tracers in the loosely packed $Fe_{91}Zr_9$ structure become possible when, as a result of thermal fluctuations, the spread-out free volume which is inherent to the relaxed amorphous state of group-I alloys contracts next to the tracer atoms, thus enabling these to jump into the so-produced vacant space of the size of about one atomic volume (Figure 13). Indeed this contraction of free volume corresponds to a negative migration entropy. Obviously the unification of two "half-vacancies" just results in a decrease of the configurational entropy by about $-k \ln 2 \approx -0.7\ k$. The fact that this mechanism involves the jumps of single, small Fe atoms makes understandable why H_R^I is small. Note that in spite of this, a collective feature is inherent to this process, namely the fluctuation-induced contraction of spread-out free volume.

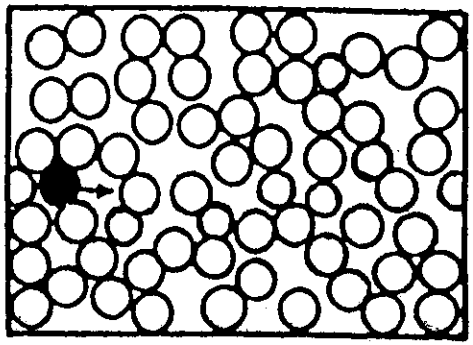

FIGURE 13 Schematic illustration of the elementary diffusion process in a group-I system (e.g., Fe in $Fe_{91}Zr_9$). The tracer atom (●) jumps into the fluctuation-induced vacant space (~) next to the tracer.

In group-III systems (e.g., Zr in $Fe_{24}Zr_{76}$) large tracer atoms have to undergo diffusion in a densely packed matrix (Figure 14). This requires that the tracers move together with their neighbouring atoms. Such a collective displacement of a group of atoms can take place where, by a thermal fluctuation, grown-in free volume is temporarily smeared out over the volume occupied by these atoms. In this way, for the duration of the fluctuation, the "viscosity" of this "droplet" of atoms is decreased. Since in this mechanism many atoms jump collectively, the large diffusion enthalpy of Zr in $Fe_{24}Zr_{76}$, $H_R^{III} = 3.2$ eV, becomes understandable.

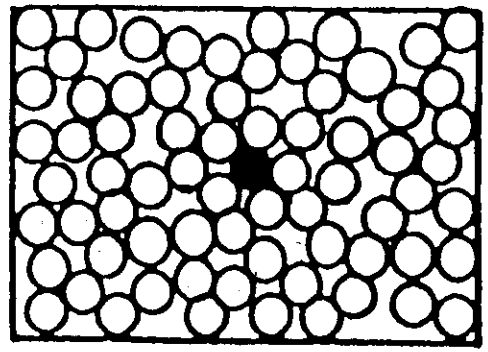

FIGURE 14 Schematic illustration of the elementary diffusion process in a group-III system (e.g., Zr in $Fe_{24}Zr_{76}$). The tracer atom (●) can only move collectively with its neighbouring atoms.

With the aid of the relationship

$$\Delta V = \frac{S_0}{\alpha K} \tag{37}$$

between the migration entropy S_0 and the migration volume ΔV, which has been derived from thermodynamic considerations,[48] one finds that the droplets of atoms participating in collective displacements comprise about 60 atomic volumes. In this estimate $S_0 = 30\ k$ (Section 3.2.3.1.1), $5.9 \times 10^{-5}\ K^{-1}$ for the isobaric volume expansion coefficient α, and $8.3 \times 10^{10}\ N/m^2$ for the isothermal bulk modulus K have been used.[48]

In the Fe–Zr systems of group II (Figure 2) a continuous transition takes place between the two diffusion mechanisms proposed above for Fe–Zr systems of groups I and III, respectively. This transition is reflected by the increase of D_0^I and H_R^I for either Fe or Zr diffusion with increasing packing density of the Fe–Zr alloys (which increases approximately monotonically with increasing Zr content) and by the fact that, in an alloy of given composition, D_0^I and H_R^I are larger for the larger Zr tracers than for the smaller Fe tracers (Figures 2 and 3, and observations (h) and (i) in Section 2.1).

3.2.3.4 Fe Diffusion in Fe-base or (Fe, Ni)-base Metal–Metalloid Alloys—According to Figure 2 these systems belong to group II. Therefore, it is tempting to interpret the corresponding diffusion data in terms of the direct collective diffusion mechanism proposed in the preceding section for group-II Fe–Zr systems. If this is done, one finds that the number of collectively diffusing atoms should increase from a few in $Fe_{78}Si_9B_{13}$ to about 10 in $Fe_{80}B_{20}$. However, in the case of the metal–metalloid alloys alternative interpretations cannot be ruled out. For instance, an exclusion of indirect diffusion via quasi-vacancies in thermal quasi-equilibrium on the basis of an *unambiguous* experiment of type (c) [Section 2..] is not yet possible for the metal–metalloid alloys. The fact that the D_0^I values of these alloys lie even closer to the pre-exponential factors of the diffusivities in crystalline metals than the D_0^I values of the group-II Fe–Zr alloys (Figure 2) might be taken pro the indirect diffusion by thermal quasi-vacancies in amorphous metal–metalloid alloys.

In this mechanism, D_0^I values which are slightly higher than in crystalline metals (e.g., $D_0^I = 7.9 \times 10^{-4}$ m²/s in $Fe_{80}B_{20}$) may be interpreted in terms of smeared-out thermal quasi-vacancies. This picture has been stimulated by a proposal of Seeger and Chik,[49] who ascribed the fact that the pre-exponential factor of the self-diffusion coefficient in crystalline germanium is more than an order of magnitude larger than in crystalline metals to the existence of smeared-out Ge vacancies.

3.2.3.5 Physical Origin of the Narrowness of the Diffusion-Enthalpy Spectra Governing Long-range Diffusion in Relaxed Amorphous Alloys—An interesting point is that the direct tracer diffusion, either collectively with neighbouring atoms (group-III Fe–Zr systems) or facilitated by local contractions of grown-in free volume (group-I Fe–Zr systems), as well as the indirect diffusion via thermal spread-out quasi-vacancies (Fe in metal–metalloid alloys?) involve activation mechanisms in which many atoms participate. Thus these mechanisms average over the inhomogeneities of the amorphous structure on the nearest-neighbour-distance scale. This may be the reason why in a given relaxed amorphous alloy the diffusion is controlled by a surprisingly narrow distribution of the activation enthalpies ($H_m = 0.14$ eV and 0.13 eV for Fe in $Fe_{80}B_{20}$ and $Fe_{78}Si_9B_{13}$, respectively), as evidenced by the quasi-Arrhenius laws obeyed by the coefficients of the transition metal self-diffusion in all relaxed amorphous metallic alloys so far thoroughly investigated.

REFERENCES

1. M. R. J. Gibbs, J. E. Evetts, and J. A. J. Leake, *J. Mater. Sci.* **18**, 278 (1983).
2. H. Kronmüller, *Phil. Mag.* **48**, 127 (1983).
3. J. E. Evetts, in *Rapidly Quenched Metals*, S. Steeb and H. Warlimont (Eds.) (Elsevier, Amsterdam, 1985), p. 607.
4. H. Kronmüller and N. Moser, in *Rapidly Quenched Metals*, S. Steeb and H. Warlimont (Eds.) (Elsevier, Amsterdam, 1985), p. 603.
5. T. Egami, in *Amorphous Metals and Semiconductors*, Acta Scripta Met., Proc. Series Vol. 3, P. Haasen and R. I. Jaffee (Eds.) (Pergamon Press, Oxford, 1986), p. 222.
6. Z. Altounian and J. O. Strom-Olsen, *J. Mater. Res.* **2**, 54 (1987).
7. H. S. Chen, in *Amorphous Metals and Semiconductors*, Acta Scripta Met., Proc. Series Vol. 3, P. Haasen and R. I. Jaffee (Eds.) (Pergamon Press, Oxford, 1986), p. 126.
8. W. Chambron and A. Chamberod, *J. de Physique* **42**, C5-511 (1981).
9. H. Kronmüller, H.-Q. Guo, W. Fernengel, A. Hofmann, and N. Moser, *Cryst. Latt. Def. and Amorph. Mater.* **11**, 135 (1985).
10. H. Kronmüller and N. Moser, in *Amorphous Metallic Alloys*, F. E. Luborsky (Ed.) (Butterworths, London, 1983), p. 341.
11. P. Allia and F. Vinai, *Phys. Rev.* **B26**, 6141 (1982).
12. H. Kronmüller, *J. Magn. Magn. Mater.* **41**, 366 (1984).
13. F. Rettenmeier and H. Kronmüller, *phys. stat. sol.* (*a*) **93**, 221 (1986).
14. H. Kronmüller, in *Amorphous Metals and Semiconductors*, Acta Scripta Met., Proc. Series Vol. 3, P. Haasen and R. I. Jaffee (Eds.) (Pergamon Press, Oxford, 1986), p. 259.
15. H. Kronmüller, in *Rapidly Quenched Metals*, T. Masumoto and K. Suzuki (Eds.) (Tohoku University, Sendai, 1982), p. 971.
16. M. R. J. Gibbs and J. E. Evetts, in *Rapidly Quenched Metals*, T. Masumoto and K. Suzuki (Eds.) (Tohoku University, Sendai, 1982), p. 479.
17. X. Z. Dong, W. Fernengel, and H. Kronmüller, *Appl. Phys.* **A28**, 103 (1982).
18. R. Hasegawa, U. R. V. Ramanan, and G. E. Fish, *J. Appl. Phys.* **53**, 2276 (1982).
19. K. Bothe and H. Neuhäuser, in *Rapidly Quenched Metals*, S. Steeb and H. Warlimont (Eds.) (Elsevier, Amsterdam, 1985), p. 735; K. Bothe, *ibid.*, p. 731.
20. H. S. Chen and N. Morito, *J. Non-Cryst. Solids* **72**, 287 (1985).
21. B. Cantor and R. W. Cahn, in *Amorphous Metallic Alloys*, F. E. Luborsky (Ed.) (Butterworths, London, 1983), p. 487.

22. B. Cantor, in *Rapidly Quenched Metals*, S. Steeb and H. Warlimont (Eds.) (Elsevier, Amsterdam, 1985), p. 595.
23. H. S. Chen, L. C. Kimerling, L. C. Poate, and W. L. Brown, *Appl. Phys. Lett.* **32**, 461 (1987).
24. F. E. Luborsky and F. Bacon, in *Rapidly Quenched Metals*, T. Masumoto and K. Suzuki (Eds.) (Tohoku University, Sendai, 1982), p. 561.
25. U. Köster and U. Herold, in *Glassy Metals I*, H.-J. Güntherodt and H. Beck (Eds.) (Springer, Berlin, 1981), p. 225.
26. Y. Limoge, G. Brebec, and Y. Adda, in *Diffusion and Defects*, F. J. Kedves and D. L. Beke (Eds.) (Trans Tech Publ., Aedermannsdorf, 1983), p. 285.
27. P. Valenta, K. Maier, H. Kronmüller, and K. Freitag, *phys. stat. sol.* (*a*) **105**, 537 (1981); **106**, 129 (1981).
28. J. Horváth, K. Pfahler, W. Ulfert, W. Frank, and H. Kronmüller, *Mater. Sci. Forum* **15–18**, 523 (1987).
29. J. Horváth, J. Ott, K. Pfahler, and W. Ulfert, *Mater. Sci. Eng.* **97**, 409 (1988).
30. J. Horváth and H. Mehrer, *Cryst. Latt. Def. and Amorph. Mater.* **13**, 1 (1986).
31. K. Pfahler, J. Horváth, W. Frank, and H. Mehrer, in *Rapidly Quenched Metals*, S. Steeb and H. Warlimont (Eds.) (Elsevier, Amsterdam, 1985), p. 755.
32. K. Pfahler, *Diplomarbeit*, University of Stuttgart (1985); K. Pfahler, J. Horváth, and W. Frank, *Cryst. Latt. Def. and Amorph. Mat.* **17**, 249 (1987).
33. F. Rettenmeier, E. Kisdi-Koszo, and H. Kronmüller, *phys. stat. sol.* (*a*) **93**, 597 (1986).
34. W. Rössle, *Diplomarbeit*, University of Stuttgart (1985).
35. H. Kronmüller, N. Moser, A. Hofmann, and W. Gehring, *Mat. Sci. Eng.* **97**, 473 (1988).
36. J. W. Haus and K. W. Kehr, *Physics Reports* **150**, 265 (1987).
37. S. Alexander, J. Bernasconi, W. R. Schneider, and R. Orbach, *Rev. Mod. Phys.* **53**, 175 (1981).
38. R. Zwanzig, *J. Stat. Phys.* **28**, 127 (1982).
39. P. J. H. Denteneer and M. H. Ernst, *J. Phys. C* **16**, L961 (1983).
40. P. J. H. Denteneer and M. H. Ernst, *Phys. Rev.* **B29**, 1775 (1984).
41. I. Webman, *Lecture Notes in Physics* **154**, 297 (1982).
42. I. Webman and J. Klafter, *Phys. Rev.* **B26**, 5950 (1982).
43. B. Movaghar and W. Schirmacher, *J. Phys. C* **14**, 859 (1981).
44. W. Frank, J. Horváth, and H. Kronmüller, *Mat. Sci. Eng.* **97**, 415 (1988).
45. R. W. Cahn, *J. Vac. Sci. Technol.* **A4**, 3071 (1986).
46. B. Cantor, in *Amorphous Metals and Semiconductors*, Acta Scripta Met., Proc. Series Vol. 3, P. Haasen and R. I. Jaffee (Eds.) (Pergamon Press, Oxford, 1986), p. 108.
47. K. H. J. Buschow, *Solid State Comm.* **43**, 171 (1982).
48. K. Pfahler, *Dr. rer. nat. thesis*, University of Stuttgart (1987).
49. A. Seeger and K. P. Chik, *phys. stat. sol.* **29**, 455 (1968).
50. T. Dosdale and R. J. Brook, *J. Am. Cer. Soc.* **66**, 392 (1983).

Materials Science and Engineering, 97 (1988) 415–418

Diffusion Mechanisms in Amorphous Alloys*

W. FRANK, J. HORVÁTH and H. KRONMÜLLER

Max-Planck-Institut für Metallforschung, Institut für Physik, and Universität Stuttgart, Institut für Theoretische und Angewandte Physik, P.O. Box 800 665, D-7000 Stuttgart 80 (F.R.G.)

Abstract

A critical analysis of experimental data shows that self-diffusion in relaxed amorphous alloys is controlled by mechanisms involving collective thermal activations. Whereas in Fe–Zr alloys both ^{59}Fe and ^{95}Zr diffuse via direct mechanisms that change with the alloy composition (e.g. in the densely packed $Fe_{24}Zr_{76}$ the large ^{95}Zr tracers move collectively with many neighbouring atoms), further experiments are needed to decide whether ^{59}Fe in metal–metalloid alloys also diffuses directly or indirectly via mobile spread-out quasi-vacancies present at thermal equilibrium. The tracer diffusivity decrease occurring in as-quenched amorphous alloys reflects that the initial contribution of a quasi-vacancy mechanism slows down because of the elimination of excess free volume during relaxation.

1. Introduction

Although amorphous alloys have been in the limelight of materials science for many years and have found numerous applications in technology, our knowledge on the mechanisms of diffusion in the amorphous state is quite poor. This is mainly because the majority of the experimental data on the diffusion in amorphous alloys scatter considerably and, in part, are even contradictory. The cause of this has been revealed by investigations at our Stuttgart diffusion laboratory by means of the radiotracer technique in combination with ion beam sputtering for serial sectioning of the specimens. In these studies, it has been demonstrated that in as-quenched amorphous alloys the diffusivity decreases markedly during diffusion annealing until a relaxed amorphous state is reached. In previous investigations in which this phenomenon was either not realized or not properly taken into account, as a consequence the scatter of the data was inexplicably large.

In a recent summary [1] and in a companion paper at this conference [2], Horváth and collaborators have presented data on the self-diffusion of ^{59}Fe in various amorphous iron-based metal–metalloid alloys and of ^{59}Fe or ^{95}Zr in amorphous metal–metal alloys of the composition Fe_yZr_{100-y}. These data are free of the deficiency described above and thus represent a sound base for the subsequent attempt to understand the diffusion in amorphous alloys.

2. Observations to be explained

A common feature of all amorphous alloys appears to be that the self-diffusivities D^T of tracer atoms in as-quenched specimens decrease during thermal annealing as a result of structural relaxations within the amorphous state. This effect may be described by the relationship

$$D^T(t, T) = \delta D^T(t, T) + D^T{}_R(T) \tag{1}$$

where $D^T{}_R$ is the diffusivity in the relaxed state and is a function of temperature T (see eqn. (2)) but not of time t. The diffusivity enhancement δD^T in the unrelaxed state drops to zero during annealing. After completion of the relaxation at an annealing temperature T_1, a temperature change to T_2 (not leading to crystallization) gives rise to a delay-free change in D^T from $D^T{}_R(T_1)$ to $D^T{}_R(T_2)$. Hence the relaxed amorphous state is a well-defined metastable equilibrium state.

A further property which has been observed in amorphous alloys so far investigated is that $D^T{}_R$ obeys an Arrhenius law

$$D^T{}_R = D^T{}_0 \exp\left(-\frac{H^T{}_R}{kT}\right) \tag{2}$$

(k is Boltzmann's constant). This is quite a surprising result, since at first sight thermally activated diffusion in non-crystalline solids is expected to involve overcoming of barriers of different heights.

The $D^T{}_R$ values are larger by five to ten orders of magnitude than the self-diffusivities obtained by extrapolation of the data measured on crystalline iron, nickel or zirconium to the low temperatures at which the $D^T{}_R$ values have been determined.

*Paper presented at the Sixth International Conference on Rapidly Quenched Metals, Montréal, August 3-7, 1987.

0025-5416/88/$3.50

The pre-exponential factors $D^T{}_0$ found in various amorphous alloys range from three orders of magnitude below to ten orders of magnitude above 10^{-4} m^2 s^{-1}, which is typical of the pre-exponential factors of the bulk self-diffusion coefficients in crystalline metals.

There is a clear tendency that, the larger the diffusion enthalpy $H^T{}_R$ in a relaxed amorphous alloy, the larger is $D^T{}_0$.

In a given Fe–Zr alloy, $H^T{}_R$ and $D^T{}_0$ are larger for the diffusion of the larger ^{95}Zr tracers than for the diffusion of the smaller ^{59}Fe tracers. For a given tracer ^{95}Zr or ^{59}Fe, $H^T{}_R$ and $D^T{}_0$ are larger in the less open $Fe_{24}Zr_{76}$ structure than in the more open $Fe_{91}Zr_9$ structure.

Replacement of 1% of the iron atoms in amorphous $Fe_{80}B_{20}$ by (large) tungsten atoms reduces the ^{59}Fe diffusivity drastically, *i.e.* by 360% at 593 K.

All the extraordinary diffusion properties of amorphous alloys reported above find a natural explanation in terms of the diffusion mechanisms to be proposed in Sections 4 and 5.

3. Theoretical background [3]

Guided by the fact that the self-diffusion coefficients in relaxed amorphous alloys show an Arrhenius-type temperature dependence, in the following it is assumed that $D^T{}_R$ may be written in the simple form

$$D^T{}_R = AD \tag{3}$$

where D is a diffusivity controlled by a single activation enthalpy. As will be seen in Section 4, an analogous expression for δD^T turns out to be useful.

3.1. Direct diffusion

If the tracer self-diffusion takes place by random walks of the tracers without any cooperation of mobile "defects" that serve as diffusion vehicles (direct diffusion mechanism), in eqn. (3) the factor A is equal to unity and D is the diffusivity of the tracers, *i.e.*

$$D^T{}_R = D^T{}_0 \exp\left(-\frac{H_T{}^M}{kT}\right) \tag{4a}$$

$$D^T{}_0 \equiv \tfrac{1}{2}\eta_T \langle x_T{}^2\rangle \nu_{T,0} \exp\left(\frac{S_T{}^M}{kT}\right) \tag{4b}$$

where $H_T{}^M$ and $S_T{}^M$ are the migration enthalpy and entropy of the tracers. The quantities $\langle x_T{}^2\rangle$, $\nu_{T,0}$ and η_T are the mean square of the jump distance components in an arbitrary x direction, the corresponding jump attempt frequency and the number of possible paths for jumps with an x component respectively.

3.2. Indirect diffusion

If the tracers diffuse with the aid of diffusion vehicles, say quasi-vacancies (Section 4), in such an indirect diffusion mechanism $A \equiv f_V C_V$ and $D \equiv D_V$, where f_V is a correlation factor and where C_V and D_V are the concentration and the diffusivity of the diffusion vehicles (The subscript V denotes, in general, "diffusion vehicles" and, in particular, "quasi-vacancies".) Provided that the diffusion vehicles are present in their equilibrium concentration (case A), *i.e.* if

$$C_V{}^{eq} = \exp\left(\frac{S_V{}^F}{k}\right)\exp\left(-\frac{H_V{}^F}{kT}\right) \tag{5}$$

we have

$$D^T{}_R = D^T{}_0 \exp\left\{-\frac{H_V{}^F + H_V{}^M}{kT}\right\} \tag{6a}$$

$$D^T{}_0 \equiv \tfrac{1}{2} f_V \eta_V \langle x_V{}^2\rangle \nu_{V,0} \exp\{(S_V{}^F + S_V{}^M)/k\} \tag{6b}$$

where $H_V{}^F$ and $H_V{}^M$ are the formation and migration enthalpies of the diffusion vehicles and where $S_V{}^F$ and $S_V{}^M$ are the corresponding entropies. The meanings of the remaining quantities in eqn. (6b) are evident by analogy to eqn. (4b). If C_V is temperature independent (case B), then

$$D^T{}_R = D^T{}_0 \exp\left(-\frac{H_V{}^M}{kT}\right) \tag{7a}$$

$$D^T{}_0 \equiv \tfrac{1}{2} f_V \eta_V \langle x_V{}^2\rangle \nu_{V,0} \exp\left(\frac{S_V{}^M}{k}\right) C_V \tag{7b}$$

4. Diffusion in the unrelaxed amorphous state

The structural relaxation of amorphous alloys from an as-quenched into a metastable state, as reflected by a decrease in D^T (Sections 1 and 2), has been investigated by means of other techniques, *e.g.* electrical resistivity [4] and volume density [5] measurements. The latter have shown that structural relaxation always leads to an increase in the volume density. This indicates that the relaxation involves an elimination of an excess of the free volume retained during the quenching from the liquid state by which the amorphous material has been produced. Obviously, during relaxation, units of free volume, henceforth referred to as "quasi-vacancies", disappear via thermally activated migration. Therefore, it is plausible that the diffusivity enhancement δD^T in the unrelaxed state is due to an indirect diffusion of the tracers via quasi-vacancies. By analogy to eqns. (7), this may be expressed by

$$\delta D^T = f_V D_V \, \delta C_V \tag{8a}$$

where

$$D_V = D_{V,0}\exp\left(-\frac{H_V^M}{kT}\right) \tag{8b}$$

$$D_{V,0} \equiv \tfrac{1}{6}\eta_V\langle x_V^2\rangle\nu_{V,0}\exp\left(\frac{S_V^M}{k}\right) \tag{8c}$$

is the quasi-vacancy diffusivity. By describing the elimination of the excess quasi-vacancies during relaxation by first-order reaction kinetics, *i.e.*

$$\delta C_V = \delta C_V^0\exp\left(-\frac{t}{\tau_V}\right) \tag{8d}$$

where δC_V^0 is the value of the concentration δC_V of these "defects" in the as-quenched state and

$$\tau_V = \tau_{V,0}\exp\left(\frac{H_V^M}{kT}\right) \tag{8e}$$

the dominating relaxation time, the quasi-vacancy migration enthalpy H_V^M and the pre-exponential factor $\tau_{V,0}$ in eqn. (8e) have been estimated for $Fe_{40}Ni_{40}B_{20}$ as about or less than 1 eV and about 10^{-13} s respectively. The value of $\tau_{V,0}$ indicates that the excess quasi-vacancies diffuse to the surfaces of the specimens, although quasi-vacancy agglomeration and annihilation of quasi-vacancies in regions with a higher than average density may also play a role.

5. Diffusion in relaxed amorphous Fe–Zr alloys

5.1. Unlikelihood of case A of indirect diffusion

As demonstrated most systematically for ^{59}Fe in $Fe_{91}Zr_9$, a temperature change from T_1 to T_2 within the relaxed state leads to a change in D^T from $D^T_R(T_1)$ to $D^T_R(T_2)$ without any measurable delay. Hence, diffusivity changes within the relaxed state induced by temperature changes cannot result from changes in the quasi-vacancy concentration provided that the quasi-vacancy generation or annihilation cannot occur by mechanisms with characteristic times that are considerably shorter than the relaxation time τ_V for the quasi-vacancy transport to the specimen surface (Section 4). Although the existence of such fast mechanisms cannot definitively be excluded, at least for the Fe–Zr alloys case A of indirect diffusion will not be considered further. This appears to be justified since, as shown in the following, a global interpretation of the diffusion of both ^{59}Fe and ^{95}Zr in all relaxed amorphous Fe–Zr alloys investigated is possible in terms of direct diffusion.

5.2. ^{59}Fe in $Fe_{91}Zr_9$

^{59}Fe in $Fe_{91}Zr_9$ possesses the smallest values of H^T_R (≈ 1.5 eV) and D^T_0 ($\approx 3\times10^{-7}$ m^2 s^{-1}) observed in the a… stigated at our laboratory. W… umptions for $\langle x_T^2\rangle$ ($=4\times1$… $\langle x_T^2\rangle$), $\nu_{T,0}$ ($=10^{13}$ s^{-1}), ν_V … η_V ($=\eta_T$), f_V ($=0.5$) and C_V … g to a density increase of abo… crystallization of amorphous … value leads to $S_T^M/k \approx -1.7$ (eq… ≈ 3.6 (eqn. (7b)) depending on whe… on or case B of indirect diffusion is as… values are reasonable. They indicate that quasi-vacancies retained in the relaxed amorphous state are spread out. If the ^{59}Fe atoms diffuse directly, immobile spread-out quasi-vacancies must be contracted next to the ^{59}Fe atoms in order to enable these atoms to jump into the so-produced vacant space. Indeed the contraction of dispersed free volume when a tracer jumps from its equilibrium to its saddle point configuration corresponds to a decrease in entropy and thus to a negative S_T^M value of the order of magnitude estimated above. If the ^{59}Fe tracers diffuse indirectly via quasi-vacancies performing random walks, the above S_V^M value is indicative of an extension of the quasi-vacancies over a few atomic volumes, similar to the extension of vacancies in crystalline germanium under high temperature equilibrium conditions [3].

On the basis of the experimental data at present available, a decision between the two alternative diffusion mechanisms of ^{59}Fe in relaxed amorphous $Fe_{91}Zr_9$ cannot be made. At first sight, either mechanism appears to be plausible for the diffusion of the quite small ^{59}Fe atoms in the loosely packed amorphous $Fe_{91}Zr_9$. However, for indirect diffusion via quasi-vacancies, these would be able to disappear at the surface via long-range migration as in unrelaxed $Fe_{91}Zr_9$ (Section 4). Hence the maintenance of a constant quasi-vacancy concentration at a constant temperature would require the existence of a dynamic equilibrium between the generation and annihilation of quasi-vacancies, but we cannot imagine that there is any mechanism leading to such a dynamic equilibrium and not depending on temperature. Therefore, for ^{59}Fe in $Fe_{91}Zr_9$, case B of indirect diffusion appears to be unlikely. It should be noted that case A of indirect diffusion has already been shown in Section 5.1 to be unlikely, so that direct diffusion assisted by local contractions of immobile spread-out quasi-vacancies, for which the difficulty of case B of indirect diffusion does not exist, is left.

5.3. ^{95}Zr in $Fe_{24}Zr_{76}$

For ^{95}Zr in $Fe_{24}Zr_{76}$, Horváth *et al.* [1, 2] have observed the largest values of H^T_R (≈ 3.2 eV) and D^T_0 ($\approx 7\times10^{-6}$ m^2 s^{-1}). Although it has been shown that

with a high … t diffusion does not occur in rela… (Sections 5.1 and 5.2), these value… e diffusion of ^{95}Zr in $Fe_{24}Zr_{76}$ can … the same direct mechanism as the … in $Fe_{91}Zr_9$ does. This is not surpris… sely packed $Fe_{24}Zr_{76}$ the concentratio… in spread-out quasi-vacancies is low, so th… likely that quasi-vacancy contractions oc… ten enough to provide a sufficient number of holes that are large enough for the large ^{95}Zr tracers to jump into. The mechanism which is left for the diffusion of ^{95}Zr in $Fe_{24}Zr_{76}$ and which is compatible with the huge D^T_0 value observed is a collective motion of the tracers with a large number of neighbouring atoms (which is a direct diffusion mechanism). With the aid of eqn. (4b), we find that $S_T^M/k \approx 29$, which according to the relationship [6]

$$V_T^M \approx \frac{S_T^M}{\alpha K} \tag{9}$$

(α is the isobaric volume expansion coefficient and K the isothermal bulk modulus) corresponds to a migration volume V_T^M of about 60 atomic volumes. In this context the prediction of collective excitations in metallic glasses by Lewis and Ashcroft [7] appears to be noteworthy.

5.4. Retrospective summary and comparison with metal–metalloid alloys

The preceding discussion has shown that in the relaxed amorphous Fe–Zr alloys the self-diffusion of either ^{59}Fe or ^{95}Zr takes place by direct diffusion. For the small ^{59}Fe tracers in the loosely packed $Fe_{91}Zr_9$ matrix the diffusional jumps are facilitated by contractions of grown-in spread-out quasi-vacancies next to the tracers, whereas for the large ^{95}Zr tracers in the densely packed $Fe_{24}Zr_{76}$ matrix the diffusion is rendered difficult by the fact that they can only move collectively with a large number of neighbouring atoms. A transition between these two diffusion mechanisms is reflected by the increase in D^T_0 and H^T_R for either ^{59}Fe or ^{95}Zr diffusion with increasing packing density of the Fe–Zr alloys (which increases approximately monotonically with increasing zirconium content) and by the fact that, in an alloy of given composition, D^T_0 and H^T_R are larger for the larger ^{95}Zr tracers than for the smaller ^{59}Fe tracers.

The ^{59}Fe self-diffusion in the amorphous iron-based metal–metalloid alloys investigated by Horváth *et al.* [1, 2] shows qualitatively the same features as the ^{59}Fe or ^{95}Zr diffusion in amorphous Fe–Zr alloys. In the relaxed state, D^T_0 and H^T_R respectively reach from 4.6×10^{-7} m^2 s^{-1} and 2.1 eV in $Fe_{78}Si_9B_{13}$ to 7.9×10^{-3} m^2 s^{-1} and 2.4 eV in $Fe_{80}B_{20}$. These data are in accordance with the direct diffusion mechanism provided that the number of atoms diffusing collectively with a tracer increases from a few in $Fe_{78}Si_9B_{13}$ to the order of magnitude of 10 in $Fe_{80}B_{20}$. However, in these metal–metalloid alloys the existing experimental data do not allow us to exclude other mechanisms definitely. For example, indirect diffusion via more or less extended quasi-vacancies which are present in temperature-dependent equilibrium concentrations (case A in Section 3.2) appears to be an alternative for this group of materials. The fact that their D^T_0 values deviate only moderately from the pre-exponential factors of the diffusivities in crystalline metals would be in accordance with this picture.

An interesting point is that the direct tracer diffusion, either collectively with neighbouring atoms or facilitated by local contractions of grown-in spread-out quasi-vacancies, as well as the indirect diffusion via spread-out quasi-vacancies in thermal equilibrium involve activation mechanisms in which many atoms participate. Thus these mechanisms average over the inhomogeneities of the amorphous structure on the nearest-neighbour distance scale. This may be the reason why in a given relaxed amorphous alloy the diffusion is controlled by a single well-defined activation enthalpy, as indicated by the Arrhenius law found by experiment. Presumably, th… astic reduction in the ^{59}Fe diffusivity in $Fe_{80}B_{20}$ by the addition of 1 at.% W may be taken as further evidence for the collective character of the diffusion.

Acknowledgments

The authors are very grateful to Professor A. Seeger for stimulating discussions and to their collaborators (see refs. 1 and 2) for their help.

References

1 J. Horváth, K. Pfahler, W. Ulfert, W. Frank and H. Kronmüller, *Mater. Sci. Forum, 15–18* (1987) 523.
2 J. Horváth, J. Ott, K. Pfahler and W. Ulfert, *Mater. Sci. Eng., 97* (1988) 409.
3 W. Frank, U. Gösele, H. Mehrer and A. Seeger, in G. E. Murch and A. S. Nowick (eds.), *Diffusion in Crystalline Solids*, Academic Press, New York, 1984, p. 63.
4 T. Komatsu, S. Sato and K. Matusita, *Acta Metall., 34* (1986) 1899.
5 T. Komatsu, K. Matusita and R. Yokota, *J. Non-Cryst. Solids, 85* (1986) 358.
6 K. Pfahler, *Dr. rer. nat. Thesis*, University of Stuttgart, 1987.
7 L. J. Lewis and N. W. Ashcroft, *Phys. Rev. B, 34* (1986) 8477.

Materials Science and Engineering, 97 (1988) 409–413

Tracer Diffusion in Amorphous Alloys*

J. HORVÁTH, J. OTT, K. PFAHLER and W. ULFERT

Max-Planck-Institut für Metallforschung, Institut für Physik, and Universität Stuttgart, Institut für Theoretische und Angewandte Physik, P.O. Box 800 665, D-7000 Stuttgart 80 (F.R.G.)

Abstract

Self-diffusion in various iron-based amorphous metal–metalloid alloys and in amorphous metal–metal systems Fe_xZr_{100-x} was investigated using radioactive ^{59}Fe and ^{95}Zr tracer atoms in combination with ion-beam sputtering for serial sectioning. It was found that the diffusion coefficients decrease significantly during isothermal annealing towards well-defined values, which are attributed to the diffusivity in a structurally relaxed metastable amorphous state. This metastable state is independent of the annealing temperature. Pre-annealing of the specimens in order to establish the metastable amorphous state leads in a subsequent diffusion experiment to self-diffusion coefficients which obey Arrhenius laws over the entire diffusion temperature regimes accessible. The activation enthalpies and the pre-exponential factors vary in the various tracer–material systems from 1.5 to 3.2 eV and from 3.1×10^{-7} to 7×10^{-4} m^2 s^{-1} respectively.

1. Introduction

Diffusion studies in amorphous alloys are of vital concern from various points of view. Generally, they are potential means for a better understanding of atomic migration in disordered or short-range-ordered media. Amorphous alloys are thermodynamically not stable and undergo structural transitions, such as relaxation and crystallization, by thermal annealing because of diffusion processes. Since in the course of these transitions the extraordinary properties of the amorphous alloys are significantly changed or even destroyed, the clarification of the diffusion mechanisms is a prerequisite for the wide span of applications of the amorphous alloys, *e.g.* as soft magnetic materials in transformer cores or as diffusion barriers against impurity atoms in semiconductors. However, diffusion experiments in amorphous alloys are difficult to perform, because the experiments are limited to very short diffusion lengths, often not more than about 10 nm. The reason for this is that the diffusion time is limited at high temperatures by the onset of crystallization, whereas at low temperatures the diffusivity is low. Another difficulty in diffusion measurements arises from the change in the diffusivity in the amorphous state as a function of the annealing time during structural relaxation. These experimental problems may explain the small number of reliable diffusion experiments which have been performed so far on amorphous alloys, although the great interest in these materials has initiated a considerable number of diffusion studies [1, 2].

In this work, we have studied the self-diffusion of radioactive ^{59}Fe tracer atoms in the amorphous alloys $Fe_{28}Zr_{72}$, $Fe_{78}Si_9B_{13}$, $Fe_{79}W_1B_{20}$ and $Fe_{80}B_{20}$ and the self-diffusion of ^{59}Fe and ^{95}Zr atoms in $Fe_{24}Zr_{76}$ and $Fe_{91}Zr_9$. Extraordinary care was devoted to the preparation of the specimens and to the effect of relaxation to the diffusivity. Optical and electron microscopy as well as X-ray diffraction investigations accompanied the diffusion experiments in order to test the amorphism of the materials. Coercive field measurements on the metal–metalloid alloys served to investigate the crystallization kinetics and also as a further test for the amorphism of those specimens which were used in diffusion experiments.

2. Experimental details

The amorphous alloys investigated were produced by the melt-spinning technique at Vacuumschmelze, Hanau ($Fe_{78}Si_9B_{13}$) or at the Max-Planck-Institut für Metallforschung, Stuttgart. The specimens, 9–10 mm in diameter and 20–40 μm thick, were produced by chemical etching from the melt-spun ribbons. By polishing the specimens, damage-free surfaces were obtained onto which the radiotracers ^{59}Fe and/or ^{95}Zr were deposited electrochemically in thin layers of about 1 nm. All annealing treatments were carried out in evacuated quartz ampoules. The concentration profiles of the diffused tracers were determined by microsectioning the specimens with the aid of the ion beam sputtering technique and subsequent measurement of the radioactivity of the sections.

*Paper presented at the Sixth International Conference on Rapidly Quenched Metals, Montréal, August 3–7, 1987.

0025-5416/88/$3.50

Crystallites larger than 200 nm in the amorphous material were made visible in an optical microscope by etching the polished specimens with oxidizing acids [3]. Smaller crystallites were detected by transmission electron microscopy or X-ray diffraction investigations. These investigations were performed on a number of specimens in the as-quenched state as well as after annealing treatments. It was found that a volume fraction of crystallites below 1% hardly influences the accuracy of diffusion measurements. The diffusion experiments were performed under conditions under which perturbations by crystallization effects may be excluded. The coercive field measurements were performed at room temperature by means of a Förster coercimeter [4].

3. Results

3.1. Magnetic measurements

Since in ferromagnetic alloys the coercive field is very sensitive to the crystalline fraction of the material [4, 5], this quantity was used to determine the activation enthalpy of crystallization and also for checking the amorphism of specimens. For $Fe_{40}Ni_{40}P_{14}B_6$, an alloy which is similar to the metal–metalloid alloys investigated in this paper, it was demonstrated that the coercive field increases proportional to the crystallized fraction until about 30% of the material has transformed to the crystalline phase [6]. Using this relationship the activation enthalpy Q of crystallization, which obviously is a thermally activated process, can be determined from $\theta \approx t \exp(-Q/kT)$. Here θ is the temperature-compensated time, t the annealing time at the temperature T required to establish a given coercive field H_c and k Boltzmann's constant. Q was determined for the metal–metalloid alloys $Fe_{78}Si_9B_{13}$, $Fe_{79}W_1B_{20}$ and $Fe_{80}B_{20}$. The results are summarized in Table 1. Figure 1 shows that for $Fe_{78}Si_9B_{13}$, for example, the equation given above is fulfilled. A parallelity of straight lines indicates that Q does not change during the thermally activated process. This is not strictly valid in a wider crystallization regime, as shown in Fig. 1. However, an error of about $\pm$ 0.1 eV in Q must be taken into account at a given H_c.

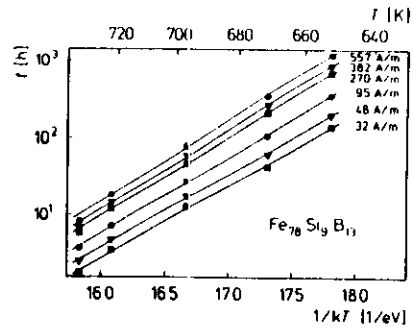

Fig. 1. Annealing times required to establish the specific values of the coercive field H_c (parameters) in $Fe_{78}Si_9B_{13}$ *vs.* the reciprocal of the annealing temperature T.

3.2. Diffusion measurements

Typical penetration profiles of the radioactive tracer atoms are shown in Fig. 2 for $Fe_{79}W_1B_{20}$ and $Fe_{80}B_{20}$. The specific radioactivity of a section at a distance x from the surface is plotted *vs.* x^2. The profiles measured at a given temperature (593 K) at

TABLE 1 The activation enthalpies Q for crystallization determined by coercive field measurements together with the activation enthalpies H^T_B and the pre-exponential factors D^T_0 for the tracer self-diffusion obtained by fitting eqn. (3) to the D^T_B data in Fig. 4

Material	*Crystallization*		*Tracer diffusion*			
	Q (eV)	*Temperature* (K)	*Tracer*	H^T_B (eV)	D^T_0 (m^2 s^{-1})	*Temperature* (K)
$Fe_{78}Si_9B_{13}$	2.2–2.4	653–733	^{59}Fe	2.1	4.6×10^{-5}	551–783
$Fe_{79}W_1B_{20}$	2.5	593–633	^{59}Fe	—	—	593
$Fe_{80}B_{20}$	2.3	573–613	^{59}Fe	2.4	7.9×10^{-2}	543–655
$Fe_{24}Zr_{76}$	—		^{59}Fe	2.3	6.0×10^{-4}	493–613
$Fe_{24}Zr_{76}$	—		^{95}Zr	3.2	7.0×10^{-4}	533–613
$Fe_{28}Zr_{72}$	—		^{59}Fe	2.6	2.6×10	533–593
$Fe_{91}Zr_9$	—		^{59}Fe	1.5	3.1×10^{-7}	473–773
$Fe_{91}Zr_9$	—		^{95}Zr	2.5	2.1×10^{-3}	633–773

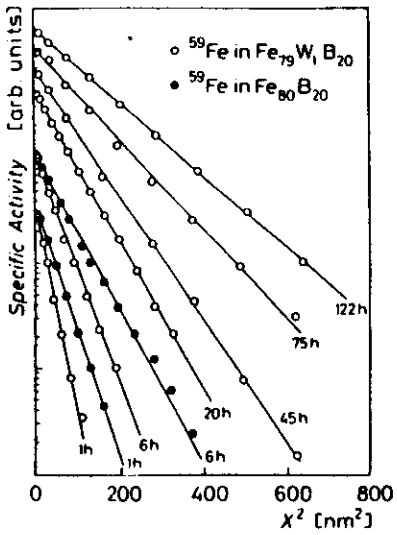

Fig. 2. ^{59}Fe diffusion profiles in $Fe_{79}W_1B_{20}$ (○) and $Fe_{80}B_{20}$ (●) at 593 K for non-pre-annealed specimens. The parameters shown on the profiles are the diffusion times applied.

various annealing times follow different straight lines and can be described by the so-called thin film solution

$$C(x,t) = A_0(\pi D^T t)^{-1/2}\exp\left(-\frac{x^2}{4D^T t}\right) \qquad (1)$$

of Fick's second law. In eqn. (1), C denotes the tracer concentration which is proportional to the radioactivity in the depth x, A_0 the tracer concentration per unit surface area at $t = 0$, t the diffusion time and D^T the tracer diffusion coefficient. The results shown in Fig. 2 were observed in specimens which did not undergo pre-annealing, *i.e.* thermal annealing prior to the diffusion annealing. By comparison of the profiles annealed for 1 and 6 h, it is obvious that diffusion of ^{59}Fe is retarded in $Fe_{79}W_1B_{20}$ in comparison with $Fe_{80}B_{20}$.

In disordered materials the structure may change because of rearrangements within the amorphous state in the course of annealing treatments. It has been demonstrated earlier for a number of alloys [7] that the diffusion coefficients decrease in the course of isothermal annealing as a result of structural relaxation. Because of the time dependence of the diffusion, the diffusion coefficients deduced from the penetration profiles are time-averaged values $\langle D^T\rangle$. If $\langle D^T\rangle(t)$ is known as a function of the annealing time t, the instantaneous tracer diffusion coefficient $D^T(t)$ follows from

$$D^T(t) = \langle D^T\rangle + t\frac{d\langle D^T\rangle}{dt} \qquad (2)$$

On each alloy, series of diffusion measurements were performed in order to determine $\langle D^T\rangle(t)$ or $D^T(t)$. In Fig. 3, D^T–t curves are presented. The main feature of these is the continuous decrease in D^T towards a plateau value, which in the following will be denoted D^T_R. This is the diffusion coefficient in a fully relaxed amorphous state.

Hitherto, in all amorphous alloys thoroughly investigated the plateau values D^T_R were found to depend on temperature via an Arrhenius law

$$D^T_R = D^T_0\exp\left(-\frac{H^T_R}{kT}\right) \qquad (3)$$

(D^T_0 is the pre-exponential factor and H^T_R the diffusion enthalpy).

Figure 4 shows that eqn. (3) is also fulfilled for all data presented in this paper. In Table 1 the values found for D^T_0 and H^T_R are summarized. The typical error in diffusion data obtained by the radiotracer technique in combination with ion beam sputtering is smaller than 10% [8]. However, although relaxation effects and crystallization can be

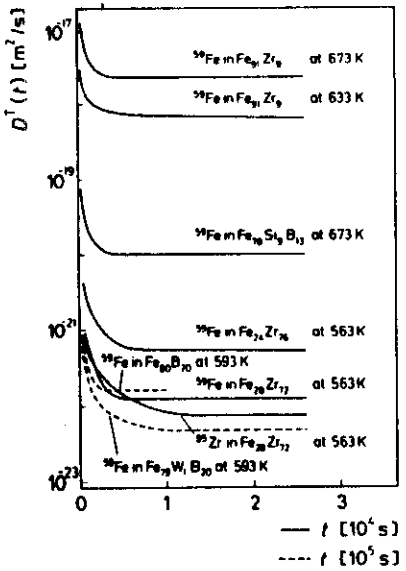

Fig. 3. Instantaneous self-diffusion coefficients $D^T(t)$ vs. the diffusion annealing time t.

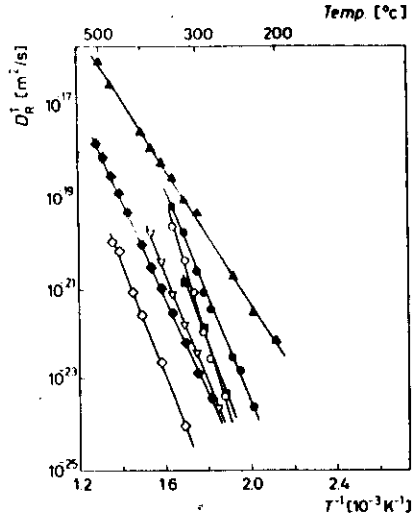

Fig. 4. Arrhenius plots of tracer diffusion coefficients in the relaxed state of the amorphous alloys.

Symbol	*Tracer*	*Alloy*
▲	^{59}Fe	$Fe_{91}Zr_9$
■	^{59}Fe	$Fe_{28}Zr_{72}$
●	^{59}Fe	$Fe_{24}Zr_{76}$
▽	^{59}Fe	$Fe_{80}B_{20}$
◆	^{59}Fe	$Fe_{76}Si_9B_{13}$
◇	^{95}Zr	$Fe_{91}Zr_9$
○	^{95}Zr	$Fe_{24}Zr_{76}$

ruled out, in some cases the scatter of the observed D^T_R values exceeds this error. As the diffusion experiments have been performed on different specimens in order to be able to diffusion anneal the specimens as long as possible, errors in D^T_R larger than ±10% presumably result from decompositions that have occurred already in the as-quenched state.

4. Summary and discussion

A detailed discussion of the results of this study has been given in a companion paper at this conference [9]. In the following, we therefore summarize and discuss only briefly the basic results and related investigations made previously at our laboratory.

(1) The activation enthalpy Q observed for crystallization exceeds in all alloys, except $Fe_{80}B_{20}$, the activation enthalpy of self-diffusion (Table 1) [3, 8]. This is not surprising since crystallization is not necessarily controlled by diffusion only but for example may be influenced considerably by the rate of nucleation. Moreover, diffusion processes contributing to crystal growth may occur in the amorphous phase, in the crystalline phase and along the phase boundaries. The interpretation of the results of crystallization kinetics in terms of diffusion quantities therefore usually is very complicated.

(2) In all materials investigated, the instantaneous tracer diffusion coefficients $D^T(t)$ decrease towards a plateau value D^T_R, which represents the diffusion coefficient in the fully relaxed amorphous state (Fig. 3).

(3) From Fig. 3, it is clear that diffusion coefficients measured in the ill-defined regime of relaxation cannot serve to determine the temperature dependence of the diffusion coefficients.

(4) After pre-annealing in order to establish the relaxed state, in a subsequent diffusion annealing D^T is equal to D^T_R from the very beginning (Fig. 3).

(5) The same relaxed state is established by annealings at any temperature [8, 10, 11].

(6) The decrease in the diffusivity from its value in the as-quenched state to D^T_R presumably occurs via a thermally activated process whose activation enthalpy is significantly smaller (less than 1 eV for $Fe_{40}Ni_{40}B_{20}$ [10, 11]) than that for self-diffusion in the relaxed state. Since structural relaxation increases the volume density in melt-spun amorphous alloys [12], the elimination of excess free volume, frozen in during the quench from the melt, must be involved in the relaxation process.

(7) In addition to the transport of free volume to the surface, a recombination of free volume with regions of higher than average density may contribute to the relaxation process.

(8) The enhanced diffusion in the unrelaxed state can be understood as an indirect vacancy-like diffusion mechanism, in which the tracer atoms use units of free volume as a diffusion vehicle.

(9) The diffusion coefficients in the relaxed state (Fig. 4) are well described by an Arrhenius law (eqn. (3)). This indicates that the dominating diffusion mechanism is the same in the entire temperature regime investigated.

(10) From alloy to alloy the D^T_0 and H^T_R values differ significantly (Table 1). Therefore different diffusion mechanisms are assumed to operate in different alloys.

(11) In partially crystallized specimens, diffusion is distinctly slower than in the relaxed amorphous state [3, 8].

Acknowledgments

The authors are very grateful to Professor W. Frank, Professor H. Kronmüller and Professor A. Seeger for stimulating discussions and their support in this study.

References

1 Y. Limoge, G. Brebec and Y. Adda, in F. J. Kedves and D. L. Beke (eds.), *Diffusion and Defect Monogr. Ser. 7*, Trans Tech, Aedermannsdorf, 1983, p. 285.
2 B. Cantor and R. W. Cahn, in F. E. Luborsky (ed.), *Amorphous Metallic Alloys*, Butterworths, London, 1983, p. 487.
3 K. Pfahler, J. Horváth and W. Frank, submitted to *Cryst. Lattice Defects Amorphous Mater.*
4 H. Mehrer, G. Flik, J. Horváth and H. Kronmüller, *Phys. Status Solidi A, 72* (1982) 215.
5 F. E. Luborsky, *Mater. Sci. Eng., 28* (1977) 139.
6 W. Fernengel, M. Rapp and H. Kronmüller, *Phys. Status Solidi A, 90* (1985) 637.
7 J. Horváth, K. Pfahler, W. Ulfert, W. Frank and H. Kronmüller, *Mater. Sci. Forum, 15-18* (1987) 523.
8 J. Horváth and H. Mehrer, *Cryst. Lattice Defects Amorphous Mater., 13* (1986) 1.
9 W. Frank, J. Horváth and H. Kronmüller, *Mater. Sci. Eng., 97* (1988) 415.
10 J. Horváth, K. Pfahler, W. Ulfert and W. Frank, *J. Phys. (Paris), Colloq. C8, 12* (1985) 645.
11 W. Ulfert, J. Horváth and W. Frank, submitted to *Cryst. Lattice Defects Amorphous Mater.*
12 R. Gerling, F. P. Schimansky and R. Wagner, in S. Steeb and H. Warlimont (eds.), *Rapidly Quenched Metals*, North-Holland, Amsterdam, 1985, p. 1377.

(5)

Materials Science Forum 15-18, 523 (1987)

DIFFUSION IN AMORPHOUS METALLIC ALLOYS

J. Horváth, K. Pfahler, W. Ulfert, W. Frank, and H. Kronmüller

Max-Planck-Institut für Metallforschung, Institut für Physik, and Universität Stuttgart,
Institut für Theoretische und Angewandte Physik, Pfaffenwaldring 57,
D-7000 Stuttgart 80, Fed. Rep. Germany

ABSTRACT

The self-diffusion of ^{59}Fe and ^{95}Zr and the diffusion of foreign ^{32}P atoms in various amorphous metal–metalloid and metal–metal alloys produced by the melt-spinning method have been investigated by means of the radiotracer technique in combination with ion-beam sputtering. In all systems investigated the self-diffusivity decreases in the course of the diffusion annealing to a value which is characteristic of a well-defined relaxed amorphous state. The diffusion coefficients in the relaxed state show Arrhenius-type temperature dependences. The diffusion enthalpy and the pre-exponential factor of the diffusion coefficient vary strongly from system to system. The increase of these quantities in the case of the self-diffusion in Fe–Zr alloys with increasing packing density of the matrix and increasing size of the diffusing atoms is interpreted in terms of a transition from diffusion along easy paths to a cooperative diffusion mechanism.

1. INTRODUCTION

The increasing interest in amorphous materials requires a better knowledge of their properties. Many of these (e.g., structural relaxations, induced anisotropy, embrittlement, and crystallization) are controlled by diffusion processes. Moreover, diffusion studies in amorphous alloys (for recent reviews see [1,2]) are of interest not only from a technological point of view but also for the understanding of the diffusion in disordered media. Unfortunately, such experiments are difficult, since in most cases the temperature regime is small within which the diffusivity is high enough to be measurable but crystallization does not take place to an unacceptable extent during diffusion annealing. As a consequence, so far only a small number of reliable diffusion studies on amorphous alloys have been performed. In amorphous materials the diffusivities may change as a function of the annealing time due to structural relaxations (Sect. 3), which may explain the large data scatter and the contradictory results in previous investigations. For this reason in the present studies special attention was paid to the relaxation processes arising from the elimination and/or redistribution of excess free volume during annealing.

We have studied the foreign-atom diffusion of ^{32}P and the self-diffusion of ^{59}Fe and ^{95}Zr in amorphous metallic alloys produced by melt-spinning either by Vacuumschmelze Hanau (FRG) [$Fe_{40}Ni_{40}B_{20}$, $Fe_{41}Ni_{41}B_{18}$, $Fe_{78}Si_9B_{13}$] or in our Stuttgart laboratories [$Fe_{24}Zr_{76}$, $Fe_{28}Zr_{72}$, $Fe_{91}Zr_9$], [3]. The radiotracer technique combined

with ion-beam sputtering — applied for the first time to the ·lic alloys by Valenta et al. [4,5] and used in the present investigatio· ir to other techniques in most systems of interest. We were able to measu· all diffusion coefficients (> 10^{-24} m^2/s) within temperature intervals u· which are significantly wider than those covered in previous diffusion studi· ·us alloys.

2. EXPERIMENTAL

The specimens, 9 mm to 10 mm in diameter and less than 40 μm thick, were produced from the melt-spun ribbons by etching. Damage-free sufaces were achieved by lapping with 1 μm-grade Al_2O_3 solution on plane glass and/or polishing with colloidal silicic acid on a metallurgical cloth. The ^{59}Fe or ^{95}Zr radiotracers were deposited electrochemically in a thin layer of about 1 nm on the polished surface. Because of its high vapour pressure, phosphorus cannot be diffused in by surface-layer deposition. Therefore, in the case of ^{32}P diffusion the tracers were implanted into the specimens with an energy of 30 keV, leading to a projected range of about 15 nm. Pre-anneals and diffusion anneals were carried out in evacuated quartz ampoules. The amorphism of the specimens was tested by optical, scanning-electron, and transmission-electron microscopy and, in the case of ferromagnetic alloys, also by coercive-field measurements.

The concentration profiles of the diffused tracers were determined by microsectioning the specimens with the aid of the ion-beam-sputtering technique and sectionwise measuring the radioactivity. For a given profile the section thickness was usually kept constant, whereas it was varied between 1 nm and 60 nm from profile to profile.

A more detailed description of the specimen preparation and the experimental techniques has been given elsewhere [6-9].

3. RESULTS

Fig. 1 shows typical ^{59}Fe- or ^{95}Zr-tracer penetration profiles. The specific activity of the radiotracers in a section at the distance x from the originally tracer-covered surface — which is proportional to the concentration C of tracers in this section — is plotted versus x^2. The fact that the data for a given temperature and time of annealing (equal symbols) follow a straight line demonstrates that the profiles obey the so-called thin-film solution

$$C(x,t_d) = C_o(\pi D^T t_d)^{-1/2} \exp(-x^2/4D^T t_d) \qquad (1)$$

of Fick's second law. In Eq. (1) C_o means the number of tracer atoms per unit area deposited on the surface, D^T the tracer diffusion coefficient, and t_d the diffusion time.

Fig. 2 shows ^{32}P profiles in $Fe_{40}Ni_{40}B_{20}$, viz., the as-implanted profile and some profiles broadened by diffusion annealing for different times at 593 K. Except in the vicinity of the implanted surface, where ^{32}P segregation has taken place, the profiles may be fitted to the appropriate solution of Fick's second law,

$$C(x,t_d) = (4\pi D^T t_d)^{-1/2} \int_0^\infty C(x',0)\left\{\exp\left[-(x'-x)^2/4D^T t_d\right] - \exp\left[-(x'+x)^2/4D^T t_d\right]\right\} dx', \qquad (2)$$

where $C(x',o)$ is the distribution of the implanted ^{32}P. A disadvantage in comparison to the thin-film-deposition technique is that here the evaluation of the data requires the measurement of the distribution of the implanted tracers.

In an amorphous material the diffusion coefficient may change in the course of isothermal annealing as a result of structural relaxations. This has indeed been demonstrated for the self-diffusivities of ^{59}Fe and ^{95}Zr in all amorphous alloys investigated. In the case of ^{32}P diffusion the existence of such an effect has not been found unambiguously, presumably because of the lesser accuracy of the ^{32}P diffusion coefficients, which is due

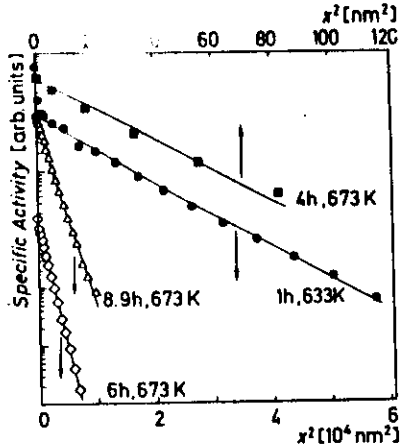

Fig. 1. Penetration profiles of ^{59}Fe in $Fe_{78}Si_9B_{13}$ (Δ, ◇) or $Fe_{91}Zr_9$ (●) and of ^{95}Zr in $Fe_{91}Zr_9$ (■). Temperatures and durations of the diffusion anneals are given in the figure.

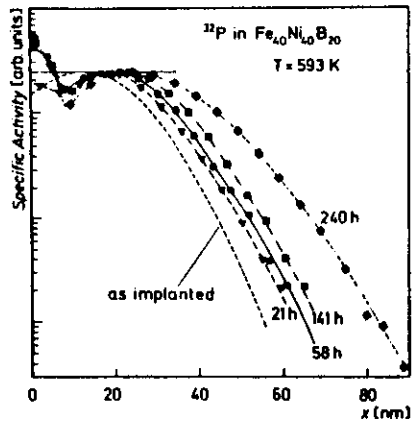

Fig. 2. Diffusion broadening of a ^{32}P implantation profile in $Fe_{40}Ni_{40}B_{20}$ at 593 K. The high ^{32}P concentration near the implanted surface at x = 0 is due to surface segregation.

to the fact that these had to be determined from small differences between two profiles.

Because of the time dependence of the ^{59}Fe and ^{95}Zr self-diffusion, the diffusion coefficients deduced from the plots in Fig. 1 have to be considered as the time averages

$$\langle D^T \rangle = t_d^{-1} \int_0^{t_d} D^T(t_d')\, dt_d' , \qquad (3)$$

since in the case of a time-dependent diffusion coefficient Eq. (1) remains a solution of Fick's second law if D^T is identified with $\langle D^T \rangle$. From (3) one finds that the instantaneous diffusion coefficient $D^T(t_d)$ is given by

$$D^T(t_d) = \langle D^T \rangle + t_d \frac{d\langle D^T \rangle}{dt_d} , \qquad (4)$$

i.e., $D^T(t_d)$ may be calculated if $\langle D^T \rangle$ is known as a function of the annealing time t_d. Therefore, on each alloy investigated series of profile measurements have been performed in which at different temperatures the annealing time has been varied. From these the instantaneous diffusion coefficients have been determined as functions of time. In Fig. 3 a selection of such D^T-versus-t_d plots is presented. One realizes that D^T decreases rapidly towards a plateau value D_R^T. A second decrease of the diffusivity found after longer durations is caused by the onset of crystallization [6,9-11].

In all our measurements the plateau values D_R^T were found to depend on the diffusion temperature T via an Arrhenius law

$$D_R^T = D_0^T \exp(-H^T/kT) \qquad (5)$$

(k = Boltzmann's constant). This is demonstrated in Fig. 4. Table 1 summarizes the diffusion enthalpies H^T and the pre-exponential factors D_0^T.

Material	Tracer	H^T [eV]	D_0^T [m^2/s]	Temperature Interval [K]
$Fe_{40}Ni_{40}B_{20}$	^{59}Fe	2.3_5	2.7×10^{-2}	571 — 643
	^{32}P	3.0_6	10^4	573 — 644
$Fe_{41}Ni_{41}B_{18}$	^{59}Fe	2.2_9	1.1×10^{-2}	552 — 643
$Fe_{78}Si_9B_{13}$	^{59}Fe	2.0_9	4.6×10^{-5}	551 — 783
$Fe_{24}Zr_{76}$	^{59}Fe	2.3_1	6.0×10^{-1}	493 — 613
	^{95}Zr	3.2_1	7.0×10^{6}	533 — 613
$Fe_{91}Zr_9$	^{59}Fe	1.4_7	3.1×10^{-7}	473 — 773
	^{95}Zr	2.5_1	2.1×10^{-3}	633 — 773

Table 1. Activation enthalpies (H^T) and pre-exponential factors (D_0^T) obtained by fitting (5) to the D_R^T data in Fig. 4.

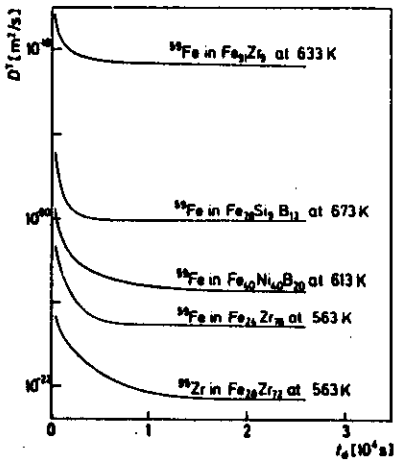

Fig. 3. Instantaneous self-diffusion coefficients D^T as a function of the annealing time t_d in various amorphous metallic alloys.

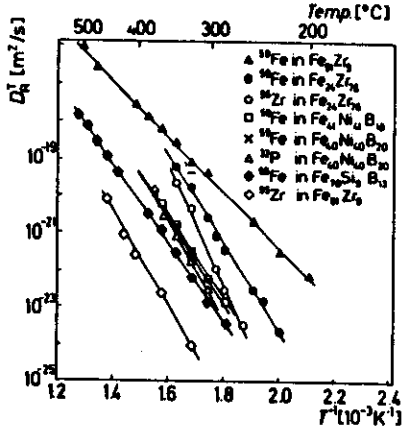

Fig. 4. Arrhenius plots of diffusion coefficients in relaxed amorphous metallic alloys.

A significant feature of the plateau-regime diffusion is that the Arrhenius law (5) is the same, irrespective of the annealing temperature at which the isothermal decrease of D^T to D_R^T has taken place. If D^T has once reached its value D_R^T at any temperature, in a subsequent diffusivity measurement D^T is no more time-dependent but possesses the D_R^T value given by (5) from the very beginning. This has been demonstrated most thoroughly for the diffusion of ^{59}Fe in $Fe_{40}Ni_{40}B_{20}$ [6,12]. These observations indicate that the as-quenched amorphous state is quite unstable and thus relaxes into a well-defined metastable amorphous state.

In spite of great efforts, in the materials investigated it has not been possible to determine the t_d dependence of D^T in the pre-plateau regime with an accuracy permitting conclusions going beyond those given in Sect. 4.1. This is so since at the short diffusion times in this part of the D^T—t_d curves the penetration depths of the tracers are usually of the order of a few nm only, so that the number of profiles measurable at sufficiently different t_d values is too small for achieving an acceptable precision. For this reason it is clear that diffusion coefficients measured in this ill-defined regime of relaxation may scatter considerably. We believe that most of the contradictory results reported in previous studies are due to the fact that this difficulty has not — or at least not fully — been taken into account, though an influence of relaxation effects on the diffusivity in amorphous materials had been expected and, in some measurements, observed (for references see [1,2,6]).

4. SUMMARY AND DISCUSSION

4.1. Relaxation mechanism and diffusion in the unrelaxed state

The fact that the relaxation from the as-quenched into the metastable amorphous state requires thermal annealing is taken as evidence that the relaxation mechanism is thermally activated. In the case of ^{59}Fe diffusion in $Fe_{40}Ni_{40}B_{20}$ we have estimated that the relaxation enthalpy must be smaller than 1 eV provided the relaxation follows an exponential time law [12,13]. Since the decrease of the diffusivity during the relaxation is accompanied by an increase of the volume density [14,15], we conclude that the relaxation involves the elimination of excess free volume and that the diffusivity enhancement in the unrelaxed state, $D^T(t_d) - D_R^T$, is due to a quasi-vacancy mechanism. The relaxation enthalpy (< 1 eV in $Fe_{40}Ni_{40}B_{20}$) is thus interpreted in terms of the migration enthalpy of these quasi-vacancies.

4.2. Diffusion in the relaxed state

Our results on the diffusion in the relaxed amorphous state may be summarized as follows: (i) The diffusivity D_R^T in a relaxed amorphous alloy does not change in the course of time until the onset of crystallization. (ii) In all systems investigated D_R^T obeys an Arrhenius law in the entire temperature regime accessible to measurements. (iii) The D_R^T values are larger by 5 to 10 orders of magnitude than the self-diffusivities found for crystalline Fe [16], Ni [17], or Zr [8] by extrapolation to the low temperatures at which the D_R^T values have been measured. (iv) The D_0^T values found for various amorphous alloys range from 3 orders of magnitude below to 10 orders of magnitude above 10^{-4} m^2/s, which is considered to be typical of the pre-exponential factors of the diffusivities in crystalline metals. (v) There is a clear tendency that the higher is the H^T value of an amorphous alloy, the higher is its D_0^T value. (vi) For a given Fe—Zr alloy H^T and D_0^T are larger for the diffusion of the bigger Zr atom than for the smaller Fe atom. (vii) For a given diffusing atom, Zr or Fe, H^T and D_0^T are larger in the less open $Fe_{24}Zr_{76}$ structure than in the more open $Fe_{91}Zr_9$ structure.

From the preceding observations we draw the following conclusions: (α) In a given relaxed amorphous alloy, diffusion of a given atom is dominated by the same mechanism in the entire temperature regime accessible, [compare (i) and (ii)]. (β) The diffusion

mechanisms in relaxed amorphous alloys presumably differ from crystalline metals [compare (iii) and (iv)].

A general discussion of diffusion mechanisms which may occur in amorphous materials has been presented elsewhere [12]. For the self-diffusion in Fe–Zr alloys the following mechanisms are tentatively proposed: (a) In alloys with open structures (e.g., $Fe_{91}Zr_9$) small atoms (e.g., Fe) can diffuse easily (low H^T) along paths formed by the free volume retained in the relaxed state. The fact that such paths may not be available for all tracers and that they may possess dead ends may explain why the diffusion entropy and thus D_0^T are smaller than in crystalline metals. (b) If the structure of the amorphous material is less open (e.g., $Fe_{24}Zr_{76}$) and/or if the tracers are fatter (e.g., Zr) the mechanism described above does not work. Under these circumstances the tracers can only perform a cooperative motion that involves considerable displacements of neighbouring atoms. This diffusion mode resembles the self-diffusion via "extended self-interstitials" in crystalline silicon [18] and will therefore be referred to as "extended-tracer" diffusion. It is obvious that with increasing size of the tracer atoms and increasing packing density of the amorphous alloy the region over which a tracer is "extended" increases and so do the diffusion entropy, i.e. D_0^T, and H^T. Like in the case of Si self-diffusion D_0^T may exceed the order of magnitude known from crystalline metals considerably.

REFERENCES

[1] Limoge, Y., Brébec, G., and Adda, Y., in: Dimeta 82 (Diffusion and Defect Monograph Series No. 7), Eds. F.J. Kedves and D.L. Beke, Trans. Tech. Publications, Switzerland 1983 (p. 285)

[2] Cantor, B., and Cahn, R.W., in: Amorphous Metallic Alloys, Ed. F.E. Luborsky, Butterworths, London 1983 (p. 487)

[3] Pfahler, K., Moser, N., Horváth, J., Frank, W., and Kronmüller, H.: Arbeitsbericht MPI/86/P1, Max-Planck-Institut für Metallforschung, Stuttgart 1986

[4] Valenta, P., Maier, K., Kronmüller, H., and Freitag, K.: phys. stat. sol. (b), 1981, 105 , 537

[5] Valenta, P., Maier, K., Kronmüller, H., and Freitag, K.: phys. stat. sol. (b), 1981, 106 , 129

[6] Horváth, J., and Mehrer, H.: Cryst. Latt. Def. and Amorph. Mater., 1986, 13 , 1

[7] Horváth, J., Freitag, K., and Mehrer, H.: Cryst. Latt. Def. and Amorph. Mater., 1986, 13 , 15

[8] Horváth, J., Dyment, F., and Mehrer, H.: J. Nucl. Mater., 1984, 126 , 206

[9] Pfahler, K., Horváth, J., and Frank, W.: Cryst. Latt. Def. and Amorph. Mater., to be submitted

[10] Horváth, J., Freitag, K., and Mehrer, H., in: Rapidly Quenched Metals, Eds. S. Steeb and H. Warlimont, Elsevier, Amsterdam 1985 (p. 751)

[11] Pfahler, K., Horváth, J., Frank, W., and Mehrer, H., in: Rapidly Quenched Metals, Eds. S. Steeb and H. Warlimont, Elsevier, Amsterdam 1985 (p. 755)

[12] Horváth, J., Pfahler, K., Ulfert, W., Frank, W., and Mehrer, H.: J. Physique, 1985, 12 , C8-645

[13] Ulfert, W., Horváth, J., and Frank, W.: Cryst. Latt. Def. and Amorph. Mater., to be submitted

[14] Gordelik, P., and Sommer, F., in: Rapidly Quenched Metals, Eds. S. Steeb and H. Warlimont, Elsevier, Amsterdam 1985 (p. 623)

[15] Gerling, R., Schimansky, F.P., and Wagner, R., in: Rapidly Quenched Metals, Eds. S. Steeb and H. Warlimont, Elsevier, Amsterdam 1985 (p. 1377)

[16] Hettich, G., Mehrer, H., and Maier, K.: Scripta Met., 1977, 11 , 795

[17] Maier, K., Mehrer, H., Lessmann, E., and Schüle, W.: phys. stat. sol. (b), 1976, 78 , 689

[18] Frank, W., Gösele, U., Mehrer, H., and Seeger, A., in: Diffusion in Crystalline Solids, Eds. G.E. Murch and A.S. Nowick, Academic Press, Orlando 1984 (p. 63)

To appear in Materials Science and Engineering A 132 (1990)

(5)

DIFFUSION AND STRUCTURAL-RELAXATION MECHANISMS IN METALLIC GLASSES

H. Kronmüller, W. Frank, and A. Hörner

Max-Planck-Institut für Metallforschung, Institut für Physik,

Heisenbergstraße 1, D-7000 Stuttgart 80 (FRG)

Abstract

Diffusion data on amorphous metal–metal (FeZr) and metal–metalloid (FeNiB, FeSiB, CoFeNiSiB) alloys have been determined by means of magnetic-after-effect (MAE), induced-magnetic-anisotropy (IMA), and radiotracer-diffusion (RTD) measurements. Whereas the self-diffusion coefficients follow Arrhenius laws, the MAE and the IMA are controlled by spectra of activation enthalpies, whose average values are distinctly smaller than the self-diffusion enthalpies. This seeming discrepancy is shown to be a consequence of the fact that MAE, IMA, and RTD are sensitive to different parts of the activation enthalpy spectra inherent to amorphous media. Models and atomic mechanisms of the diffusion in disordered media are proposed and compared with experimental results.

1. Introduction

The existence of structural-relaxation phenomena in amorphous alloys and their relation to diffusion processes belong to the most challenging features of these materials. After it had been realized that in thermally pre-treated specimens both relaxation times and diffusion coefficients reversibly depend on temperature, pressure, and specific volume (i.e. that — like in crystalline materials — these quantities are variables of state in the sense of thermodynamics), reliable results on the diffusion in amorphous alloys were obtained from systematic investigations [1—3]. Since amorphous alloys are thermodynamically metastable, quasi-reversible diffusion behaviour indicates that the enthalpy barriers against diffusion are smaller than those governing crystallization.

Diffusion in amorphous alloys was reviewed by various authors. Whereas Cahn [4], Egami and Waseda [5], and Sharma et al. [6] concentrated on the relation between diffusion properties and the glass-forming ability, Cantor [7] emphasized that the diffusivity of metals and metalloids in metallic glasses scales with the glass transition temperature.

As expected for disordered media, the relaxation phenomena observed in MAE [8-10], IMA [11], and enthalpy-relaxation [12] studies reveal the presence of wide spectra of activation enthalpies. This is contrasted by the finding that the self-diffusion coefficients of metallic glasses, as measured in RTD experiments, exclusively obey Arrhenius laws [3], which seemingly indicates that the diffusion of a given tracer species in a given alloy is controlled by a single activation enthalpy. This paradoxon, to which we shall return below, was resolved by Kronmüller and Frank [13]. The present paper presents the effective activation enthalpies in amorphous $Co_{58}Ni_{10}Fe_5Si_{11}B_{16}$, which were recorded by means of different techniques operating in different intervals of measuring time and measuring temperature. These results are compared with current models of diffusion in disordered media and interpreted in terms of atomic mechanisms.

2. Experimental results

The almost non-magnetostrictive amorphous alloy $Co_{58}Ni_{10}Fe_5Si_{11}B_{16}$ was chosen as a model substance for studying diffusion and relaxation phenomena. By thermal pre-annealing between 350°C and 460°C for several hours, irreversible processes were eliminated. Fig. 1 summarizes the results obtained by MAE, IMA, and RTD measurements. The spectra $p(H)$ of activation enthalpies were deduced from isothermal MAE and IMA relaxation curves under the assumption that the relaxation times are related to activation enthalpies H via Arrhenius laws. The distribution functions $p(H)$ are of Gaussian shape on their low-enthalpy sides and show abrupt decreases on their high-enthalpy sides as a result of the cut-off of the relaxation times arising from the finiteness of the measuring times. The discrete activation enthalpies lying above the MAE and IMA spectra have been taken from the Arrhenius laws

$$D_R^T(T) = D_0^T \exp(-H_R^T/kT) \qquad (1)$$

for the tracer self-diffusion coefficients D_R^T, which were found in RTD studies of the long-range diffusion of Fe, Ni, or Co [14]. Fig. 1 shows that MAE, IMA, and RTD selectively probe the activation-enthalpy spectra of amorphous alloys in their low-, medium-, and high-enthalpy regimes, respectively.

The RTD data on amorphous $Co_{58}Ni_{10}Fe_5Si_{11}B_{16}$ reported above are typical of the diffusion of transition-metal atoms in amorphous metallic alloys. This follows from the extensive investigations which have been performed at the Max-Planck-Institut für Metallforschung in Stuttgart by means of the RTD technique in combination with ion-beam sputtering for serial sectioning [3]. In all systems investigated so far (for a representative selection see Fig. 2) the tracer diffusion coefficients D_R^T in the relaxed amorphous state, which is attained by thermal pre-annealing of the specimens, were found to obey Arrhenius laws (1), in which the superscripts "T" and the subscripts "R" stand for "tracer diffusion" and "relaxed state", respectively. It is of interest to note that within the groups of FeZr alloys and of metal–metalloid alloys the pre-exponential factors D_0^T in Eq. (1) increase with increasing enthalpies H_R^T according to the empirical relationships of the form

$$\ln D_0^T = A(H_R^T - B) \qquad (2)$$

indicated by the broken lines in Fig. 2. Such relationships have been found as well in diffusion studies on amorphous NiZr and for the diffusivity of hydrogen in amorphous metallic alloys by Sharma et al. [6]. By contrast, the pre-exponential factors of the self-diffusion coefficients of crystalline metals range approximately from 10^{-5} m^2s^{-1} to 10^{-4} m^2s^{-1}, virtually independent of the diffusion enthalpies (solid line in Fig. 2).

3. Models of the Diffusion in Disordered Media

It is evident from Fig. 1 that techniques operating in different regimes of measuring time and measuring temperature monitor different parts of the activation-enthalpy spectra of diffusion in amorphous alloys. The increase of the effective enthalpies with increasing time and temperature is intimately related to the concomitant increase of the range of diffusion: MAE arises from local atomic rearrangements governed by short-range diffusion; IMA is generated by the alignment of the axes of atom pairs as a result of medium-range diffusion; RTD measurements can exclusively be done in the long-range diffusion limit.

The description of diffusion in disordered media is based on the following

assumptions: The jump frequency of a particle from a site i to a neighbouring site j obeys an Arrhenius law

$$\nu_{ij} = \nu_{ij,0} \exp[-(h_{ij}-h_i)/kT] , \qquad (3)$$

where the attempt frequency $\nu_{ij,0}$ includes the migration-entropy term and where h_i and h_{ij} denote the enthalpies at i and at the saddle point between i and j, respectively. The motion of the particle is governed by the Markoffian master equation

$$\frac{d}{dt} P_i(t) = \sum_j [\nu_{ji} P_j(t) - \nu_{ij} P_i(t)] , \qquad (4)$$

where $P_i(t)$ is the probability of occupation of site i at time t. The diffusion coefficient is then defined as

$$D(t) = \frac{1}{2d} \frac{\partial}{\partial t} \langle R^2 \rangle \equiv \frac{1}{2d} \frac{\partial}{\partial t} \sum_i R_i^2 P_i(t) , \qquad (5)$$

where the sum extends over all sites and where R_i and d are the site vectors and the dimensionality of diffusion, respectively.

It is noteworthy that even qualitative features of $D(T,t)$ depend strongly on the dimensionality of diffusion and on details of the diffusion potential. This is demonstrated for the three different types of diffusion potentials shown on the left-hand sides of Figs. 3a to c and referred to as (a) the random-barrier model (RBM) [h_i independent of i, Gaussian distribution $p(h_{ij})$ with variance h^2_{RB}], (b) the random-trap model (RTM) [h_{ij} independent of i and j, Gaussian distribution $p(h_i)$ with variance h^2_{RT}], and (c) the mixed model (MM) [independent Gaussian distributions $p(h_i)$ and $p(h_{ij})$ with $h^2_{RB} = h^2_{RT}$]. Within the framework of the effective-medium approximation [15–17] and under the assumptions that the initial site-occupation probabilities are Boltzmann-type and the topological structures of three-dimensional disordered media are fcc-like, in the limiting cases of short times (st) and long times (lt) these models yield the temperature dependences of D shown schematically on the right-hand sides of Figs. 3a to c. In the RBM (Fig. 3a), both the st and the lt limits (solid curves) of $D(T)$ lie above the (broken straight) Arrhenius line for the average activation enthalpy $H_0 \equiv \langle h_{ij} - h_i \rangle$, since in three-dimensional diffusion surmounting of high barriers can be avoided. In the RTM [15] (Fig. 3b), $D(T)$ is time-independent (solid curve) and lies below the (broken straight) Arrhenius line for H_0, since trapping is unavoidable. In the MM (Fig. 3c), the st limit of $D(T)$ coincides with the (broken straight) Arrhenius law for H_0, since the effects of the fluctuations in the barrier heights and trap depths cancel, whereas in the lt limit (curved solid line) $D(T)$ lies below this Arrhenius line due to the dominance of the traps at long times.

Obviously, the three-dimensional MM is most appropriate for describing diffusion in amorphous alloys. Therefore, in the framework of this model time-averaged D–T^{-1} curves have been computed for different measuring times (Fig. 4). Using $H_0 = 1.65$ eV, $h_{RB} = h_{RT} = 0.22$ eV, and $\nu_{ij,0} = 10^{12}$ s^{-1} *), for $t = 10^5$ s (which is a typical measuring time in RTD and IMA experiments) Curve 1 is obtained, whereas Curve 2 holds for $t = 10^3$ s (which is typical of MAE measurements). The hatched areas in Fig. 4 represent the regimes covered in RTD, IMA, and MAE experiments, respectively. In accordance with our statement that different techniques probe different parts of the activation-enthalpy spectra in amorphous alloys, the slopes $H_{eff} \equiv -\frac{\partial}{\partial(1/kT)} \ln D$ of the D–T^{-1} curves running through hatched arens referring to different techniques span different intervals of activation enthalpies.

4. Diffusion Mechanisms

It is widely accepted that in amorphous alloys the diffusion of small atoms such as H, B, C, or Si takes place via quasi-interstitial-type mechanisms [4]. Therefore, in this section we shall concentrate on the discussion of the diffusion mechanisms of transition metals [13,18].

As indicated by the quasi-Arrhenius-type temperature dependences of the diffusion coefficients, a given transition-metal species diffuses in a given amorphous alloy via the same mechanism in the entire temperature regime accessible in RTD experiments.

---

*) This choice of parameters is in accordance with the data on the ^{59}Fe RTD and the MAE in amorphous $Co_{58}Ni_{10}Fe_5Si_{11}B_{16}$.

The fact that — even within the group of amorphous FeZr alloys — D_0^T varies over 14 orders of magnitude (Fig. 2) allows us to exclude a vacancy-type mechanism similar to that controlling self-diffusion in "normal" crystalline metals, since for such a mechanism D_0^T is of the order of magnitude of 5×10^{-6} m^2s^{-1}.

There is evidence that transition metals undergo direct diffusion in amorphous alloys, i.e., they do not diffuse indirectly with the aid of diffusion vehicles, viz. quasi-vacancies and/or quasi-self-interstitials: (i) The self-diffusion enthalpies H_R^T of transition metals in amorphous transition-metal—metalloid alloys are smaller by 0.5 eV to 1 eV than the self-diffusion enthalpies of crystalline metals of the iron group. This may indicate that the H_R^T values are equal to the migration enthalpies of the tracer atoms, but not to the sums of the formation enthalpies and the migration enthalpies of diffusion vehicles, as it is the case for the self-diffusion enthalpies in crystalline metals. (ii) In pre-annealed amorphous alloys, a sudden temperature change results in instantaneous changes of the transition-metal diffusion coefficients. This is in contrast to what is expected for indirect diffusion. In this case the tracer diffusion should reflect the gradual establishing of a new equilibrium concentration of the diffusion vehicles.

Concerning the mechanisms of diffusion in amorphous alloys, we restrict ourselves to the extreme cases of Zr diffusion in $Zr_{76}Fe_{24}$ (H_R^T = 3.2 eV, $D_0^T = 10^{+7}$ m^2s^{-1}) and Fe diffusion in $Fe_{91}Zr_9$ (H_R^T = 1.5 eV, $D_0^T = 10^{-7}m^2s^{-1}$). The diffusion of the relatively large Zr atoms in the quite densely packed Zr-rich matrix requires the cooperative movement of a large number of neighbouring atoms, which is reflected by a large migration enthalpy and a large, positive migration entropy (the latter depending logarithmically on D_0^T). By contrast, in the more loosely packed Fe-rich matrix, due to their smallness, single Fe atoms may jump onto vacant neighbouring sites with a relatively small migration enthalpy. The fact that $D_0^T = 10^{-7}m^2s^{-1}$ corresponds to a slightly negative migration entropy is interpreted in terms of a low availability of vacant neighbouring sites. Presumably, the vacant sites have to be produced by the contraction of spread-out free volume as a result of thermal fluctuations.

It should be noted that between the two diffusion mechanisms just described a continuous spectrum of intermediate mechanisms may exist. Among these, there is a mechanism in which a single atom jumps onto vacant neighbouring sites whose number is of the order of magnitude of the nearest-neighbour atoms. Obviously, this is a direct quasi-interstitial mechanism. Fig. 2 suggests that the self-diffusion of the iron-group elements in amorphous $Co_{68}Ni_{10}Fe_5Si_{11}B_{16}$ occurs via this mechanism.

References

1 M. R. Gibbs, J. E. Evetts, and J. A. J. Leake, *J. Mater. Sci., 18* (1983) 278.

2 H. Kronmüller, in P. Haasen and R. I. Jaffee (eds.), *Amorphous Metals and Semiconductors, Acta Scr. Metall. Proc. Ser. 3*, Pergamon, Oxford, 1986, p. 259.

3 J. Horváth, J. Ott, K. Pfahler, and W. Ulfert, *Mat. Sci. Eng., 97* (1988) 409.

4 R. W. Cahn, in *Proc. 2nd Intern. Workshop on Non-Crystalline Solids*, San Sebastian, 1989.

5 T. Egami and Y. Waseda, *J. Non-Cryst. Solids, 64* (1984) 113.

6 S. K. Sharma, S. Banerjee, Kuldeep, and A. K. Sain, *J. Mater. Res., 4* (1989) 603.

7 B. Cantor, in *Amorphous Metals and Semiconductors, Acta Scr. Metall. Proc. Ser. 3*, Pergamon, Oxford, 1986, p. 108.

8 H. Kronmüller, *J. Magn. Materials, 41* (1984) 366.

9 P. Allia and F. Vinai, *Phys. Rev. B, 26* (1982) 6141.

10 M. Bourrous and H. Kronmüller, *phys. stat. sol. (a), 113* (1989).

11 H. Kronmüller, H.-Q. Guo, W. Fernengel, A. Hofmann and N. Moser, *Cryst. Latt. Def. and Amorph. Mat., 11* (1985) 135.

12 Z. Altounian, *Mat. Sci. Eng., 97* (1988) 461.

13 H. Kronmüller and W. Frank, *Rad. Eff. and Def. in Solids, 108* (1989) 81.

14 P. Scharwaechter, *Diplomarbeit*, Universität Stuttgart, 1989.

15 J. W. Haus and K. W. Kehr, *Physics Reports, 150* (1987) 263.

16 I. Webmann and J. Klafter, *Phys. Rev. B, 26* (1982) 5950.

17 A. Hörner, *Diplomarbeit*, Universität Stuttgart, 1990.

18 W. Frank, J. Horváth, and H. Kronmüller, *Mat. Sci. Eng. 97* (1988) 415.

Figure Captions

Fig. 1. Self-diffusion enthalpies as well as MAE and IMA activation-enthalpy spectra for amorphous $Co_{68}Ni_{10}Fe_5Si_{11}B_{16}$. The average temperatures and times of measurement were 400 K/10^2 s, 500 K/10^5 s, and 700 K/10^5 s in the MAE, IMA [10], and RTD [14] measurements, respectively.

Fig. 2. $\log D_0^T - H_R^T$ plot of the diffusion enthalpies H_R^T and the pre-exponential factors D_0^T of the diffusion coefficients of transition metals in amorphous alloys [● FeZr alloys ; (1) $\underline{Fe}_{80}B_{20}$, (2) $\underline{Fe}_{40}Ni_{40}B_{20}$, (3) $\underline{Fe}_{41}Ni_{41}B_{18}$, (4) $\underline{Fe}_{40}Ni_{40}P_{14}B_6$, (5) $\underline{Fe}_{78}B_{13}Si_9$; (6) $\underline{Ni}$, (7) $\underline{Co}$, (8) $\underline{Fe}$, and (9) $\underline{Ta}$ in $Co_{68}Ni_{10}Fe_5Si_{11}B_{16}$]. The underlined elements indicate the radioactive diffusers. For comparison self-diffusion data in crystalline metals (dashed circle and full squares) are included.

Fig. 3. Schematic representation of diffusion models and corresponding Arrhenius plots of the diffusion coefficients [$D_0 \equiv D(T^{-1} = 0)$]. a) Random-barrier model, b) random-trap model, c) mixed model. The horizontal lines in the H—x diagrams mark $H = 0$, $H = \langle h_i \rangle$, and $H = \langle h_{ij} \rangle$, respectively. For further details see text.

Fig. 4. Arrhenius representation of time-averaged diffusion coefficients according to the mixed model for different diffusion times. The curves "st" and "lt" represent the limiting cases $t \to 0$ and $t \to \infty$. The hatched areas indicate the regimes in which MAE, IMA, and RTD experiments have been performed. For further details see text.

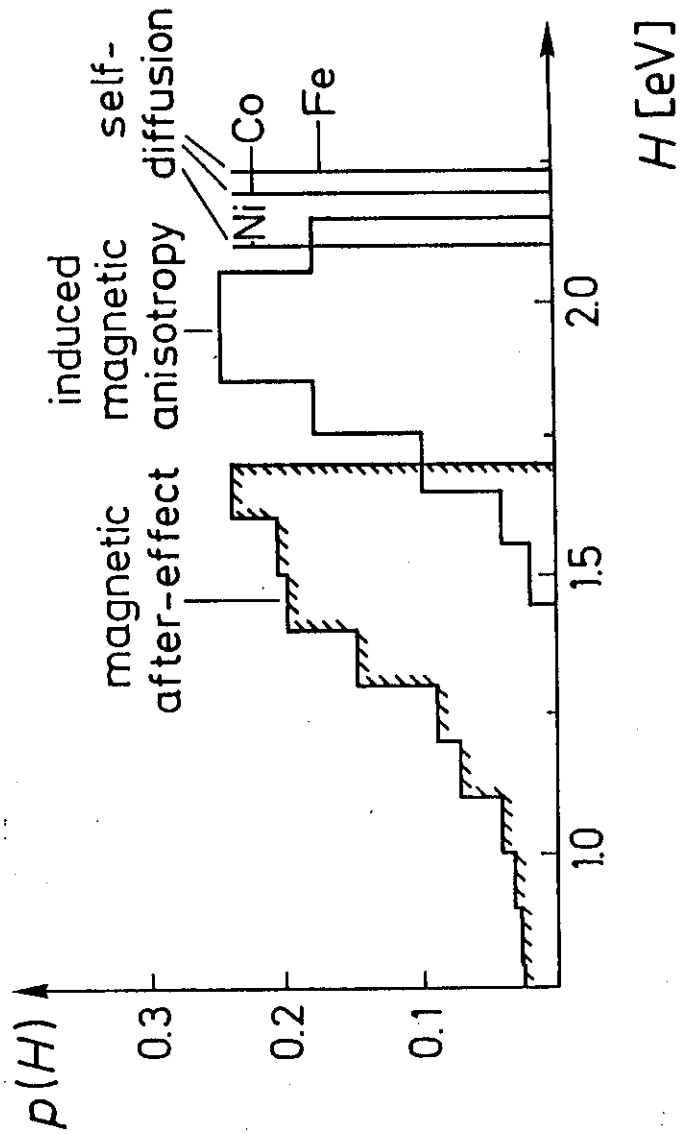

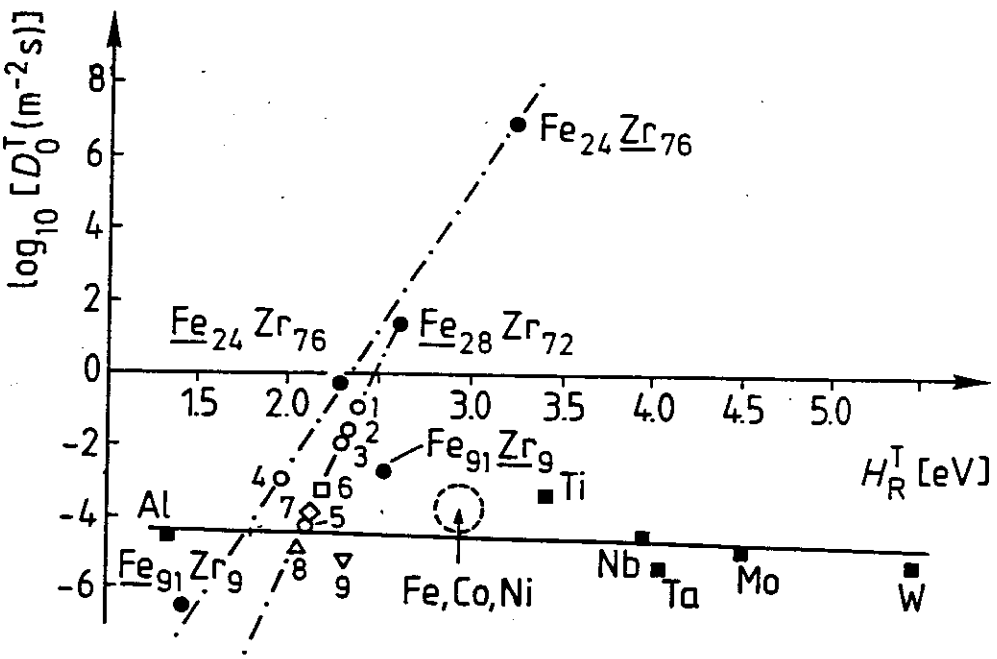
$\log_{10}[D_0^T(m^{-2}s)]$
8
6
4
2
0
-2
-4
-6
1.5
2.0
3.0
3.5
4.0
4.5
5.0
H_R^T [eV]
$Fe_{24}Zr_{76}$
$Fe_{28}Zr_{72}$
$Fe_{91}Zr_9$
Ti
Al
$Fe_{91}Zr_9$
Fe,Co,Ni
Nb
Ta
Mo
W
1
2
3
4
5
6
7
8
9

Fig. 2

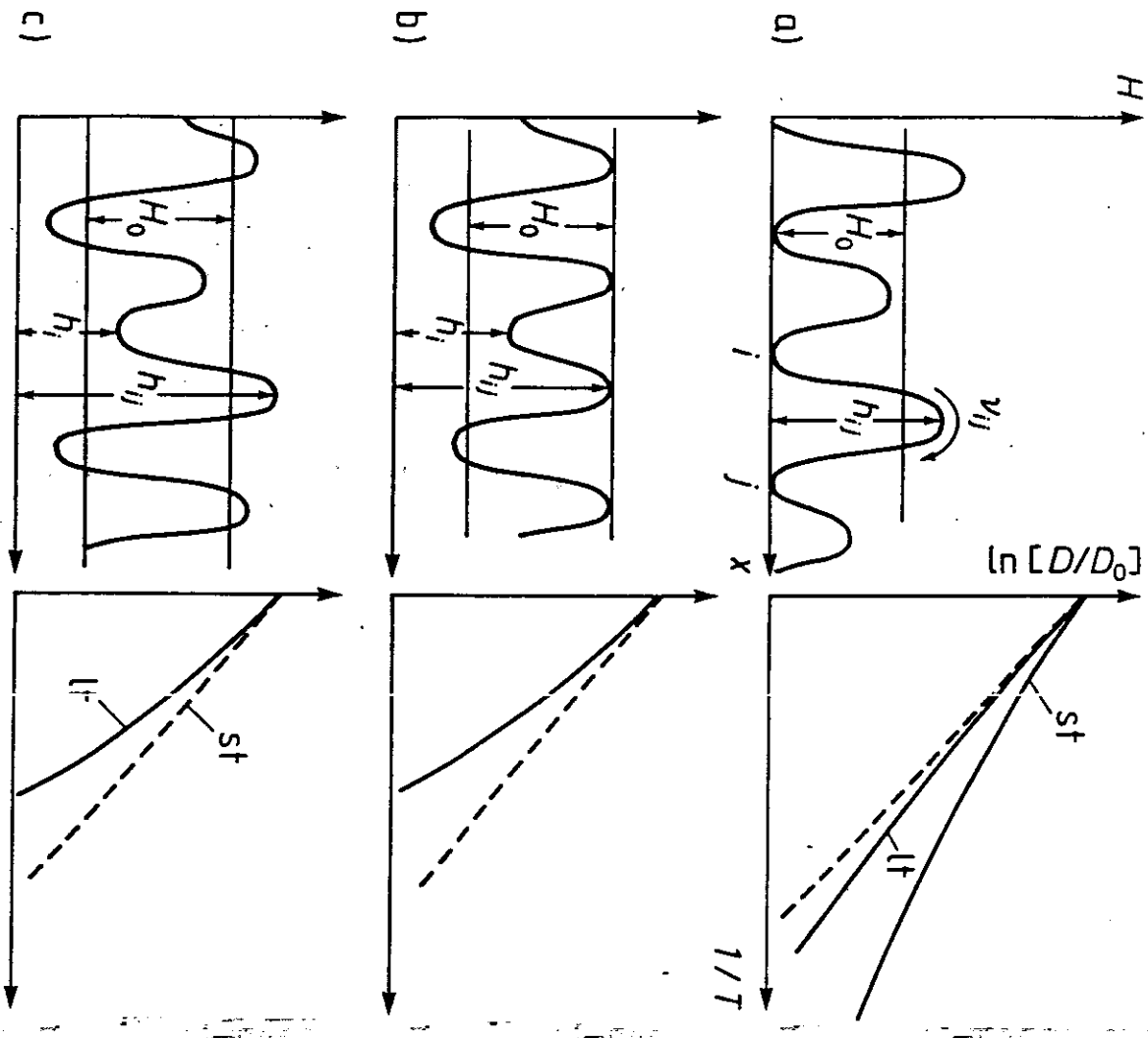
c
b
a
H
H_0
h_I
h_{II}
h_{II}
h_{II}
I
II
x
ln [D/D₀]
lf
st
st
lf
1/T

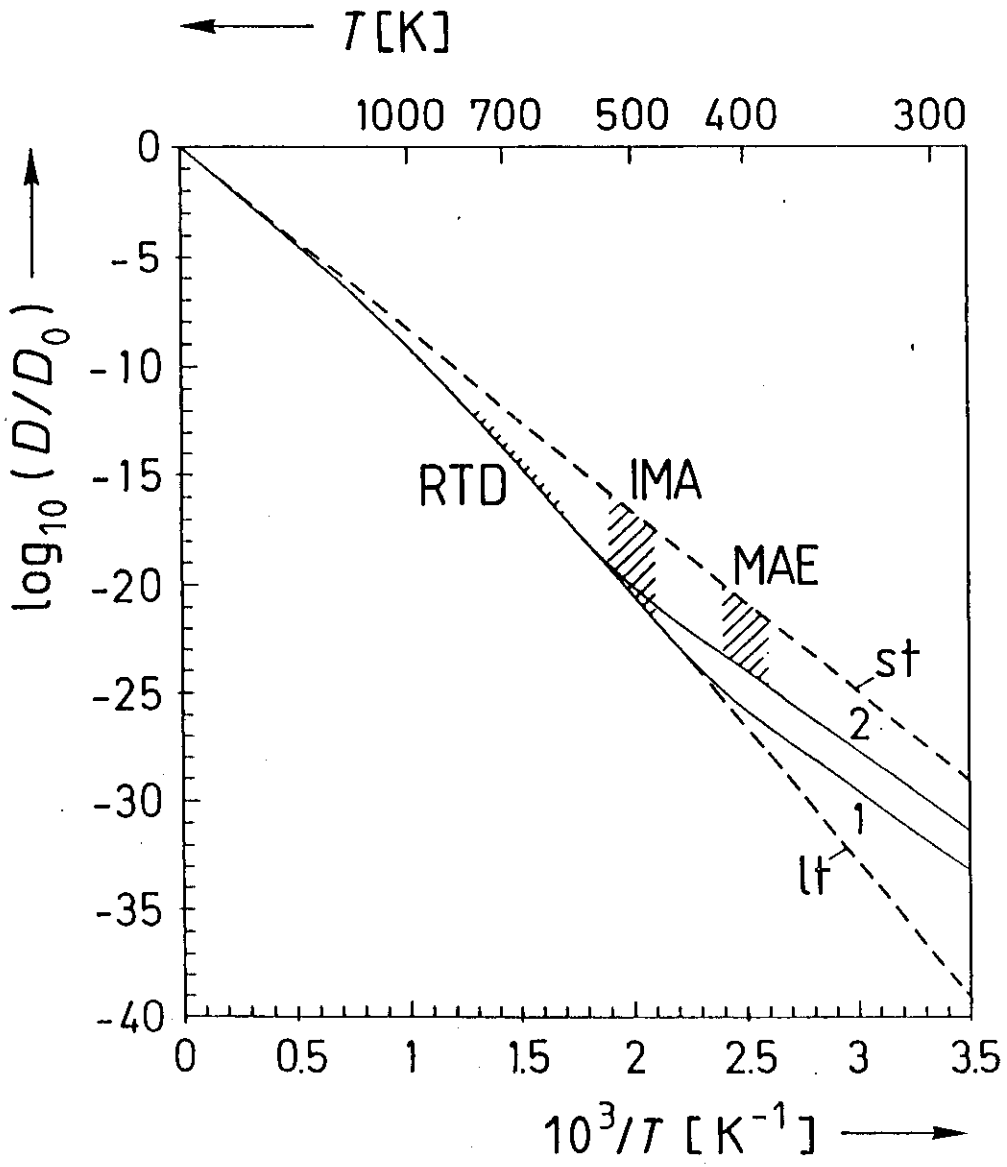
T [K]
1000 700 500 400 300
0
-5
-10
-15
-20
-25
-30
-35
-40
log10 (D/D0)
RTD
IMA
MAE
st
2
1
lt
0 0.5 1 1.5 2 2.5 3 3.5
10^3/T [K^-1]